REPUBLIQUE DU CAMEROUN
Paix – Travail – Patrie
****
UNIVERSITE DE YAOUNDE I
FACULTE DES SCIENCES
DEPARTEMENT DE PHYSIQUE
****
LABORATOIRE DE MODÉLISATION ET SIMULATION EN INGÉNIERIE, BIOMIMÉTISME ET PROTOTYPES

REPUBLIC OF CAMEROUN
Peace – Work – Fatherland
****
UNIVERSITY OF YAOUNDE I
FACULTY OF SCIENCE
DEPARTMENT OF PHYSICS
****
LABORATORY OF MODELLING AND SIMULATION IN ENGINEERING, BIOMIMETICS AND PROTOTYPES

Quantum Study of Optical and Geometrical Nonlinearities in Fabry-Pérot Optomechanical Cavity

Thesis
Submitted and defended for the award of
Doctorat/ PhD in Physics

Par : **DJORWÉ Philippe**
Master in Physics

Sous la direction de
NANA ENGO Serge Guy
Associate Professor
WOAFO Paul
Professor

Année Académique : 2014

Faculty List

Dean	:	BILONG Paul, Professor
Vice-Dean (DPSAA)	:	NJOPWOUO Daniel, Professor
Vice-Dean (DSSE)	:	DONGO Etienne, Professor
Vice-Dean (DRC)	:	ESSIMBI ZOBO Bernard, Professor
Head of Division (AARR)	:	ABOSSOLO Monique, Senior Lecturer
Head of Division (AF)	:	NDOYE FOE M. C. F., Senior Lecturer

1 - DEPARTMENT OF BIOCHEMISTRY (BC) (41)			
01	MOUNDIPA FEWOU Paul	Professor	Head of Dept
02	OBEN Julius ENYONG	Professor	on duty
03	BENG born NINTCHOM P. V.	Associate Professor	on duty
04	FEKAM BOYOM Fabrice	Associate Professor	on duty
05	FOKOU Elie	Associate Professor	on duty
06	KANSCI Germain	Associate Professor	on duty
07	MBACHAM Wilfried	Associate Professor	Head of Dept/FSBM
08	MINKA Samuel	Associate Professor	on duty
09	NGUEFACK Julienne	Associate Professor	on duty
10	ACHU Mercy BIH	Senior Lecturer	on duty
11	ATOGHO Barbara Mma	Senior Lecturer	on duty
12	BELINGA born NDOYE FOE Marie C. F.	Senior Lecturer	Head DAF / FS
13	BIGOGA Jude	Senior Lecturer	on duty
14	BIYITI BI ESSAM born AKAM ADA L. F.	Senior Lecturer	GI MINRESI
15	BOUDJEKO THADEE	Senior Lecturer	on duty
16	DEMMANO Gustave	Senior Lecturer	on duty
17	DJOKAM TAMO Rosine Rachel	Senior Lecturer	on duty
18	DJUIDJE NGOUNOUE Marcelline	Senior Lecturer	on duty
19	EFFA ONOMO Pierre	Senior Lecturer	on duty
20	EVEHE BEBANDOUE Marie-Solange.	Senior Lecturer	on duty
21	EWANE Cécile Anne	Senior Lecturer	on duty
22	MOFOR née TEUGWA Clautilde	Senior Lecturer	IA3 MINESUP
23	NGONDI Judith Laure	Senior Lecturer	on duty
24	NJAYOU Frédéric Nico	Senior Lecturer	on duty
25	TCHANA NKOUATCHOUA A.	Senior Lecturer	on duty
26	WAKAM née NANA Louise	Senior Lecturer	on duty
27	AKINDEH MBUH NJI	Assistant	on duty
28	BEBEE FADIMATOU	Assistant	on duty
29	BEBOY EDZENGUELE Sara Nathalie	Assistant	on duty
30	DAKOLE DABOY Charles	Assistant	on duty
31	DJUIKWO NKONGA Ruth Viviane	Assistant	on duty
32	DONGMO LEKAGNE Joseph Blaise	Assistant	on duty
33	KOTUE KAPTUE Charles	Assistant	on duty
34	FONKOUA Martin	Assistant	on duty
35	LUNGA Paul KAILAH	Assistant	on duty
36	MANANGA Marlyse Joséphine	Assistant	on duty
37	MBONG ANGIE MOUGANDE Mary Ann	Assistant	on duty
38	MBOUCHE FANMOE Marcelline Joëlle	Assistant	on duty
39	PACHANGOU NSANGOU Sylvain	Assistant	on duty
40	Palmer MASUMBE NETONGO	Assistant	on duty
41	TIENTCHEU DJOKAM Léopold	Assistant	on duty

2 - DEPARTMENT OF ANIMAL BIOL. AND PHYSIOL. (BPA) (45)			
01	BILONG BILONG Charle Félix	Professor	Head of Dept
02	DIMO Théophile	Professor	on duty
03	FOMENA Abraham	Professor	on duty
04	KAMTCHOUING Pierre	Professor	on duty
05	MINFOUNDI Remy	Professor	on duty
06	NGASSAM Pierre	Professor	on duty
07	NJIOKOU Flobert	Professor	on duty
08	NOLA Moïse	Professor	on duty
09	DJIETO Lordon Champlain	Associate Professor	on duty
10	ESSOMBA born NTSAMA M.	Associate Professor	MINSANTE
11	FOTO MENBOHAN Samuel	Associate Professor	CT2 MINEE
12	KAMGANG René	Associate Professor	CS MINRESI
13	NJAMEN Dieudonné	Associate Professor	on duty
14	TAN Paul	Associate Professor	on duty
15	TCHUEM TCHUENTE Louis	Associate Professor	Coord. Progr MINSANTE
16	AJEAGAH Gidéon AJHAINDUM	Senior Lecturer	on duty
17	ALENE Désirée Chantal	Senior Lecturer	on duty
18	BELLET EDIMO Oscar R.	Senior Lecturer	on duty
19	BILANDA Danielle Claude	Senior Lecturer	on duty
20	DJIOGUE Séfirin	Senior Lecturer	on duty
21	DZEUFIET DJOMENI Paul D.	Senior Lecturer	on duty
22	GOUNOUE KAMKUMO Raceline	Senior Lecturer	on duty
23	JATSA MEGAPTCHE Hermine	Senior Lecturer	on duty
24	KEKEUNOU Sévilor	Senior Lecturer	on duty
25	MEGNEKOU Rosette	Senior Lecturer	on duty
26	MONY NTONE Ruth	Senior Lecturer	on duty
27	NGUEGUIM TSOFACK Florence	Senior Lecturer	on duty
28	NGUEMBOCK	Senior Lecturer	on duty
29	TOMBI Jeannette	Senior Lecturer	on duty
30	ZEBAZE TOGOUET Serge H.	Senior Lecturer	on duty
31	ATSAMO Albert Donatien	Assistant	on duty
32	ETEME ENAMA Serge	Assistant	on duty
33	KANDELA KAVAYE Antoine	Assistant	on duty
34	KOGA MANG'Dobara	Assistant	on duty
35	LEKEUFACK FOLEFACK Guy B.	Assistant	on duty
36	MAHOB Raymond Joseph	Assistant	on duty
37	MBENOUN MASSE Paul Serge	Assistant	on duty
38	MOUNGANG NGAMENI Luciane	Assistant	on duty
39	MUH Bernice FIEN	Assistant	on duty

40	MVEYO NDANKEU Yves Patrick	Assistant	on duty
41	NGOUATEU KENFACK Omer BEBE	Assistant	on duty
42	NJUA Clarisse YAFI	Assistant	on duty
43	OBI OBEN Esther	Assistant	on duty
44	TADU Zéphirin	Assistant	on duty
45	YEDE	Assistant	on duty

3 - DEPARTMENT OF PLANT BIOLOGY (BPV) (25)			
01	YOUMBI Emmanuel	Professor	on duty
02	AMBANG Zachée	Associate Professor	**Vice-Dean/FSE**
03	BELL Joseph Martin	Associate Professor	on duty (CDPi)
04	DJOCGOUE Pierre F.	Associate Professor	on duty
05	MOSSEBO Dominique C.	Associate Professor	on duty
06	ZAPFACK Louis	Associate Professor	on duty
07	ANGONI Hyacinthe	Senior Lecturer	on duty
08	BIYE Elvire Hortense	Senior Lecturer	on duty
09	KENGNE NOUMSI Yves M.	Senior Lecturer	on duty
10	MALLA Armand William	Senior Lecturer	on duty
11	MBARGA BINDZI Marie A.	Senior Lecturer	IA2 MINESUP
12	MBOLO Marie	Senior Lecturer	on duty
13	NDONGO BEKOLO	Senior Lecturer	CE/MINRESI
14	NGODO MELINGUI Jean B.	Senior Lecturer	on duty
15	NGONKEU MAGAPTCHE E. L.	Senior Lecturer	on duty
16	NGOUO Lucas Vincent	Senior Lecturer	on duty
17	NSOM ZAMO Annie Claude	Senior Lecturer	National expert/UNESCO
18	TONFACK Libert Brice	Senior Lecturer	on duty
19	TSOATA Esaïe	Senior Lecturer	on duty
20	DJEUANI Astride Carole	Assistant	on duty
21	MAHBOU SOMO TOUKAM Gabriel	Assistant	on duty
22	MAFFO MAFFO Nicole Liliane	Assistant	on duty
23	NGALLE Hermine BILLE	Assistant	on duty
24	NNANGA MEBENGA Ruth Laure	Assistant	on duty
25	NOUKEU KOUAKAM Armelle	Assistant	on duty

4 - DEPARTMENT OF INORGANIC CHEMISTRY (CI) (33)			
01	NDIFON Peter TEKE	Professor	IGS MINRESI
02	NGAMENI Emmanuel	Professor	DEAN FS / UDs
03	NJOPWOUO Daniel	Professor	Vice-Dean/DPSAA
04	AGWARA ONDOH M.	Associate Professor	IGS MINPMEA
05	AVOM Jérôme	Associate Professor	Dir. IAI Gabon
06	BABALE née DJAM DOUDOU	Associate Professor	CM PR
07	DJOUFAC WOUMFO E.	Associate Professor	on duty
08	ELIMBI Antoine	Associate Professor	on duty
09	GHOGOMU Paul MINGO	Associate Professor	Dir. cab. PM
10	KETCHA MBADCAM J.	Associate Professor	Head of Dept.
11	LAMINSI Samuel	Associate Professor	on duty
12	MELO née CHINJE Uphie F.	Associate Professor	Dir. MIPROMALO
13	NANSEU Charles Péguy	Associate Professor	on duty
14	NENWA Justin	Associate Professor	on duty
15	NDIKONTAR Maurice KOR	Associate Professor	Vice-Dean/UBa
16	NGOMO Horace MANGA	Associate Professor	SG of MINESUP
17	YOUNANG Elie	Associate Professor	on duty
18	BAIZOUMI ZOUA	Senior Lecturer	Head of Div. MINTOUR
19	EMADACK Alphonse	Senior Lecturer	on duty
20	GWET Simon-Pierre	Senior Lecturer	on duty
21	KEUMEGNE MBOUGUEM J.C.	Senior Lecturer	on duty
22	KONG SAKEO	Senior Lecturer	CM of P.M
23	NJIOMOU C. wife DJANGANG	Senior Lecturer	on duty
24	NJOYA Dayirou	Senior Lecturer	on duty
25	SIGNING Pierre	Senior Lecturer	on duty
26	ACAYANKA Elie	Senior Lecturer	on duty
27	CHEUMANI YONA Arnaud	Senior Lecturer	on duty
28	KAMGANG YOUBI Georges	Senior Lecturer	on duty
29	NYAMEN Linda Dyorisse	Senior Lecturer	on duty
30	PABOUDAM GBAMBIE Awaou	Senior Lecturer	on duty
31	TCHAKOUTE KOUAMO H.	Senior Lecturer	on duty
32	BELIBI BELIBI Placide Désiré	Assistant	on duty
33	NDI Julius NSAMI	Assistant	on duty

5 - DEPARTMENT OF ORGANIC CHEMISTRY (CO) (34)			
01	DONGO Etienne	Professor	on duty
02	GHOGOMU TIH Raphäel	Professor	on duty
03	MBAFOR Joseph	Professor	on duty
04	NGADJUI TCHALEU B.	Professor	Head of Dept /FMBS
05	NGOUELA Silvère A.	Professor	on duty
06	NKENGFACK Augustin E.	Professor	Head of Dept.
07	NYASSE Barthélemy	Professor	Deputy VC /UBa
08	PEGNYEMB Dieudonné Emmanuel	Professor	DAUQ MINESUP
09	WANDJI Jean	Professor	on duty
10	Alex de Théodore ATCHADE	Associate Professor	CS Rect./UY1
11	FOLEFOC G. NGOSONG	Associate Professor	Vice-Dean U.B.
12	KAPNANG Henriette	Associate Professor	on duty
13	KEUMEDJIO Félix	Associate Professor	on duty
14	KOUAM Jacques	Associate Professor	on duty
15	NOUNGOUE TCHAMO D.	Associate Professor	on duty
16	TCHOUANKEU Jean-Claude	Associate Professor	DAAC UYI
17	YANKEP Emmanuel	Associate Professor	on duty
18	TIH born NGO BILONG E.A.	Associate Professor	on duty
19	AMBASSA Pantaleon	Senior Lecturer	on duty
20	EYONG Kenneth OBEN	Senior Lecturer	on duty
21	KENMOGNE Marguerite	Senior Lecturer	on duty
22	MBAZOA born DJAMA C.	Senior Lecturer	on duty
23	MKOUNGA Pierre	Senior Lecturer	on duty
24	NGO MBING Josephine	Senior Lecturer	on duty
25	NGONO BIKOBO Dominique Serge	Senior Lecturer	on duty
26	NOTE LOUGBOT Olivier	Senior Lecturer	on duty
27	OUAHOUO WACHE Blandine Marlyse	Senior Lecturer	on duty
28	TABOPDA KUATE Turibio	Senior Lecturer	on duty
29	TAGATSING FOTSING Maurice	Senior Lecturer	on duty
30	ZONDENDEGOUMBA Ernestine	Senior Lecturer	on duty
31	FOTSO WABO Ghislain	Assistant	on duty
32	KAMTO Eutrophe Ledoux	Assistant	on duty
34	NGINTEDO Dominique	Assistant	on duty
35	NGOMO Orléans	Assistant	on duty

6 - DEPARTMENT OF COMPUTER SCIENCE (IN) (25)			
01	TCHUENTE Maurice	Professor	PCA UB
02	ATSA ETOUNDI Roger	Associate Professor	Head of Dept./Head Div. MINFOPRA
04	FOUDA NDJODO Marcel	Associate Professor	IGA MINESUP/Head of Dept. ENS
05	NDOUNDAM René	Associate Professor	on duty
06	CHEDOM FOTSO D. E.	Senior Lecturer	on duty
07	MELATAGIA YONTA P.	Senior Lecturer	on duty
08	MOTO MPONG Serge A.	Assistant	on duty
09	TINDO Gilbert	Senior Lecturer	on duty
10	TSOPZE Norbert	Senior Lecturer	on duty
11	WAKU KOUAMOU Jules	Senior Lecturer	on duty
12	ABESSOLO ALO'O Gislain	Assistant	on duty
13	BAYEM Jacques Narcisse	Assistant	on duty
14	DJOUWE MEFFEJA Merline Flore	Assistant	on duty
15	EBELE Serge Alain	Assistant	on duty
16	HAMZA Adamou	Assistant	on duty
17	KAMDEM KENGNE Christiane	Assistant	on duty
18	KAMGUEU Patrick Olivier	Assistant	on duty
19	KENFACK DONGMO Clauvice Viliane	Assistant	on duty
20	DOMGA KOMGUEM Rodrigue	Assistant	on duty
21	KOUOKAM KOUOKAM E. A.	Assistant	on duty
22	MEYEMDOU Nadège S.	Assistant	on duty
23	MONTHE DJIADEU V. M.	Assistant	on duty
24	JIOMEKONG AZANZI Fidel	Assistant	on duty
25	TAPAMO KENFACK Hyppolite	Assistant	on duty

7 - DEPARTMENT OF MATHEMATICS (MA) (35)			
01	BEKOLLE David	Professor	Deputy Vice-Chancellor UN
02	BITJONG NDOMBOL	Professor	DIPD UY II
03	DOSSA COSSY Marcel	Professor	on duty
04	NGUETSENG Gabriel	Professor	Head of Div. UIT-Bois, UYI
05	NOUTCHEGUEME Norbert	Professor	on duty
06	EMVUDU WONO Yves S.	Associate Professor	Head of Div. MINESUP
07	NKUIMI JUGNIA Célestin	Associate Professor	on duty
08	TCHAPNDA NJABO S. B.	Associate Professor	on duty
09	TONGA Marcel	Associate Professor	on duty
10	WAMON François	Associate Professor	Head of Dept
11	AGHOUKENG JIOFACK Jean Gérard	Senior Lecturer	on duty
12	AYISSI Raoult Domingo	Senior Lecturer	on duty
13	FOMEKONG Christophe	Senior Lecturer	on duty
14	KIANPI Maurice	Senior Lecturer	on duty
15	KIKI Maxime A.	Senior Lecturer	on duty
16	MBAKOP Guy Merlin	Senior Lecturer	on duty
17	MBANG Joseph	Senior Lecturer	on duty
18	MBIANDA Gilbert	Senior Lecturer	on duty
19	MENGUE MENGUE David Joe	Senior Lecturer	on duty
20	NGUIMTSA Charles	Senior Lecturer	on duty
21	NOUNDJEU Pierre	Senior Lecturer	on duty
22	TCHANGANG Roger D.	Senior Lecturer	on duty
23	TCHOUNDJA Edgar Landry	Senior Lecturer	on duty
24	TIAYA TSAGUE N. A.-M.	Senior Lecturer	on duty
25	CHENDJOU Gilbert	Assistant	on duty
26	DJIADEU NGAHA Michel	Assistant	on duty
27	MBEHOU Mohamed	Assistant	on duty
28	MBELE BEDIMA Martin	Assistant	on duty
29	MBIAKOP Hilaire George	Assistant	on duty
30	NGUEFACK Bertrand	Assistant	on duty
31	NIMPA PEFOUKEU Romain	Assistant	on duty
32	POLA DOUNDOU Emmanuel	Assistant	on duty
33	TAKAM SOH Patrice	Assistant	on duty
34	TANG AHANDA Barnabé	Assistant	Head of Serv. MINPLAMAT
35	TETSADJIO TCHILEPECK M. E.	Assistant	on duty

8 - DEPARTMENT OF MICROBIOLOGY (MB) (13)			
01	ETOA François-Xavier	Professor	Head of Dept./CT PM
02	ESSIA NGANG Jean Justin	Associate Professor	Head of Div IMPM
03	NWAGA Dieudonné M.	Associate Professor	on duty
04	BODA Maurice	Senior Lecturer	on duty
05	BOYOMO ONANA	Senior Lecturer	on duty
06	ENO Anna Arey	Senior Lecturer	on duty
07	ESSONO OBOUGOU Germain Gabriel	Senior Lecturer	on duty
08	NYEGUE Maximillienne Ascension	Senior Lecturer	on duty
09	RIWOM Sara Honorine	Senior Lecturer	on duty
10	SADO KAMDEM Sylvain Leroy	Senior Lecturer	on duty
11	BOUGNOM Blaise Pascal	Assistant	on duty
12	NJIKI BIKOÏ Jacky	Assistant	on duty
13	TCHIKOUA Roger	Assistant	on duty

9 - DEPARTMENT OF PHYSICS (PH) (40)			
01	ESSIMBI ZOBO Bernard	Professor	Vice-Dean (DRC)
02	KOFANE Timoléon Crépin	Professor	Head of Dept
03	NDJAKA Jean Marie B.	Professor	on duty
04	NJOMO Donatien	Professor	on duty
05	WOAFO Paul	Professor	on duty
06	BEN-BOLIE Germain H.	Associate Professor	on duty
07	EKOBENA FOUDA H. P.	Associate Professor	Head of Dept /UN
08	NJANDJOCK NOUCK P.	Associate Professor	Head of Serv. MINRESI
09	NOUAYOU Robert	Associate Professor	on duty
10	OUMAROU BOUBA	Associate Professor	Vice-Chancellor UYII
11	PEMHA Elkana	Associate Professor	on duty
12	TABOD Charles TABOD	Associate Professor	Dean UBda
13	TCHAWOUA Clément	Associate Professor	on duty
14	ZEKENG Serge Sylvain	Associate Professor	on duty
15	BIYA MOTTO Frédéric	Senior Lecturer	Gener. Manag. MEKIN Dam
16	BODO Bernard	Senior Lecturer	on duty
17	DJUIDJE K. G. wife ALOYEM	Senior Lecturer	on duty
18	EDONGUE HERVAIS	Senior Lecturer	on duty
19	EYEBE FOUDA Jean Sire	Senior Lecturer	on duty
20	FEWO Serge Ibraid	Senior Lecturer	on duty
21	FOUEDJIO David	Senior Lecturer	on duty
22	HONA Jacques	Senior Lecturer	on duty
23	MBANE BIOUELE	Senior Lecturer	on duty
24	MBONO SAMBA Yves C.U.	Senior Lecturer	on duty
25	NANA NBENDJO Blaise	Senior Lecturer	on duty
26	NDOP Joseph	Senior Lecturer	on duty
27	OBOUNOU Marcel	Senior Lecturer	on duty
28	SAIDOU	Senior Lecturer	on duty
29	SIEWE SIEWE Martin	Senior Lecturer	on duty
30	SIMO Elie	Senior Lecturer	on duty
31	TABI Conrad Bertrand	Senior Lecturer	on duty
32	TCHOFFO Fidèle	Senior Lecturer	on duty
33	VONDOU DERBETINI Appolinaire	Senior Lecturer	on duty
34	BEYA Annie wife WAKATA	Senior Lecturer	Head of Serv. MINESUP
35	WOULACHE Rosalie Laure	Senior Lecturer	on duty
36	ABDOURAHIMI	Assistant	on duty
37	CHAMANI Roméo	Assistant	on duty
38	ENYEGUE A NYAM F. épouse BELINGA	Assistant	on duty
39	MBINACK Clément	Assistant	on duty
40	MBOUSSI NKOMIDIO Aissatou	Assistant	on duty

10 - DEPARTMENT OF EARTH SCIENCE (ST) (43)			
01	BILONG Paul	Professor	Dean Fac. Science/ Head Dept
02	NZENTI Jean-Paul	Professor	on duty
03	BITOM Dieudonné L.	Professor	Dean/UN
04	FOUATEU Rose wife YONGUE	Associate Professor	on duty
05	KAMGANG Pierre	Associate Professor	on duty
06	MEDJO EKO Robert	Associate Professor	Dir UIT Bois UYI
07	MVONDO ONDOA J.	Associate Professor	on duty
08	NDAM NGOUPAYOU J.-R.	Associate Professor	on duty
09	NDJIGUI Paul-Désiré	Associate Professor	CSMM
10	NGOS III Simon	Associate Professor	DAAC/UMa
11	NJILAH Isaac KONFOR	Associate Professor	on duty
12	NKOUMBOU Charles	Associate Professor	on duty
13	TEMDJIM Robert	Associate Professor	on duty
14	ABOSSOLO born ANGUE M.	Senior Lecturer	Head of DAASR
15	BEKOA Etienne	Senior Lecturer	on duty
16	BISSO Dieudonné	Senior Lecturer	Head of Project Barrage Memvelle
17	EKOMANE Emile Marie	Senior Lecturer	CS/MINMIDT
18	ESSONO Jean	Senior Lecturer	CEA MINIMDT
19	GANNO Sylvestre	Senior Lecturer	on duty
20	GHOGOMU Richard TANWI	Senior Lecturer	on duty
21	LAMILEN BILLA Daniel	Senior Lecturer	on duty
22	LIENOU Gaston	Senior Lecturer	on duty
23	MBIDA YEM	Senior Lecturer	CS/LABOGENIE
24	MINYEM Dieudonné	Senior Lecturer	on duty
25	MOUAFO Lucas	Senior Lecturer	on duty
26	MOUNDI Amidou	Senior Lecturer	IS1 MINIMDT
27	NGO BIDJECK Louise Marie	Senior Lecturer	on duty
28	NGUETCHOUA Gabriel	Senior Lecturer	on duty
29	NJOM Bernard de Lattre	Senior Lecturer	on duty
30	NYECK Bruno	Senior Lecturer	S/Dir MINMIDT
31	ONANA Vincent	Senior Lecturer	on duty
32	TCHAKOUNTE J. wife NUMBEN	Senior Lecturer	CEA MINRESI
33	TCHOUANKOUE Jean-Pierre	Senior Lecturer	on duty
34	YENE ATANGANA J. Q.	Senior Lecturer	Head of Div. MINFOF
35	ZO'O ZAME Philémon	Senior Lecturer	SG MINTP
36	ANABA ONANA Achille Basile	Assistant	on duty
37	FUH Calistus Gentry	Assistant	Sec State/MINMIDT
38	METANG Victor	Assistant	on duty
39	NGO BELNOUN Rose Noël	Assistant	on duty
40	NOMO NEGUE Emmanuel	Assistant	on duty
41	TCHAPTCHET TCHATO. De P. I	Assistant	on duty
42	TEHNA Nathanaël	Assistant	CS/ MINMIDT
43	TEMGA Jean Pierre	Assistant	on duty

REPARTITION OF LECTURERS IN THE FACULTY OF SCIENCE ACCORDING TO DEPARTMENTS (31 July 2014)

DEPARTMENT	**NUMBER OF LECTURERS**				
	Prof.	**Ass. Prof.**	**Sen. Lect.**	**Asst.**	**Total**
BC	2 (0)	7 (2)	17 (11)	15 (6)	**41 (19)**
BPA	8 (0)	7 (0)	15 (7)	15 (5)	**45 (12)**
BPV	1 (0)	5 (0)	13 (3)	6 (5)	**25 (8)**
CI	3 (0)	14(2)	14 (3)	2 (0)	**33 (5)**
CO	9 (0)	9 (2)	12 (6)	4 (0)	**34 (8)**
IN	1 (0)	4 (1)	6 (0)	14 (4)	**25 (5)**
MA	5 (0)	5 (0)	14 (1)	11 (1)	**35 (2)**
MB	1 (0)	2 (0)	7 (3)	3 (0)	**13 (3)**
PH	5 (0)	9 (0)	21 (3)	5 (2)	**40 (5)**
ST	2 (0)	11 (1)	22 (3)	8 (1)	**43 (5)**
Total	**37 (0)**	**73 (8)**	**141 (40)**	**83 (23)**	**334 (72)**

So a total of: 334 (72) with

- Professors 37 (0)
- Associate Professor 73 (8)
- Senior Lecturer 141 (40)
- Assistants 83 (23)
- () = Number of Women.

Dedications

To the **Almighty God**, the Father of Beauties, the Beloved Son and the Holy One, always loving, living and laboring

Acknowledgements

All glory is for **God**, the Exalted and Almighty, without whom the completion of this project would have not been possible.

This thesis is the fruit of moral and financial support of the special persons whom I would like to address my very king gratitude:

My special thanks go to my promoter **Prof. Serge Guy NANA ENGO** who accompanied my work with lot of attentions, rigor, criticism science spirit and also with confidence. But most importantly, he trusted in me and its advices helped me to have self-confidence; briefly, I have inherited from his scientific mind and his simplicity.

My deepest and endless gratitude go to my supervisor **Prof. Paul WOAFO**, who not only gave me the opportunity to work in his group and entrusted me with an exciting research topic, but also accompanied rigorously my work with lot of attentions, fruitful discussions, and advice in all aspects of this research. Most importantly, his open-minded and kind attitude towards his students created a very familiar and cooperative atmosphere, which I appreciated very much. This passionate researcher challenges me scientifically and I benefited both from his skills and his organizational abilities.

I adress a special thank to my collaborator **Dr. Jimmi Hervé TALLA MBE** for fruitful discussions on the basic of optomechanics.

I am grateful to **Prof. Timoléon Crépin KOFANE**, the head of the Department of Physics, Faculty of Science, UYI and the teaching staff of his department for their encouragements and their fruitful advices.

I am grateful to the head of the Department of Physics, Faculty of Science, University of Ngaoundéré and the teaching staff of his department for their valuable teachings.

I wish to express my thanks to the members of the Laboratory of Atom and radiation, especially to Prof. Germain H. BEN-BOLIE, for their encouragements and the fruitful discussions during my thesis audition.

I wish to express my acknowledgments to all the members of the jury who have accepted to discuss and appreciate the results of this thesis, in spite of their numerous duties.

I would like to thank all my lab elders and mates of LaMSEBP: **Dr. Bonaventure NANA**, **Dr. Blaise Roméo NANA NBENDJO**, **Dr. Aissatou MBOUSSI**, **Dr. Guy KOL**, **Dr. Omer FOSSI**, **Dr. Sifeu TAKOUGANG KINGNI**, **Dr. Serges NGUEUTEU**, **Dr. Fulbert TOGUE**, **Dr. Hervé SIMO**, **Mr. Lejuste ABOBDA**, **Mr. Armand NANHA**, **Mr. Ahoudou NDOUKOUO**, **Mr. Andre CHAMGOUE**, who have participated to the seminars organized monthly at the LaMSEBP. Their various questions during my presentations helped me to improve the quality of this work.

I would like to thank all my lab mates of the Laboratory of Photonics at the University of Ngaoundéré for their constant encouragement during my laborious moments.

I also want to express my thanks to **Dr. Noël DJONYANG** and **Pauline Mai SELE** for their financial support and their encouragement.

The bests of my thanks go to my family, especially to my father **Victor WAMBA**, my brothers **Jean-Marie MENWA** and **Mermoz LAWA** and to my mother **OUIGA NINBE**, for their endless financially and morally support.

All those who by near or far have anyway contributed for the success of this intellectual masterpiece, recognize yourself in these thanks and be sure that I keep you in the deep of my heart.

Contents

List of Abbreviations

CM: Covariance Matrix
CV: Continuous Variable
EIT: Electromagnetically induced Transparency
EPR: Einstein-Podolsky-Rosen
FWHM: Full Width at Half Maximum
LIGO: Laser Interferometer Gravitational wave Observatory
NODEs: Nonlinear Ordinary Differential Equations
NL: Nonlinear
NQLEs: Nonlinear Quantum Langevin Equations
NR: Nanoresonator
ODEs: Ordinary Differential Equations
QFT: Qunatum Fourier Transform
QKD: Quantum Keys Distribution
QLEs: Quantum Langevin Equations
RK4: 4^{th} order Runge-Kutta
RPSN: Radiation Pressure Shot Noise
SEM: Scanning Electron Microscope
SQL: Standard Quantum Limit
WGM: Whispering-Gallery Mode
ZPF: Zero Point Fluctuation

List of Figures

List of Tables

Abstract

Considering the technological advances, phonon number less than unity have been achieved ($n_{eff} < 1$) during these five last years. However, reaching the Standard Quantum Limit ($n_{eff} = 0$) remains an experimental challenge which seems to be explained in nonlinear terms. To give a satisfactory explanation to this problem, we focused our thesis works on the nonlinear phononics study at the single-phonon level in optomechanical systems. We have shown that:

- Softening geometrical nonlinearity allows a classical control of the nanoresonator. The nonlinear term, through a semiclassical study, gives results which agree well with the quantum ones;
- Geometrical nonlinearity as the quantum decoherence, adds some of amount of phonons on the lowest result, and then limits the quantum ground state achievement. This allows us to show that high finesse structures ($\Omega_m \gg 1$) could be used to reduce the nonlinear effects and therefore suppress the quantum decoherence;
- At the mechanical and optical resonances where the geometrical and optical nonlinearities reach their maximum value, the squeezing is limited;
- At the blue detuning sideband, geometrical nonlinearity enhances the generation of robust CV entanglement against thermal decoherence.

The relevant fact of these results is that nonlinear effects not only contribute to the advance of the fundamental science but also appear as pillar elements for an improvement of quantum applications.

Keywords: Optomechanical oscillator, geometrical nonlinearity, optical nonlinearity, ground state, cooling, squeezing, entanglement.

Résumé

Avec les avancées technologiques, des nombres de phonons inférieurs à l'unité ($n_{eff} < 1$) ont été atteints lors ces cinq (05) dernières années. Cependant, parvenir à la limite quantique standard ($n_{eff} = 0$) reste un verrou expérimental qui semble s'expliquer en termes de non-linéarités. Afin de donner une explication satisfaisante à ce chalenge, nous focalisons nos travaux de thèse sur l'étude phononique non-linéaire à un niveau de phonon dans les systèmes optomécaniques. Nous avons montré que:

- La non-linéarité géométrique de type "softening" permet un contrôle classique du nanoresonateur. Une étude sémi-classique avec cette non-linéarité donne des résultats qui corroborent avec les attentes quantiques;
- La non-linéarité géométrique, pareil que la décohérence quantique, rajoute un supplément de phonons au résultat connu, limitant ainsi l'atteinte de l'état quantique fondamental. Cela nous a permis de montrer que des structures de grandes finesse ($\Omega_m \gg 1$) réduirait les effets non-linéares, supprimant la décohérence quantique;
- Aux résonances mécanique et optique où les non-linéarités géométriques et optiques sont maximales, la compression des états est limitée;
- A la bande latéral bleu "blue sideband", la non-linéarité géométrique améliore la génération d'états intriqués continus robustes thermiquement.

Il ressort de ces résultats que les effets non-linéaires contribuent non seulement à l'avancée de la science fondamentale mais aussi, se révèlent comme un levier pour améliorer les applications quantiques.

Mots clés: Oscillateur optomécanique, nonlinéarité géométrique, nonlinéarité optique, état fondamental, refroidissement, compression, intrication.

General Introduction

Light carries momentum which gives rise to radiation pressure forces. Such forces were already postulated in 1619 by Kepler, who conjectured that the dust tails of comets point away from the sunlight during a comet transit. Some 250 years later, this empirical observation of the mechanical effect of light, known as radiation pressure, was theoretically derived through the famous equations of Maxwell's theory on electromagnetic radiation. In early 1909, Einstein derived the statistics of the radiation pressure force fluctuations acting on a movable mirror, including the frictional effects of the radiation force, and this analysis allowed him to reveal the dual wave-particle nature of blackbody radiation. In pioneering experiments, both the linear and angular momentum transfer of photons to atoms and macroscopic objects were demonstrated by Frisch [1] and by Beth [2], respectively. But none satisfactory explanation about radiation pressure was not given experimentally.

The situation drastically changed with the advent of lasers in the 1970s, which enables highly focused and coherent light sources. Laser cooling was subsequently realized experimentally in the 1980s and has became since then an extraordinarily important technique [3]. It was soon suggested to use optical force to manipulate the motion of mechanical objects in a controlled manner. Radiation pressure is then used to cool atoms [3–6], to trap small particles [7, 8] and also to cool ions to their motional ground state. Some decades after, laser cooling enabled many applications [9] including what can be considered as true revolution in atomic physics, pivotal for discoveries such as Bose-Einstein condensation, optical atomic clocks, precision measurements of the gravitational field and systematic studies of quantum many-body physics in trapped clouds of atoms [10].

At the fundamental level, these experiments have established the fact that the motion of laser-cooled atoms or ions oscillating in their trapping potential can only be understood in quantum mechanical terms. For instance, when the quantum ground state is reached [11], the generation of the non-classical states such as Fock or Schrödinger cat states [12] becomes possible through optical manipulation. In the same sense, quantum fluctuations of the cooling light give rise to the Doppler limit in the temperature [13]. This

was the first time that such quantum effects have been observed with massive oscillators. To handle this limit sets by quantum fluctuations, optomechanical coupling has been proposed. Such coupling consists of confining highly laser light into an optical cavities. Under the radiation pressure exerted by light on these cavities or these mechanical structures, they begin to vibrate leading to an optomechanical interaction. There are many optomechanical system configurations such as Fabry-Perot cavity with one end moving mirror, suspended macroscopic mirrors, trampoline resonators, microtoroid and optical microsphere resonator. Using the quantum theory, one easily describes the optomechanical systems like photon-phonon interactions. During the last decade, these new systems have been proposed as potential candidates for laser cooling.

Several optomechanical cooling schemes, both theoretically and experimentally have been proposed. Among whose we have the resolved sideband cooling [14], back-action cooling [15–17] cooling by light scattering [18], cryogenic cooling [19–21], quadratic cooling [22] and modulation cooling [23]. Despite these numerous efforts, cooling remains limited by the Standard Quantum Limit (SQL). This limitation is experimentally induced by the Radiation Pressure Shot Noise (RPSN) [24] and is theoretically explained by thermal fluctuations [25] and laser phase noise [26–30]. Thus, ground state cooling or making measurement beyond the SQL was the first optomechanical challenge.

In recent years, the tremendous progresses both in cryogenic dilution techniques and in micro/nanofabrication technologies have provided unprecedented opportunities to engineer novel optomechanical devices [31]. These new devices have led to cooling improvement, since phonon numbers less than unity have been achieved in optomechanics devices [32] and in superconducting microwave circuits [33, 34]. With this achievement, ultrasensitive measurements beyond the SQL became possible. This was a step forwards the detection of ultra weak signals in the community of gravitational astronomy. Indeed, in order to detect wobbles in space-time induced by gravitational waves, these scientists conceived today's most sensitive displacement meters: kilometer-scale laser-driven interferometers, the mirrors of which are suspended as pendula to isolate them from seismic and technical noise (see Fig.1).

These exploits on ground state cooling were of great interest for the improvement of quantum applications in quantum information and quantum computing, thanks to quantum states as squeezed and entangled states. The generation of robust quantum states is often limited by the thermal decoherence and certain instabilities. This is why the authors of [34] stated that, new opportunities would be available as well as the generation of highly non-classical states, if the study of nonlinear phononics at the single-phonon

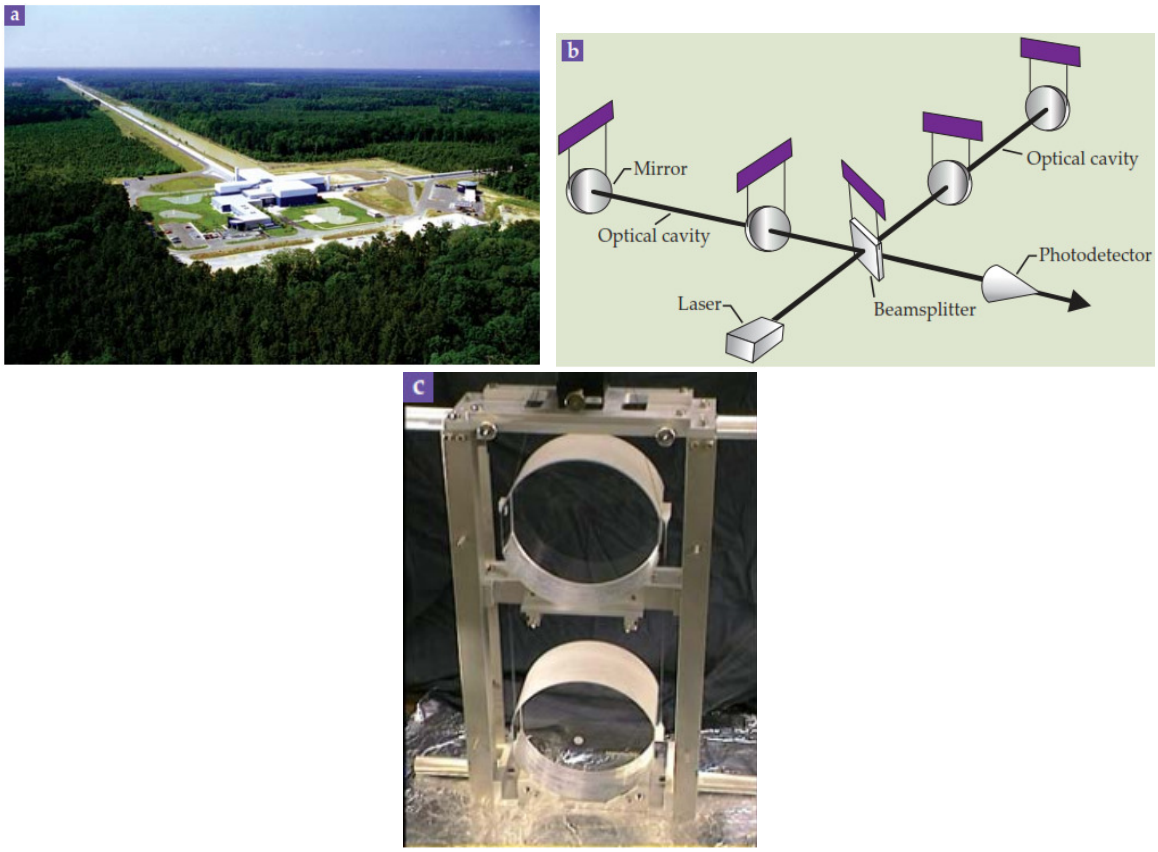

Figure 1: *Description of Laser Interferometer Gravitational Wave Observatory (LIGO). (a) LIGO laboratory in Livingston, Louisiana. (b) Schematic of LIGO. It consists of massive mirrors suspended to form a pair of optical cavities, each some kilometers long. The cavities behave as the arms of a Michelson interferometer and can detect changes in distance as small as* 10^{-21} *relative to the cavity length. (c) Mirrors used in the gravitational Wave detector GEO600, located near Sarsteat, Germany [35].*

level is done. We aim to tackle this problem in this thesis **by studying at the single-phonon level, the nonlinear phononics in optomechanical systems. We focus this study on the so-called geometrical (softening) nonlinearity in order to show its effects on quantum ground state cooling. We also need to bring out the influence of optical nonlinearity on the optomechanical coupling.**

To do this, we organize this thesis in three chapters.

In chapter one, elementary concepts of cooling are described and overview of nanomechanical cooling efforts is done.

The second chapter is devoted to the description of the mathematical tools used in this thesis. The rate equations of the models used are also established.

The third chapter which presents and discusses our results is structured in four specific points as follows:

The first point studies the effect of the geometrical nonlinearity on both the dynamical behavior of optomechanical system and on the optical bistability.

In the second point, the quantum ground state cooling is analyzed regarding on the geometrical nonlinear term.

The third point is devoted to investigate the effect of geometrical and optical nonlinearities on the squeezing.

Finally, the fourth point studies the effect of the geometrical nonlinear term on the generation of CV entanglement.

We end by a summary and outlook for feature challenges in nanomechanics.

Chapter 1

Literature Review

1.1 Introduction

This chapter starts with an overview of optomechanics, where some earlier interests that have led researchers to explore this new field are highlighted. After that, some basic concepts of opto/electromechanical quantum ground state cooling are presented. Later on, various experimental and theoretical efforts to reach quantum ground state will be reviewed. The section after describes briefly a new challenge poses by the geometrical nonlinearity in quantum ground state cooling, which will enable us to figure out the problem that our thesis aims to handle.

1.2 Overview

Pioneering experimental observation of optomechanical interaction was addressed by the Braginsky's group at Moscow State University. Conducting their research on general theory of quantum measurements [36–38], they developed a comprehensive understanding of optomechanical interactions as they occur in the fundamental building block of a gravitational wave observatory (see Fig.3.2). Their setup consisted to trap a monochromatic light in a high-finesse Fabry-Perot cavity resonator. This light exerts radiation pressure on the massive end-mirrors which couples their oscillatory motion to the light. Similar physics was explored theoretically for solid-state vibrations by Dykman [39]. In 1983, Dorsel et al. [40] demonstrated for the first time in a cavity optomechanical experiment, the bistability of the radiation pressure force acting on a macroscopic end-mirror. In 1967, Braginsky and coworkers showed that radiation pressure can change the dynamics of the mechanical degree of freedom, by effectively adding an optically induced viscous damping to the mirror motion. This was understood as dynamical back-action [41–44] which could be used to amplify or cool the motion of the mirror [39, 45]. For high enough light powers, quantum fluctuations in radiation pressure start to induce random motion in the mirror, masking the displacement to be detected [43], effect which is similar to the one of the quantum back-action of the measurement. This inspired Braginsky to address the fundamental consequences of the quantum fluctuations of radiation pressure, which impose a limitation to detect the position of a moving mass [43]. This ponderomotive role of quantum noise in interferometers is analyzed and clarified by Caves [46]. These works set the standard quantum limit for continuous position detection, which is essential for gravitational wave detectors such as LIGO or VIRGO.

Since then, optomechanics started to attract much attention of researchers in the quantum optics community, resulting in a variety of proposals exploring quantum effects

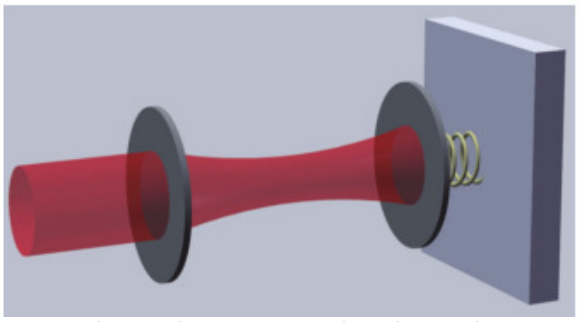

Figure 1.1: *Generic optomechanical system, with a laser driven Fabry-Perot optical cavity. The left mirror is fixed while the right one is attached to a spring which captures its motion [53].*

in these systems. To mention just a few examples, quantum non-demolition measurements of the light intensity or single quadratures of the mechanical displacement have been suggested in Refs. [36, 37, 47]. The generation of non-classical states, such as squeezing of light [48, 49], mechanical squeezed states [50, 51] and entangled states [52] have also been put forward. Such quantum properties are used to characterize and measure weak forces [43, 54, 55], to make ultrasensitive optical measurement in interferometric systems and both in optical accelerometers and sensors [56–59]. The squeezed and entangled states are used to improve the quantum teleportation, quantum key distribution, quantum information and quantum computing tasks. The observation of these quantum effects is enhanced if optomechanical cooling at the quantum ground state is achieved.

However, there are some experimental challenges to reach quantum ground state. The weakness of optomechanical coupling by radiation pressure causes limitations on ground state optomechanical cooling. This is due to the fact that the momentum transfer of a single reflected photon changes the velocity of a free gram-scale mass by some $10^{-15}\,\mathrm{nm/s}$ only. At the same time, the oscillator displacements associated with quantum effects are typically on the scale of its zero-point fluctuations $x_{ZPF} = \sqrt{\frac{\hbar}{2M\Omega}}$, where M and Ω_m are its mass and the resonance frequency, respectively. The increase of the optomechanical coupling can be done by the reduction of the resonator size, in order to make them more sensitive to the laser beam. Another challenge is the thermal noise which tends to mask quantum signatures as long as the thermal energy $k_B T$ largely exceeds the energy scale $\hbar\Omega_m$ of a motional quantum. Here, k_B is the Boltzmann's constant, $\hbar$ is the reduced Planck constant and T is the temperature.

According to the potential quantum opportunities offered by optomechanics, researchers from diverse fields have been interested by this new research field. With a joint effort of these researchers combined to the tremendous progress in micro/nano-fabrication technologies, new optomechanical devices have been devised and characterized. Some of these

optomechanical devices are grouped in the devices's zoo on figure Fig.3.3. The aim of these devices is to induce strong optomechanical coupling, enabling to approach fundamental quantum limit both in terms of the quality of displacement sensitivity and the occupation of the mechanical oscillator or phonon occupancy. This opens the way to the research field of cavity quantum optomechanics [60, 61].

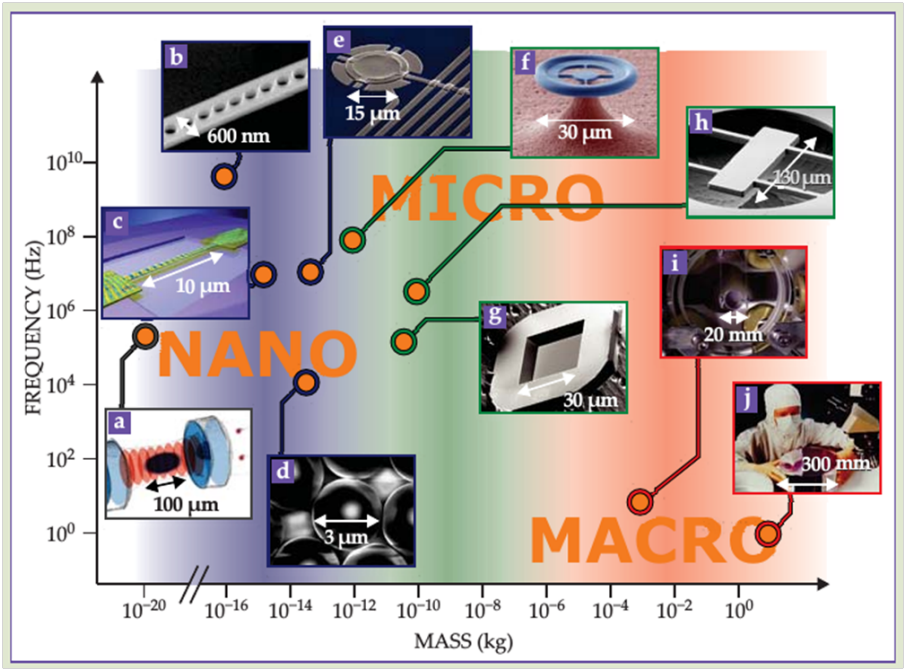

Figure 1.2: *Optomechanical devices's zoo illustrating the variety of optomechanical cavities, arranged according to mass and frequency. They are ranged from nanometer-sized structures (10^{-20} kg), to micromechanical structures (10^{-11} kg) and to macroscopic, centimeter-sized mirrors weighing several kilograms. To get details about each of these optomechanical devices, see Ref. [35].*

Nano-structures exhibits the nonlinearities which are non negligible [62–64]. These nonlinear effects pose a new experimental challenge to surpass the quantum ground state limits. **This new challenge constitutes the focus point that our thesis try to elucidate. Two others research teams [65, 66], have devoted their works in this sense.**

1.3 Basic concepts for optomechanical cooling

As the optical forces exerting on mechanical structure are typically weak, optical cavities are employed to resonantly enhance the intracavity light intensity, so that the optical forces become pronounced. Our investigations in this work, are based on a Fabry-Perot

cavity where one end-mirror is attached to a spring while the other is fixed, as shown in Fig.3.2. The advances in nano-fabrication lead to the simplification of this system where the system end-mirror+spring is replaced by a cantilever elastic beam mirror (see Fig.3.4). These two configurations have the same dynamics but, the former is cumbersome due to its size while the later can be easily integrated in small devices since its size is reduced. Here and below, unless otherwise specified, mechanical cooling refers to the center-of-mass motion.

When the light circulates inside the cavity, it exerts a radiation pressure on the cantilever mirror which begins to vibrate. This mechanism induces a coupling between the photon number of the intracavity field and the mechanical position of the movable mirror which behaves as a harmonic oscillator. When it is coupled to the radiation pressure, its mechanical susceptibility is modified given rise to two important optomechanical effects: the optical spring and the optical damping. During the optomechanical interaction, the vibrations of the movable mirror induce a shift in the effective mechanical resonant frequency, it is the the optical spring. Similarly, these vibrations of the movable mirror change the effective damping of the mechanical oscillator which is known as the optical damping. Both optical spring and optical damping scale linearly with the laser power, and depend on the relative detuning of the laser frequency from the cavity resonance. These two effects can be used to identify the nature of the back-action force which is important in the cooling process in optomechanics. Thus, quantum ground state cooling is deeply influenced by these optical effects [67].

Another important factor which is influenced by the optomechanical coupling is the temperature. When the movable mirror vibrates, its mechanical modes are coupled to the thermal bath temperature T, which fluctuates, leading to a Brownian motion of the mirror [19]. Using the fluctuation-dissipation theorem, one shows that the optomechanical interaction modifies the damping rate, but it does not change the thermal Brownian drive. This means a change in the effective temperature of the mechanical mode [68]. To appreciate this change, one considered a mean energy E_m of a mechanical mode subjected to a Brownian noise from the thermal bath at temperature T. Without optomechanical interaction, the mean energy follows

$$\dot{E} = -\Gamma E_m + \Gamma k_B T, \tag{1.1}$$

where Γ is the intrinsic mechanical damping rate. The steady state solution of this equation is $E_m = k_B T$.

In the optomechanical interaction picture, when the laser or the optical field is intro-

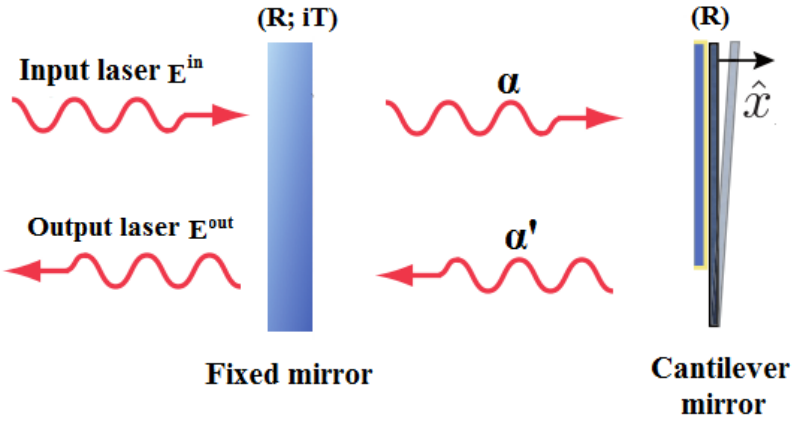

Figure 1.3: *Simplified Fabry-Perot optomechanical cavity. The system right-mirror+spring of the generic setup Fig.3.2 is replaced by a cantilever elastic beam mirror.*

duced, Eq.(1.1) becomes

$$\dot{E} = -\Gamma_{eff} E_m + \Gamma k_B T, \tag{1.2}$$

where the steady state solution yields

$$E_m = k_B T \frac{\Gamma}{\Gamma_{eff}} = k_B T_{eff}. \tag{1.3}$$

Γ_{eff} is the effective damping as it will be shown below and $T_{eff} = T\frac{\Gamma}{\Gamma_{eff}}$ is the effective temperature modified by the optomechanical interaction. Eq.(1.3) shows that an optomechanical interaction can modify the effective temperature of a system putting it either in a cooling ($\Gamma_{eff} > \Gamma$) or in a heating ($\Gamma_{eff} < \Gamma$) regime.

Adopting the corpuscular aspect of light, we can use the photon-phonon interaction picture to give deep explanation of the cooling and heating processes. Let us characterize the photon by the laser frequency ω_0 while the phonon is characterized by the resonant frequency Ω_m of the nanoresonator (cantilever mirror). After the reflection of one photon on the mirror, its frequency changes due to effect similar to an inelastic Raman scattering creating a Stokes and anti-Stokes processes. Stokes process corresponds to the physical process of creating one extra phonon by extracting energy from the optical mode while the Stokes process, one phonon is absorbed and the energy $\hbar\Omega_m$ is transferred from the mechanical mode towards the photon as shown on Fig.3.5a. These processes create two sidebands around the optical frequency ω_0 respectively at $\omega_0 \pm \Omega_m$ as indicated on Fig.3.5b. The cooling and the heating of the mechanical mode correspond respectively to the anti-Stokes and the Stokes process which are equivalent to blue and red detuning. These two processes are equivalent at the optical resonance $\omega_0 = \omega_c$, where ω_c is the cavity frequency. This situation corresponds to the case where there is no energy transfer between

mechanical and optical mode. To enhance one of these two phenomena, an asymmetry between Stokes and anti-Stokes sideband needs to be induced. In the cooling process, the anti-Stokes sideband requires to be put at the cavity resonance ω_c (see Fig.3.5b), while the heating process is enhanced when the Stokes sideband is accorded with the cavity frequency. Practically, quantum ground state cooling is reached in the resolved sideband limit which requires a large mechanical frequency compared to the cavity linewidth ($\Omega_m \gg \kappa$). The theoretical effective minimum phonon number achieved at this limit,

$$n_{eff} = \left(\frac{\kappa}{4\Omega_m}\right)^2, \tag{1.4}$$

is experimentally limited by the radiation pressure shot noise and others sources which always add a small amount of phonon. κ is the cavity decay rate.

In order to enhance ground state cooling, both high light intensity and high mechanical factor $Q_m = \frac{\Omega_m}{\Gamma_m}$ are needed. This means that, an efficient cooling is achieved for both high optical Q-factor $Q \gg 1$ ($Q = \frac{\omega_0}{\kappa}$) and high mechanical Q factor $Q_m \gg 1$.

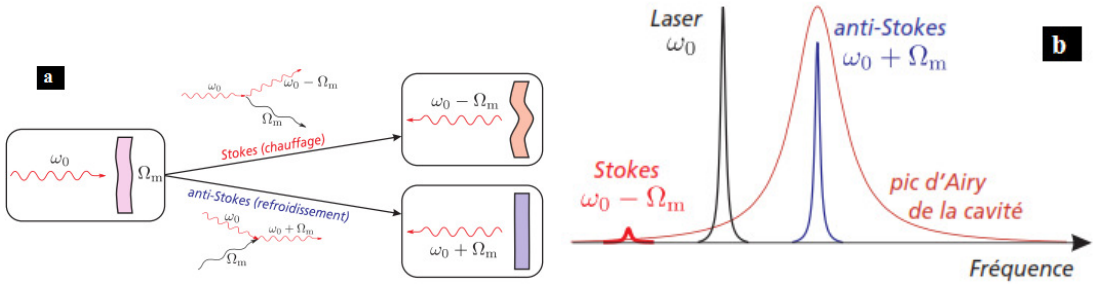

Figure 1.4: *Photon-phonon interaction in optomechanics. Corpuscular consideration of light and mechanical mode can be used to explain cooling and heating which refer respectively to the anti-stokes and Stokes process. (a) Elementary anti-stokes and Stokes process. (b) Cooling process where the anti-stokes process is accorded with the cavity frequency (or where the Stokes process is desaccorded with the cavity frequency).*

1.4 Quantum cooling review

Many theoretical and experimental schemes have been proposed to study the quantum ground state cooling of the mechanical vibrating mode of resonators. These schemes cover both the field of quantum optomechanics and electromechanics. Depending on the kind of the driving source which can be an optical beam or a microwave beam, one distinguishes an optomechanical and electromechanical coupling respectively. According to their high frequency of vibration and their easy integration on chip, the mechanical

resonators using in the superconducting microwave circuits are the most promising to be cooled in its quantum ground state rather than those used in optomechanical systems. In the following, we review some important theoretical and experimental results on the cooling in optomechanical systems.

In [11], the authors developed the cooling scheme based on the dynamical back-action which is introduced by the radiation pressure. They showed that final phonon number below unity can be attained at the resolved sideband. After having established an analogy between their scheme and the sideband cooling, they showed that the final average occupancy can be retrieved directly from the optical output spectrum. The parameters they used are those for a wide range of experimental realizations of cavity self-cooling [8, 10]. Comparative study between the back-action cooling via a detuned cavity and cold-damping via quantum-feedback cooling in optomechanical systems is done in [69], for the full parameters range of a stable cavity. It is found that back-action cooling is more efficient in the resolved sideband cooling ($\Omega_m \gg \kappa$) while the cold-damping is more suitable in regime of unresolved sideband cooling.

Favero and Karrai [12] investigated the cooling by light scattering in a high finesse Fabry-Perot cavity of small mode volume, within which a nanorod which constitutes the nanoresonator acts as a position-dependent perturbation by scattering. In return, the back-action induced by the cavity affects the nanoresonator dynamics and can cool its fluctuations. They predicted the ground-state cooling in optomechanics by using such a scheme, based on light scattering. Schliesser and co-workers combine for the first time in 2009, a cryogenic pre-cooling and resolved-sideband laser cooling to cool experimentally the silica whispering gallery mode (WGM) microcavities having the mechanical frequency range of $62-122\,\mathrm{MHz}$ [13]. Using the input laser power of $0.2\,\mathrm{mW}$ which increases the total damping rate to $\Gamma_{eff} = 370\,\mathrm{kHz}$, the mode temperature is reduced to $T_{eff} = 200 \pm 60\,\mathrm{mK}$ and the final phonon occupancy reaches $n_{eff} = 63 \pm 20$. This was a best performance in the context of experimental cavity optomechanical cooling reported in 2009; since the occupancy of $n_{eff} = 25$ phonons was attained three years before only, in the context of conventional dilution refrigeration of a nanomechanical resonator [14]. During the same year, Groblacher and co-worker [15] demonstrated an ultracooling of a micro-optomechanical oscillator in a cryogenic cavity. They used the optomechanical laser cooling to cool in a cryogenic cavity, a nanoresonator having the fundamental frequency of $\Omega_m = 2\pi \times 945\,\mathrm{kHz}$ with an effective mass of $m = 43 \pm 2\,\mathrm{ng}$. Starting from environment temperature of $5.3\,\mathrm{K}$ which corresponds to 53×10^3 quanta, the final occupancy achieves $n_{eff} = 30$ quanta at the cryogenic temperature of $1.3\,\mathrm{mK}$. According to the large laser cooling rates attained,

the performance of this method is proved to be no longer limited by residual absorption or phase-noise effects. This is why at the end of 2009, Rabl and co-workers investigated the effect of laser phase noise on the ground state cooling in optomechanical systems [20]. They elucidated that phase fluctuations of the driving laser induce modulations of the linearized optomechanical coupling as well as a fluctuating force on the mirror due to variations of the mean cavity intensity. They showed out that laser phase noise induces limitations on cooling in optomechanical systems. Other works confirmed this result some years after, precisely in 2011 [21–23] and 2013 [24].

In Ref. [70], the authors showed how parametric interaction can enhance cooling. They proposed an optical cavity which contains a nonlinear crystal which is pumped by a laser to produce parametric amplification and to change photon statistics in this cavity. They demonstrated how the addition of a parametric amplifier in a cavity can lead to cooling of the micromirror to a temperature which is much lower than what is achieved in an identical experiment without the use of a parametric amplifier. This method cools a micromechanical mirror by radiation pressure from room temperature of 300 K to sub-Kelvin temperatures and it could provide a way to cool the mirror to its quantum ground state or even squeeze it.

Genes and co-workers in [71] used the electromagnetically induced transparency (EIT) to cool towards ground state a mechanical resonator in the unresolved sideband cooling. To do this, they investigated a hybrid optomechanical system composed of a micromechanical oscillator as a movable membrane and an atomic three-level ensemble within an optical cavity. They showed that a suitably tailored cavity field response via electromagnetically induced transparency in the atomic medium allows for strong coupling of the membrane mechanical oscillations to the collective atomic ground-state spin, which facilitates ground-state cooling of the membrane motion, even in the unresolved sideband cooling. In 2009 [72], the same authors showed inhibition of the Stokes-scattering process or enhancement of anti-Stokes scattering, leading to ground-state cooling of micromechanical oscillators, even for short low-finesse optical cavities. They processed by modeling the particles as a two-level ensemble which creates intracavity narrow bandwidth loss or gain and induce tailored asymmetric structuring of the cavity noise spectrum interacting with the oscillator.

In 2012, sequence of fast pulses laser were used to achieve quantum ground state [73]. These pulses add a term to the effective optomechanical interaction Hamiltonian which tunes the cooling operator. This technique is shown to be experimentally feasible in both the good cavity limit ($\Omega_m \gg \kappa$), where it is capable of reaching the ground state much

faster than the oscillator frequency, and the bad cavity limit ($\Omega_m < \kappa$) , where sideband cooling is incapable of approaching the ground state. It was shown that this scheme can be implemented for strongly and weakly coupled optomechanical systems in both weakly and highly dissipative cavities. Parametrically modulated optomechanical systems were proposed in [16] as simple and efficient setting for the quantum ground state cooling. Both sinusoidal modulations of the mechanical frequency and of the input laser intensity are introduced in such system. The relevant result is that, the choice of the relative phase between the two modulations can either enhance or cancel the desired quantum effects, opening new possibilities for optimal quantum control strategies.

In 2013, a cavity mirror was cooled in the presence of an incoherently pumped atomic medium [74]. The authors showed that the strong optomechanical coupling regime can be reached by increasing the incoherent pump strength which increases the cooling rate and enhances the minimum attainable phonon number. Both dispersive and dissipative effects resulting from the modulation of the cavity frequency and the cavity linewidth respectively were investigated on optomechanical cooling in [75]. They showed that in the purely dissipative coupling, cooling is limited while it is enhanced in the purely dispersive coupling. In the combining case of the dispersive and dissipative optomechanical couplings, they showed that the cooling is more efficient. Their work then showed how to beneficially combine dispersive and dissipative optomechanical couplings to boost cooling.

These techniques can also be used for cooling processes in electromechanical systems. Indeed, a single-electron transistors are used to detect the position approaching that set by the Heisenberg uncertainty principle limit in [76,77] while the superconducting circuits capacitively coupled are used to reach small phonon number in [14,27,28]. Particularly, small phonon number of $n_{eff} \approx 0.3$ and $n_{eff} = 0.07$ are respectively reached in electromechanical superconducting microwave circuit in Ref [27] and Ref [28].

1.5 New challenges: Towards the nonlinear quantum optomechanics

So far, scientists considered the linear optomechanical coupling between the oscillator displacement and the optical or microwave field. Until 2008, there were only few studies on nonlinear optomechanical coupling reported in the literature. In 2008, a quadratic optomechanical coupling was proposed by Harris's group at Yale University [78]. In the same way, Painter's group at the California Institute of Technology [26] suggested in 2011 the nonlinear study, as candidate for the improvement of quantum applications in

optomechanics.

Since our thesis begun in 2010, it aimed to explore theoretically these new aspects of the optomechanical coupling, which refer to the field of (nonlinear) quantum optomechanics. In order to bring out the problematic of our thesis, let us briefly describe at first the works done in [26, 78].

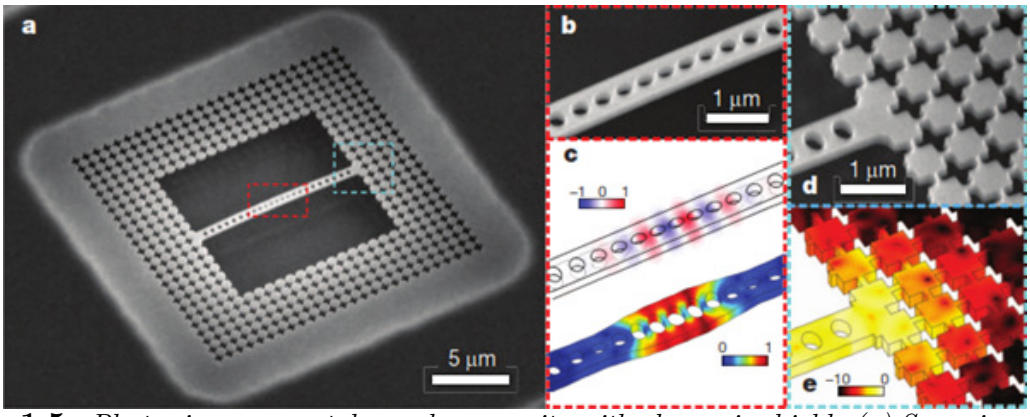

Figure 1.5: *Photonic nanocrystal nanobeam cavity with phononic shield. (a) Scanning electron microscope (SEM) image of the patterned silicon nanobeam and the external phononic bandgap shield. (b) Enlarged image of the central region of the nanobeam. (c) Simulation of the optical and mechanical modes. (d) Enlarged image of the nanobeam-shield interface. (e) Simulation of the localized acoustic resonance at the nanobeam-shield interface [26].*

In the Painter's group, a nanomechanical oscillator was successfully cooled into its quantum ground state by using the resolved sideband laser cooling technique. The mechanical frequency of the oscillator used in this experiment is $\Omega_m = 2\pi \times 3.68$ GHz. Both mechanical factor ($Q_m \approx 1.05 \times 10^5$) and optical factor ($Q \approx 4 \times 10^5$) used are enough for a good cooling expectation towards quantum ground state, at the resolved sideband limit. They used an optomechanical structure with co-located photonic and phononic band gaps in a suspended on-chip waveguide. Their optomechanical resonator is represented on Fig.3.6. The structure was pre-cooled to $20K$, corresponding to about 100 thermal quanta, and then cooled via radiation pressure to $n_{eff} = 0.85 \pm 0.08$. Considering the laser cooling technique, this phonon occupancy is the lowest to date reported, apart those reported in [27, 28] where the final occupancies less than unity ($n_{eff} < 1$) have been achieved by using the superconducting microwave cavities. **In order to improve their result, the authors of [26] suggested that many new opportunities would be available if the regime of strong coupling at the single-quantum level could be reached, not least the study of nonlinear phononics at the single-phonon level and the generation of highly non-classical quantum states in mechanical or optical systems. This means that nonlinearities limit quantum ground state**

achievement at the single-phonon level by adding some amount of phonon. Thus, we take into account the nonlinear properties which appear in nano-systems in order to improve quantum ground state cooling, given rise to possible enhancement of quantum applications in optomechanics.

In the Harris's group, a so-called membrane-in-the-middle optomechanical cavity was designed for the first time in 2008. Such geometry is most interesting since it exhibits a quadratic coupling in the displacement. As implied by its name, this geometry involves an oscillating mechanical membrane placed inside a Fabry-Perot cavity fixed end-mirrors (see Fig.3.7). An attractive feature of membrane-in-the-middle configurations is the ability to realize easily either linear or quadratic optomechanical couplings, depending on the precise equilibrium position of the membrane (see section **??**). Quadratic coupling opens the way to numerous interesting possibilities in optomechanics, including the direct measurement of energy eigenstates of the mechanical element, rather than the position detection characteristics of linear coupling. As estimated by Harris and coworkers, such coupling may be used in the future to observe particular behaviors as quantum jumps of a mechanical system [79], quantum tunneling of an optomechanical system and can allow the study of the quantum Zeno effect in a mechanical context [80]. This coupling provides also a comparatively simple scheme for the preparation and characterization of non-classical mechanical states of interest for quantum metrology and sensing [80]. Particularly, the quadratic coupling has appeared as key element to enhance optomechanical cooling and squeezing even for high temperatures and weak coupling [16].

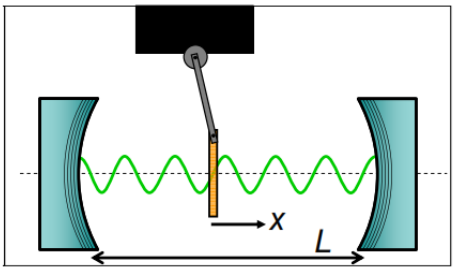

Figure 1.6: *Conceptual illustration of the quadratic or dispersive optomechanical coupling. The cavity is defined by rigid mirrors. The only mechanical degree of freedom is that of a thin dielectric membrane (orange) in the cavity mode (green) [78].*

So, in this work, we focus on the improvement of the quantum ground state cooling at the single-phonon level, through nonlinearities.

Therefore, we proceed to the study of nonlinear phononics at the single-phonon level by taking into account a geometrical nonlinearity, which occurs for large displacements of the mechanical resonator. Such nonlinearity is used

to correct the dynamics of the system and merges in the nanoscale systems [62–64]. This allows to,

- **Predict the dynamical behaviors such as quantum jump and chaos phenomena in optomechanical systems. The effects of geometrical nonlinearity as well as the quantum operator's fluctuations on optical bistability are also studied;**
- **Investigate the effects of geometrical nonlinearity on quantum ground state cooling at the single-phonon level;**
- **Study the effect of optical and geometrical nonlinearities on the squeezed states generation;**
- **Generate highly Continuous Variables entanglement via geometrical nonlinearity.**

1.6 Conclusion

The purpose of this chapter was to give an overview of various efforts done to reach quantum ground state, through otpomechanics. The phonon occupancies less than unity are achieved in [26–28]. However, nonlinear effects which are non-negligible at the nanoscale, constitute new challenge which limits quantum ground state cooling.

Hereafter, we will highlight important points of these nonlinear effects on optomechanics, in order to surpass this limitation. To this end, we organize the rest of our thesis as follows. Chapter two describes the analytical and numerical tools that have been used. Chapter three explains and models the anharmonic terms of our optomechanical system. The corresponding results will be also reported and discussed. Finally, we summarize and will bring out future directions of the nonlinear quantum optomechanics.

Chapter 2

Methods and Materials

2.1 Introduction

This Chapter is devoted to the establishment of the optomechanical rate equations. Both classical and semiclassical approaches are used. Analytical and Numerical methods as well as the computational techniques used are briefly reviewed. The organization of this chapter is as follows. The second section establishes the optomechanical rate equations both in classical and semiclassical limits. Analytical methods used are described in section three while numerical methods are presented in section fourth. We then end by a conclusion in section five.

2.2 Modelling of optomechanical oscillators

We use both the energy conservation method [19] and the theory of elastic thin beam equations [62,63] through optomechanical cavity to derive the rate equations in the classical limit. In the semiclassical limit, these equations come from the derivation of the system Hamiltonian [81].

2.2.1 Classical limit

Optical part

Equations of the optical part are obtained by using the energy conservation method. Let us consider the system represented on Fig.3.4, where $E^{in}(t)$, $E^{out}(t)$, α and α' denote respectively the amplitude of the input field, the amplitude of the output field, the intracavity transmitted field and the intracavity reflected field. R and T denote respectively the reflection and transmission coefficients. They are given by:

$$R = 1-\gamma \text{ and } T = \sqrt{1-R^2} \approx \sqrt{2\gamma},\ \gamma \ll 1. \tag{2.1}$$

Considering the optical energy conservation through each element of the cavity, one has the following conservation relations,

$$\alpha(t) = iTE^{in}(t) + R\alpha'(t), \tag{2.2}$$

$$E^{out}(t) = iT\alpha'(t) - RE^{int}(t), \tag{2.3}$$

$$\alpha'(t) = \alpha(t-\tau)e^{i\Psi(t)}, \tag{2.4}$$

where $\tau = \frac{2d_0}{c}$ is seen either as the round trip time of the light in the cavity or as the time

delay of α' with respect to α. d_0 and c are the cavity length and the celerity respectively. $\Psi(t) = 2kd(x(t)) + \sigma$ is the phase shift between α' and α. k is the wavenumber and $\sigma = i\frac{\varepsilon_0 d_0}{2}$ characterizes the linear attenuation in the resonator where ε_0 (in m^{-1}) is a coefficient caused by scattering, absorption and radiation. i is the complex number defined by $i^2 - 1$.

The phase shift can be written as the superposition of a linear part and nonlinear part as [82]

$$\Psi(t) = \Psi_L + \Psi_{NL} = \Psi_0 + \sigma + \Psi_{NL} = 2kd_0 + \sigma + 2kf(x), \tag{2.5}$$

where $f(x)$ is a function characterizing the optical nonlinearity induced by the radiation pressure exerted on the cantilever nanobeam. After some arrangements, $\Psi(t)$ takes the form,

$$\Psi(t) = \sigma + 2k\left(d_0 + x + \frac{x^2}{2d_0} + \cdots\right). \tag{2.6}$$

Close to resonance, both phase shift and round trip are small, so that [19]

$$e^{i\Psi(t)} \approx 1 + i\Psi(t) + \cdots, \tag{2.7}$$

$$\alpha(t-\tau) \approx \alpha(t) - \tau\frac{d\alpha(t)}{dt}. \tag{2.8}$$

By inserting Eqs.(2.6) - (2.7) in Eq.(2.1), one finds that α satisfies the following differential equation,

$$\dot{\alpha} = \left[-\frac{\gamma}{\tau} + i\frac{\sigma}{\tau} + i\left(\frac{2\pi c}{\lambda n_0} - \frac{2\pi c\gamma}{\lambda n_0}\right) + i\left(\frac{4\pi}{\lambda\tau}(1-\gamma)x\right)\right]\alpha(t) + i\frac{\sqrt{2\gamma}}{\tau}E^{in}(t), \tag{2.9}$$

where the second order nonlinear term ($\propto x^2$) in Eq.(2.6) is neglected, since it is to small as we will show later. n_0, λ and c are respectively the refraction index of the intracavity medium, the wavelength of the laser and the celerity. Equation(2.9) can be rewritten as,

$$\dot{\alpha} = \left[i\left(\Delta_0 + \frac{g_M}{x_{ZPF}}x\right) - \frac{\kappa}{2}\right]\alpha(t) + i\sqrt{\kappa}E^{in}(t), \tag{2.10}$$

where $\Delta_0 = \frac{2\pi c}{\lambda n} - \frac{2\pi c\gamma}{\lambda n} = \omega_0 - \omega_{cav}$, $g_M = \frac{\omega_{cav}x_{ZPF}}{d_0}$, $x_{ZPF} = \sqrt{\frac{\hbar}{2M\Omega_m}}$, $\omega_{cav} = \frac{4\pi}{\lambda\tau}(1-\gamma)$, $\frac{\kappa}{2} = i\frac{\sigma}{\tau} - \frac{\gamma}{\tau} = -\left(\frac{1}{2\tau_0} + \frac{1}{2\tau_{ex}}\right) = -\frac{1}{2\theta}$, $\sqrt{\kappa} = \frac{\sqrt{2\gamma}}{\tau} = \sqrt{\frac{1}{\tau_{ex}}}$. ω_0 is the laser frequency and ω_{cav} is the cavity resonance frequency. The other parameters κ, Δ_0 and g_M are respectively, the cavity decay rate, the laser detuning and the cantilever-cavity coupling.

Mechanical part

The dynamics of the cantilever nanobeams is derived according to Euler-Bernoulli theory, which reads the following nonlinear space-time equation [62–64],

$$EI\frac{\partial^2}{\partial r^2}\left[\frac{\partial^2 y(r,t)}{\partial r^2}\left(1+\left(\frac{\partial y(r,t)}{\partial r}\right)^2\right)^{-\frac{3}{2}}\right]+\rho s\frac{\partial^2 y(r,t)}{\partial t^2}+\mu\frac{\partial y(r,t)}{\partial t}=f_{rad}(r,t), \tag{2.11}$$

where E, I, ρ and s are respectively, the Young modulus, moment of inertia, density and the section of the cantilever nanobeam which has the length ℓ. $f_{rad}(r,t)$ is the radiation pressure force which is exerted on an infinitesimal length element of the cantilever beam. The term $\left(\frac{\partial y(r,t)}{\partial r}\right)^2$ is the geometrical nonlinear term which is neglected here.

Using the Galerkin method, which allows us to separate the spatial and temporal solutions and using the boundary conditions of cantilever beams known in the literature [62–64], the modal solution of equation (2.11), by excluding the damping term and the pressure force is,

$$\begin{aligned} y(r,t) &= u_n(r)x_n(t) \\ &= \left\{-\frac{\sin k_n\ell+\sinh k_n\ell}{\cos k_n\ell+\cosh k_n\ell}(\cos k_n r-\cosh k_n r)+(\sin k_n r+\sinh k_n r)\right\}x_n(t), \end{aligned} \tag{2.12}$$

where $x_n(t)$ is the time dependent component.

According to the form of equations of motion of the nanobeam, the radiation pressure force can be written as

$$f_{rad}(r,t)=u_n(r)f_{rad}(t)=2\hbar kI(t)\frac{c}{2d_0}u_n(r)=\frac{\hbar g_M}{x_{ZPF}}|\alpha(t)|^2u_n(r). \tag{2.13}$$

Note that, for convenience, we have switched to normalization of $|\alpha(t)|^2$ to photon number, and will pursue this consistently sometimes in the following. Equivalently, $|E^{in}(t)|^2$ denotes the photon flux impinging on the coupling region.

By inserting equations (2.12) and (2.13) in equation (2.11) and integrating the resulting equation over the entire length of the nanobeam, considering a single mode dynamics, it comes

$$\ddot{x}+\Gamma_m\dot{x}+\Omega_m^2x=\frac{\hbar g_M}{Mx_{ZPF}}|\alpha(t)|^2, \tag{2.14}$$

where $M=\rho s$, $\Omega_m=\sqrt{\frac{EI}{\rho s}}k_1^2$, $\Gamma_m=\frac{\mu}{\rho s}=\frac{\Omega_m}{Q}$ and $k_1=\frac{1.875}{\ell}$. Ω_m and Γ_m are respectively

the frequency of the cantilever beam and damping rate of the cantilever beam motion.

Finally, the rate equations describing the linear optomechanical coupling device in the classical approach is [83]:

$$\dot{\alpha} = \left[i\left(0\Delta + \frac{g_M}{x_{ZPF}}x\right) - \frac{\kappa}{2}\right]\alpha(t) + i\sqrt{\kappa}E^{in}(t), \tag{2.15}$$

$$\ddot{x} + \Gamma_m \dot{x} + \Omega_m^2 x = \frac{\hbar g_M}{M x_{ZPF}}|\alpha(t)|^2. \tag{2.16}$$

2.2.2 Semiclassical limit

Rate equations are derived from the semiclassical Hamiltonian, which describes the coupling between the optical and mechanical degrees of freedom. The formulation of this Hamiltonian is given by Law in [81],

$$\hat{H} = \frac{(p+\Gamma_m)^2}{2m} + V(q) + \hbar\sum_k \omega_k(q)\hat{\alpha}_k^\dagger\hat{\alpha}_k - \frac{\hbar c\pi}{24q}. \tag{2.17}$$

In this Hamiltonian, k is the longitudinal mode number and $\omega_k(q) = \frac{k\pi c}{q}$, $\hat{\alpha}_k$ and $\hat{\alpha}_k^\dagger$ are respectively the corresponding frequency, annihilation and creation operators; Γ_m corresponds to an effective momentum in the optomechanical interaction, arising from the mixing of different spatial modes. $V(q)$ is the mechanical potential and the last term Casimir term for one-dimensional space.

By considering only a single optical mode and assuming all others are unpopulated, Γ_m must be zero since it gives rise only to terms that mix the different modes [81]. Such result suppose that we have treated the optical field in an adiabatic limit; if the mechanical motion is not slow compared to the round trip time of a photon in the cavity, it will cause coupling between the different modes, even if only one is initially occupied. Then Eq.(2.17) takes the form,

$$\hat{H} = \frac{p^2}{2m} + V(\hat{q}) + \hbar\omega_{cav}(q)\hat{\alpha}^\dagger\hat{\alpha} - \frac{\hbar c\pi}{24q}, \tag{2.18}$$

where ω_{cav} is the frequency of the single populated intracavity optical mode. Equation Eq.(2.18) can be further simplified by ignoring the Casimir term, which is negligibly weak for most optomechanical systems, and by assuming that the mechanical potential is harmonic about some equilibrium position d_0, we find

$$V(q) = \frac{1}{2}m\Omega_m^2 x^2, \tag{2.19}$$

where $x = q - d_0$ is the displacement from equilibrium. Considering only small motion of the resonator around this equilibrium position ($x \ll d_0$), we can tailored ω_{cav} around this equilibrium point and Eq.(2.18) then yields

$$\hat{H} = \frac{p^2}{2m} + \frac{1}{2}M\Omega_m^2 x^2 + \hbar \left[\omega_{cav}(d_0) + x \left. \frac{d\omega_{cav}(q)}{dq} \right|_{q=d_0} + \cdots \right] \hat{\alpha}^\dagger \hat{\alpha}. \tag{2.20}$$

Both mechanical position and momentum can be written with respect to their quantum counter-parts as,

$$x = x_{ZPF}\hat{x}_m, p = \frac{\hbar}{2x_{ZPF}}\hat{p}_m, \ [\hat{x}_m, \hat{p}_m] = 2i. \tag{2.21}$$

This allows to write the mechanical energy as

$$\frac{p^2}{2m} + \frac{1}{2}m\Omega_m^2 x^2 = \frac{\hbar\Omega_m}{4}(\hat{p}_m^2 + \hat{x}_m^2). \tag{2.22}$$

By taking into account the optical energy and after the rotating wave approximation, the Hamiltonian takes its final form,

$$\hat{H} = -\hbar(\Delta_0 + g_M\hat{x}_m)\hat{\alpha}^\dagger\hat{\alpha} + \frac{\hbar\Omega_m}{4}(\hat{p}_m^2 + \hat{x}_m^2) + \hbar\sqrt{\kappa}E^{in}(\hat{\alpha}^\dagger + \hat{\alpha}) + \hat{H}_\kappa + \hat{H}_\Gamma, \tag{2.23}$$

where $\hat{H}_\kappa$ and $\hat{H}_\Gamma$ are the Hamiltonian terms which capture respectively the decay of a photon and the mechanical damping of the cantilever mirror beam. The optomechanical coupling term is $g_M = gx_{ZPF} = -x_{ZPF} \left. \frac{d\omega_{cav}(q)}{dq} \right|_{q=d_0}$, with $g = -\left. \frac{d\omega_{cav}(q)}{dq} \right|_{q=d_0} = \frac{\omega_{cav}}{d_0}$ for the Fabry-Perot cavities.

It should be noted that the quantum Hamiltonian can be deduced from Eq.(2.23) by setting $\hat{x}_m$ and $\hat{p}_m$ as,

$$\hat{x}_m = \hat{b}^\dagger + \hat{b} \text{ and } \hat{p}_m = i(\hat{b}^\dagger - \hat{b}), \tag{2.24}$$

where $\hat{b}$ and $\hat{b}^\dagger$ are the annihilation and creation operators of the mechanical mode.

2.3 Analytical methods

This section describes the analytical methods that have been used in this work.

2.3.1 Langevin derivation method

The Langevin equations of the system are the stochastic differential equations, describing the time evolution of a subset of degrees of freedom, where the mean value of the system

slowly varies and is treated dynamically, while the small fluctuations around the mean value are treated probabilistically. Initially, Paul Langevin considered the Brownian motion of particles [84] and assumed that such particles are subject to a systematic force, i.e., a viscous drag, and a rapidly fluctuating force, which comes from surrounding particles randomly impacting on the system under investigation with a mean amplitude of zero, i.e. the net force is zero on average. He treated this rapid force statistically, assuming that it was independent from the viscous drag and arrived to an expression for the mean motion of the particle. Indeed, for a given operator O, its Langevin equation is

$$\frac{\partial O}{\partial t} = \frac{i}{\hbar}\left[\hat{H}, O\right] + N, \tag{2.25}$$

where N is the corresponding noise operator of O. Using this Langevin relation and taking into account some commutators relation, one obtains the following quantum Langevin equations (QLEs) of optomechanical systems,

$$\dot{x}_m = \Omega_m p_m, \tag{2.26}$$

$$\dot{p}_m = -\Omega_m x_m - \Gamma_m p_m + 2g_M \alpha^\dagger \alpha + F_{th}, \tag{2.27}$$

$$\dot{\alpha} = \left[i\left(\Delta_0 + g_M x_m\right) - \frac{\kappa}{2}\right]\alpha - i\sqrt{\kappa}E^{in} + \sqrt{\kappa}\alpha^{in}, \tag{2.28}$$

where F_{th} and α^{in} are the Brownian stochastic force and the optical vacuum input noise, both with zero mean amplitude.

2.3.2 Stability analysis

To analyze the stability of our system, we have used some specific approaches.

Steady states and dynamics fluctuations

The steady state values are obtained by setting the time derivatives in the Langevin equations to zero. Applying to the system Eqs.(2.26)-(2.28), one gets the following steady state values,

$$x_s = 2\frac{g_M}{\Omega_m}|\bar{\alpha}|^2, \;\; |\alpha_s|^2 = \frac{2\kappa P_{in}}{\hbar\omega_0\left(\Delta^2 + \frac{\kappa^2}{4}\right)}, \tag{2.29}$$

where $\Delta = \Delta_0 + g_M x_m$ is the effective detuning.

By assuming a strong intracavity amplitude field, i.e., $|\alpha_s| \gg 1$, needed for a strong coupling, one can write a steady state amplitude for each operator with small zero-mean

fluctuations. For the generic operator O, one has

$$O = O_s + \delta O, \tag{2.30}$$

where O_s is its mean value and δO its corresponding the fluctuation operator. The Langevin equations can then be linearized by replacing each operator by its corresponding form given by Eq.(2.30) as,

$$\delta\dot{x}_m = \Omega_m \delta p_m, \tag{2.31}$$

$$\delta\dot{p}_m = -\Omega_m \delta x_m - \Gamma\delta p_m + G\delta I + \delta F_{th}, \tag{2.32}$$

$$\delta\dot{I} = -\frac{\kappa}{2}\delta I - \Delta\delta\varphi + \sqrt{\kappa} I^{in}, \tag{2.33}$$

$$\delta\dot{\varphi} = -\frac{\kappa}{2}\delta\varphi + \Delta\delta I + G\delta x_m + \sqrt{\kappa}\varphi^{in}, \tag{2.34}$$

where the higher order of fluctuations are safely neglected. The linearized QLEs show that the mechanical mode is coupled to the cavity mode quadrature fluctuations by the effective optomechanical coupling $G = g_M|\alpha_s|$. An appropriate method can be now used to analyze the stability of our system.

Routh-Hurwitz criterion

The solution of a stochastic Ordinary Differential Equations (ODEs) given by its general form (see subsection 3.4.1),

$$\dot{u}(t) = Au(t) + n(t), \tag{2.35}$$

is,

$$u(t) = M(t)u(0) + \int_0^t ds M(s)n(s), \tag{2.36}$$

where $M(t) = e^{At}$. This system is stable and reaches its steady state as $t \longrightarrow \infty$ only if the real parts of all the eigenvalues of the matrix A are negative so that $M(\infty) = 0$ [85]. One can then use the Jacobian matrix method or the Routh-Hurwitz criterion to analyze the stability of such a system. As we have used the Routh-Hurwitz criterion here, we briefly describe it.

Let us consider a linearized stochastic ODEs given by its compact form of Eq.(2.35). The stability of this system depends on the nature of the solutions of its characteristic equation defined by,

$$\det(A - \lambda\mathbb{I}) = 0 \Leftrightarrow \lambda^n + a_1\lambda^{n-1} + a_2\lambda^{n-2} + \cdots + a_{n-1}\lambda + a_n = 0, \tag{2.37}$$

where $\mathbb{I}$ is a $n \times n$ identity matrix, $a_{i=1,n} \in \mathbb{R}$ are the coefficients and $\lambda \in \mathbb{C}$ are the eigenvalues of the matrix A and the roots of the characteristic equation. The Routh-Hurwitz determinants are defined as,

$$H_1 = \left|a_1\right|, H_2 = \begin{vmatrix} a_1 & 1 \\ a_3 & a_2 \end{vmatrix}, H_3 = \begin{vmatrix} a_1 & 1 & 0 \\ a_3 & a_2 & a_1 \\ a_5 & a_4 & a_3 \end{vmatrix}, \tag{2.38}$$

$$\vdots$$

$$H_j = \begin{vmatrix} a_1 & 1 & 0 & \cdots & 0 \\ a_3 & a_2 & a_1 & \cdots & 0 \\ a_5 & a_4 & a_3 & \cdots & 0 \\ \vdots & \vdots & \vdots & \vdots & \\ a_{2j-1} & a_{2j-2} & a_{2j-3} & \cdots & a_j \end{vmatrix}, \tag{2.39}$$

$$\vdots$$

$$H_n = \begin{vmatrix} a_1 & 1 & 0 & \cdots & 0 \\ a_3 & a_2 & a_1 & \cdots & 0 \\ \vdots & \vdots & \vdots & \vdots & \\ 0 & 0 & 0 & \cdots & a_n \end{vmatrix}. \tag{2.40}$$

Proposition 2.1. *For a $n \times n$ matrix, the h_{jk} elements $(j,k = 1,\cdots,n)$ of the Routh-Hurwitz determinants are defined as,*

- $h_{jk} = a_{2j-k}$ *for* $0 < 2j-k \leq n$;
- $h_{jk} = 1$ *for* $2j = k \Leftrightarrow 2j-k = 0$;
- $h_{jk} = 0$ *for* $2j < k \Leftrightarrow 2j-k < 0$ *or* $2j > n+k \Leftrightarrow 2j-k > n$.

Proposition 2.2. *The system is stable if only if* $\forall_i\ \Re(\lambda) < 0 \Leftrightarrow \forall_i\ H_i > 0$.

As a simplified Routh-Hurwitz criterion in $\mathbb{R}^4$, the characteristic equation is,

$$\lambda^4 + a_1\lambda^3 + a_2\lambda^2 + a_3\lambda + a_4 = 0. \tag{2.41}$$

The corresponding determinants are,

$$H_1 = \left|a_1\right| = a_1, H_2 = \begin{vmatrix} a_1 & 1 \\ a_3 & a_2 \end{vmatrix} = a_1a_2 - a_3, \tag{2.42}$$

$$H_3 = \begin{vmatrix} a_1 & 1 & 0 \\ a_3 & a_2 & a_1 \\ 0 & a_4 & a_3 \end{vmatrix} = a_1 \begin{vmatrix} a_2 & a_1 \\ a_4 & a_3 \end{vmatrix} - a_3 \begin{vmatrix} 1 & 0 \\ a_4 & a_3 \end{vmatrix} = a_1 a_2 a_3 - a_1^2 a_4 - a_3^2, \tag{2.43}$$

$$H_4 = \begin{vmatrix} a_1 & 1 & 0 & 0 \\ a_3 & a_2 & a_1 & 0 \\ 0 & a_4 & a_3 & a_2 \\ 0 & 0 & 0 & a_4 \end{vmatrix} = a_4 H_3. \tag{2.44}$$

One then finds that the Routh-Hurwitz criterion for the stability in $\mathbb{R}^4$ is satisfied for the following conditions,

$$\begin{cases} a_1 > 0, \\ a_1 a_2 > a_3, \\ a_1 a_2 a_3 - a_1^2 a_4 - a_3^2 > 0, \\ a_4 > 0. \end{cases} \tag{2.45}$$

Cardano's Method

Generally in the nonlinear approach, the steady state equations or the equilibrium equations lead to the m-order polynomial equation ($m > 2$) which needs specific method to be solved. Particularly for $m = 3$, the roots of the namely third-order polynomial equation are obtained by using the method known as Cardano's Method. The roots of this equation, in the steady state equations case, are helpful to analyze the stability of the system.

Let us consider the following third-order polynomial equation,

$$ax^3 + bx^2 + cx + d = 0. \tag{2.46}$$

To solve it, we have first to set,

$$x = z - \frac{b}{3a}, \tag{2.47}$$

which allows us to transform Eq.(2.46) on the form,

$$z^3 + pz + q = 0, \tag{2.48}$$

with $p = \frac{-b^2}{3a^2} + \frac{c}{a}$ and $q = \frac{b}{27a}\left(\frac{2b^2}{a^2} - \frac{9c}{a}\right) + \frac{d}{a}$.

The roots of Eq.(2.48) depend on the sign of the discriminant $\Delta = q^2 + \frac{4}{27}p^3$ as follows:

- For $\Delta > 0$, it has one real root z_0 and two complex roots z_1, z_2 as,

$$\begin{cases} z_0 = u + v, \\ z_1 = ju + \bar{j}v, \\ z_2 = j^2u + \bar{j}^2v, \end{cases} \tag{2.49}$$

where $j = -\frac{1}{2} + i\frac{\sqrt{3}}{2} = e^{i\left(\frac{2\pi}{3}\right)}$ with $\bar{j}$ its conjugate, $u = \sqrt[3]{\frac{-q+\sqrt{\Delta}}{2}}$ and $v = \sqrt[3]{\frac{-q-\sqrt{\Delta}}{2}}$.

- For $\Delta = 0$, it has one real root z_0 and one double real root $z_1 = z_2$ as,

$$\begin{cases} z_0 = 2\sqrt[3]{\frac{-q}{2}} = -2\sqrt{\frac{-p}{3}} = \frac{3q}{p}, \\ z_1 = z_2 = -\sqrt[3]{\frac{-q}{2}} = \sqrt{\frac{-p}{3}} = \frac{-3q}{2p}. \end{cases} \tag{2.50}$$

- For $\Delta < 0$, it has three distinct real roots z_0, z_1 and z_2 defined as,

$$z_k = 2\sqrt{\frac{-p}{3}}\cos\left(\frac{1}{3}\arccos\left(\frac{-q}{2}\sqrt{\frac{27}{-p^3}} + \frac{2k\pi}{3}\right)\right), k \in \{1,2,3\}. \tag{2.51}$$

2.3.3 Quantum Fourier Transform and fluctuation spectrum

Quantum Fourier Transform (QFT) is used to solve analytically the ODEs by transforming them into the frequency domain. For a given operator $O(t)$, depending on the time, its expression in the Fourier domain is,

$$O(\Omega) = \int_{-\infty}^{+\infty} dt\, e^{i\Omega t} O(t), \tag{2.52}$$

$$O^\dagger(\Omega) = \int_{-\infty}^{+\infty} dt\, e^{-i\Omega t} O^\dagger(t) = (O(-\Omega))^\dagger. \tag{2.53}$$

From these relations, the QFT of the time derivative and of the fluctuation of operators can be deduced.

By replacing each operator in a ODEs system with its corresponding QFT, one obtains a simple algebra system of the dynamics fluctuations which be easily solved. From this dynamics system of the fluctuations, all informations induce by small change in the system can be extracted, revealing so the quantum aspects of the system.

The quantum effects of the system are contained in the spectrum fluctuations of each operators in system and in their variance, which allow both to quantify the minimum phonon occupancy, the squeezing and the entangling in the system. The spectrum fluc-

tuation $S_O(\Omega)$ of an operator O is defined by

$$2\pi\delta(\Omega+\Omega')S_O(\Omega) = \langle\delta O(\Omega)\delta O^\dagger(\Omega')\rangle. \tag{2.54}$$

The symmetrized spectrum $\bar{S}_O(\Omega)$ of the operator O is defined by,

$$\bar{S}_O(\Omega) = \frac{1}{2}(S_O(+\Omega) + S_O(-\Omega)), \tag{2.55}$$

which allows us to defined its variance as,

$$\langle\delta O^2(\Omega)\rangle = \int_{-\infty}^{+\infty} \frac{d\Omega}{2\pi}\bar{S}_O(\Omega). \tag{2.56}$$

Characterization of Squeezing

For two given quadrature operators ΔX and ΔY, squeezing is used to reduce their quantum noise. As coherent states, squeezed states minimize the Heisenberg relation as follows,

$$\Delta X\Delta Y \geq |\frac{1}{2}[X,Y]|. \tag{2.57}$$

For the coherent states, there is a symmetry between the two quadratures (see Fig.3.13a below):

$$\Delta X = \Delta Y = \sqrt{|\frac{1}{2}[X,Y]|}, \tag{2.58}$$

which then minimizes the Heisenberg relation as

$$\Delta X\Delta Y = |\frac{1}{2}[X,Y]|. \tag{2.59}$$

For the squeezed states, this symmetry disappears as shown on Fig.3.13b. One remarks that this asymmetry reduces quantum fluctuations along the quadrature ΔX,

$$\Delta X < \sqrt{|\frac{1}{2}[X,Y]|}, \tag{2.60}$$

and adds them along the quadrature ΔY,

$$\Delta Y > \sqrt{|\frac{1}{2}[X,Y]|}. \tag{2.61}$$

Despite this asymmetry, squeezed states also verify the standard quantum limit (SQL),

$\Delta X \Delta Y = |\frac{1}{2}[X,Y]|$. The quadrature ΔX is said to be squeezed while the ΔY one is said to be unsqueezed.

Minimum phonon occupancy

Quantum cooling is characterized by the final phonon occupancy in a system. When this occupancy decreases, the cooling process increases on the mechanical mode of the system. The effective phonon number n_{eff} is extracted from the mean mechanical energy of the system defined by,

$$\langle E_m \rangle = \frac{\hbar\Omega_m}{4}(\langle \delta x_m^2 \rangle + \langle \delta p_m^2 \rangle) = \hbar\Omega_m(n_{eff} + \frac{1}{2}), \tag{2.62}$$

where $\langle \delta x_m^2 \rangle$ and $\langle \delta p_m^2 \rangle$ are the position and momentum variances of the mechanical resonator which satisfy the commutation relation $[x_m, p_m] = 2i$. Analytical expression of n_{eff} is found by integrating the variances $\langle \delta x_m^2 \rangle$ and $\langle \delta p_m^2 \rangle$ using Eq.(2.56). This can be accomplished in a straightforward manner using the residue theorem.

Residue theorem

This theorem is used to evaluate the integrals in the complex domain. Let consider a complex function $f(z) = \frac{g(z)}{h(z)}$ which has n $(n \in \mathbb{N}^*)$ singularities at certain points z_j, $j = 1, \cdots, n$. Applying residue theorem to f leads to

$$\int_{-\infty}^{+\infty} dz f(z) = \int_{-\infty}^{+\infty} dz \frac{g(z)}{h(z)} = 2i\pi \sum_{j=1}^{n} Res(f, z_j), \tag{2.63}$$

where $Res(f, z_j)$ is the residue of the function f at the singular point z_j. There are different ways to evaluate the residue of a function f $(Res(f, z_j))$ depending on the type of its singularities:

- $Res(f, z_j) = \frac{1}{(m-1)!} \lim_{z \longrightarrow z_j} \left[\frac{d^{m-1}}{dz^{m-1}} (z - z_j)^m f(z) \right]$, if z_j is a $m-$order singular point of the function f;
- $Res(f, z_j) = \frac{g(z_j)}{h'(z_j)}$, if z_j is a simple singular point of the function f which can be written on the form $\frac{g(z)}{h(z)}$.

2.3.4 Logarithmic negativity $E_{\mathcal{N}}$

Logarithmic negativity is used to quantify the level of the quantum entanglement in a system. When it is positive, the system is said to be entangled and when it is negative, the system is not entangled. For high values of $E_{\mathcal{N}}$, the entanglement is said to be robust. Entanglement characterized the intrication between different parts of a system, similarly to the EPR effect. Such quantum effects are then used to share information in the quantum networks as dense coding, quantum teleportation and quantum cryptography.

Let us consider a bipartite system describes by the compact form given by Eq.(2.36). Assuming that the quantum noises are zero-mean quantum Gaussian noises and that the dynamics is linearized, the quantum steady state for the fluctuations is a zero-mean bipartite Gaussian state, fully characterized by its 4×4 correlation matrix which has the components $V_{ij}=\frac{1}{2}\langle u_i(\infty)u_j(\infty)+u_j(\infty)u_i(\infty)\rangle$. When the system is stable, one obtains

$$V_{ij}=\sum_{kl}\int_0^\infty ds\int_0^\infty ds' M_{ik}(s)M_{jl}(s')\Phi_{kl}(s-s'), \tag{2.64}$$

where $\Phi_{kl}(s-s')=\frac{1}{2}\langle n_k(s)n_\ell(s')+n_\ell(s')n_k(s)\rangle$ is the matrix of stationary noise correlation functions. Using the fact that the three components of $n(t)$ are uncorrelated, we find $\Phi_{kl}(s-s')=D_{kl}\delta(s-s')$, where $D=Diag[0,\Gamma_m(2n_{th}+1),\kappa,\kappa]$ is a diagonal matrix and Eq.(2.64) becomes $V=\int_0^\infty dsM(s)DM(s)^T$ which leads, for a stable system ($M(\infty)=0$) and after applying Lyapunov's first theorem, to

$$AV+VA^T=-D. \tag{2.65}$$

V is known as the system covariance matrix (CM) and it contains all information about the steady state. Equation (2.65) can be straightforwardly solved. The entanglement of the steady state can then be quantified by means of the logarithmic negativity $E_{\mathcal{N}}$ which, in the continuous variable (CV) case, is defined as [86–88]

$$E_{\mathcal{N}}=\max[0,-\ln 2\eta], \tag{2.66}$$

where

$$\eta=\sqrt{\frac{\sum(V)-\sqrt{\sum(V)^2-4\det V}}{2}}, \tag{2.67}$$

is the lowest symplectic eigenvalue of the partial transpose of the CM, with $\sum(V)$ ex-

pressed in terms of 2×2 block matrix

$$V = \begin{bmatrix} V_m & V_{corr} \\ V_{corr}^T & V_{cav} \end{bmatrix}, \tag{2.68}$$

as $\sum(V) = \det V_m + \det V_{cav} - 2\det V_{corr}$. The matrix V_m is associated to the oscillating mirror, V_{cav} to the cavity mode and V_{corr} describes the optomechanical correlations. According to Eq.(2.66), a Gaussian state is entangled ($E_{\mathcal{N}} > 0$) if only if $\eta < \frac{1}{2}$, which is equivalent to Simon's necessary and sufficient entanglement nonpositive partial transpose criterion for Gaussian states.

2.4 Numerical methods

These methods, that can be sustained by various reasons, are used to solve directly the rate equations of optomechanical systems. They are used to analyze complex dynamical behaviors as well as the dynamical behavior of the systems for which the rate equations are not readily apparent or solvable. When analytical solutions are not apparent, numerical integration can be used to obtain information about the trajectory. Many numerical methods exist and are used to solve various types of ODEs.

However, the Runge-Kutta family of algorithms comes arguably the most well-known and used methods for numerical integrations. Thus, we choose to review briefly two kinds of numerical integration methods namely 4^{th} order Runge-Kutta ($RK4$) for ODEs and some computational techniques that we have used to characterize the dynamical behaviors of our system. These numerical methods are run on a Laptop computer using MS Windows 7 operating system and three major softwares: Fortran, Matlab and Maple.

2.4.1 Fourth-order Runge-Kutta method for first-order ordinary differential equation

According to the fact that it is the commonly used method, this numerical integration method gives more accurate solutions of the nonlinear ordinary differential equations (NODEs). Let us consider the first order differential equation

$$\frac{du(t)}{dt} = f(t, u(t)), \text{ with } u(t_0) = u_0, \tag{2.69}$$

where $u(t) = (x_1(t), x_2(t), \cdots, x_n(t))^T$ and the vector of noises $f = (f_1, f_2, \cdots, f_n)^T$.

The $RK4$ method gives the solutions of this problem after each time step h. Next solution is a function of the previous one. The solutions are given with respect to the following scheme:

$$u(t+h) = u(t) + \frac{1}{6}(\ell_1 + 2\ell_2 + 2\ell_3 + \ell_4). \tag{2.70}$$

where

$$\ell_1 = hf(t, u(t)), \tag{2.71}$$

$$\ell_2 = hf(t + \frac{h}{2}, u(t) + \frac{\ell_1}{2}), \tag{2.72}$$

$$\ell_3 = hf(t + \frac{h}{2}, u(t) + \frac{\ell_2}{2}), \tag{2.73}$$

$$\ell_4 = hf(t + h, u(t) + \ell_3). \tag{2.74}$$

For a given an initial value $u(t_0) = u_0$, this procedure runs and evaluates all the other values taken by the function u after other times separated by the time step h.

2.4.2 Dynamical behaviors characterization

Behaviors of nonlinear systems are usually characterized with a number of numerical tools such as the time history diagram, phase portraits diagrams, Poincaré section and bifurcation diagrams. Here, we briefly summarize the computational techniques which are used to characterize the dynamical behaviors of optomechanical systems used in this thesis.

Time histories and phase portraits diagrams

Time histories diagrams gives the evolution of each system parameter versus the time. It is constructed straight form the RK4 procedure described above. This diagram shows different forms of traces which inform about the regular and the complex behaviors of the system. The limit of this techniques is the fact that, it can not offer sufficient information to make difference between complex behaviors such as the quasi-periodicity and chaos phenomenon.

A phase portrait is a mathematical space having orthogonal coordinate directions which represent each of the variables needed to specify the instantaneous state of the system. The commonly coordinates used to construct a phase diagram are the position and velocity. It reveals information such as whether an attractor or limit cycle is present for the chosen parameter value. As the time histories diagrams, it is not easy to distinguish

the quasi-periodicity and chaos phenomena by using the phase portrait diagram.

One of reliable numerical tools used to know if a dynamical system exhibits a chaotic phenomenon for a given parameter values is the Poincaré section.

Poincaré section

Poincaré map is the intersection of an orbit in the state space of a continuous dynamical system with a certain lower dimensional subspace. This map known as Poincaré section, provides sufficient informations to distinguish easily different behavior in nonlinear system. Generally for an $n-$dimensional flow, the Poincaré section will be an $(n-1)$ dimensional hypersurface transverse to the flow. To construct the Poincaré section for a three dimensional attractor, choose a plane transverse to the direction of motion of the trajectories. Put a point on this plane every time the trajectory crosses it. This plane then constitutes the Poincaré section for the attractor. Noting that motion of the trajectories only in one direction has to be considered and the time interval between successive intersections need not be equal. Regarding the distribution of points on a computer generated Poincaré section, one easily distinguishes between different motions.

- A $k-$periodic motion maps to $k-$ points on the Poincaré section, i.e., period-1 motion maps to a single point on the Poincaré section, period -2 motion maps to two points, etc.;
- A quasiperiodic motion which contains a finite number of incommensurable frequencies traces a continuous closed curve on the Poincaré map since it does not converge to a single point;
- If the Poincaré map does not consist of either a finite set of points or a closed curve, the motion is chaotic.

2.5 Conclusion

This chapter has presented the mathematical formalisms used for analytical investigations and the numerical methods used to integrate the optomechanical ordinary differential rate equations. We started by the presentation of the analytical methods and some mathematical formalism used. After that, the numerical methods and some computational techniques used both to solve the ODEs and to characterize dynamical behavior of the system have been described. The hardware as well as the software used are indicated. The next chapter focuses on the results and discussions.

Chapter 3

Results and discussions

3.1 Introduction

This chapter investigates the effect of geometrical and optical nonlinearities in optomechanical systems. The geometrical nonlinearity comes from the bending of a mechanical structure, the cantilever nanobeam mirror, when it moves under large excitations while the optical nonlinearity originates form the interaction between laser beam and the nanomirror.

We organize the chapter as follows. In the second section we perform the modelling of the nonlinear Fabry-Pérot optomechanical cavity by taking into account the geometrical nonlinear term. In the third section, we study both the effect of nonlinear term and quantum noises on the dynamical behavior of the system, considering the classical and semiclassical limit. This study is focused on the optomechanical behaviors such as the instabilities which includes chaos, jump phenomena and the bistability. We have represented the hysteresis cycles to characterize this bistability. In the fourth section , we investigate the effect of geometrical nonlinearity on the quantum ground state cooling. The section five is devoted to the study of the geometrical and optical nonlinear effects on the generation of optical and mechanical squeezed states. The last section investigates the effect of geometrical nonlinearity on the generation of continuous variables entangled states in optomechanical systems. The interest allowed to the last two sections comes to the fact that squeezed and entangled states are useful for in quantum information processing and other quantum technologies applications.

3.2 Effects of geometrical and optical nonlinearities in nano-optomechanics

3.2.1 Nonlinear optomechanical rate equations

The meaning of nonlinear optomechanical equations here refers to those which contain the geometrical nonlinear term. Such a nonlinearity is used to correct the dynamics of a mechanical structure when it is subjected to a strong external excitation. As strong external excitation induces large displacement of the structure (Fig.3.1), geometrical nonlinearity then depends on the bending moment of the nanoresonator (nanobeam mirror) and becomes important for its large deflections. The curvature of the nano-mirror when it deflects under various loads such as molecules in suspension in the air contributes also to increase this nonlinearity [62, 89].

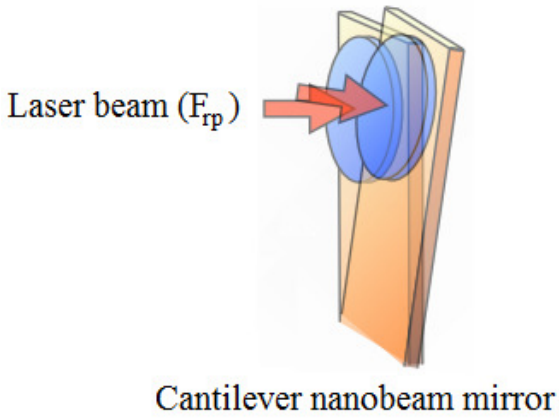

Figure 3.1: *Large displacements of a nanobeam mirror under high laser beam excitation [25].*

In order to take into account the geometrical nonlinearity, we refer to the Eq.(2.11) where the geometrical nonlinear term $\left(\frac{\partial y(r,t)}{\partial r}\right)^2$ is considered.

Using the ansatz approach and boundary conditions of cantilever beams equations [62–64], one obtains the modal solution of Eq.(2.11) given by Eq.(2.12). By following the same procedure as for the linear limit presented in paragraph 2.2.1, one obtains the nonlinear equation,

$$\ddot{x}+\Gamma_m\dot{x}+\Omega_m^2 x-\beta' x^3=\frac{\hbar g_M}{M x_{ZPF}}|\alpha(t)|^2, \tag{3.1}$$

where the nonlinear term is captured by

$$\beta'=\frac{3EI}{2\rho s}\frac{\int_0^l\left[u_n''''(u_n')^2+6u_n'''u_n''u_n'+2(u_n'')^3\right]dr}{\int_0^l u_n(r)dr}. \tag{3.2}$$

By combining Eq.(3.1) with the optical one (Eq.(2.10)), one easily obtains the following nonlinear optomechanical rate equations,

$$\dot{\alpha}=\left[i\left(\Delta_0+\frac{g_M}{x_{ZPF}}x+\frac{g_M}{2x_{ZPF}d_0}x^2\right)-\frac{\kappa}{2}\right]\alpha+i\sqrt{\kappa}E^{in}, \tag{3.3}$$

$$\ddot{x}+\Gamma_m\dot{x}+\Omega_m^2 x-\beta' x^3=\frac{\hbar g_M}{M x_{ZPF}}|\alpha|^2, \tag{3.4}$$

where $\frac{g_M}{2x_{ZPF}d_0}x^2$ is the second order optical nonlinear term [90].

The variables t, x and α can be rescaled as $t_a=\Omega_m t$, $x_a=\frac{g_M}{\Omega_m x_{ZPF}}x$ and $\alpha_a=\frac{\Omega_m}{2i\sqrt{\kappa}\bar{E}^{in}}\alpha$, so that the coupled equations of motion contain only the dimensionless parameters Ψ, $\frac{\Delta}{\Omega_m}$,

$\frac{\kappa}{\Omega_m}$, $\frac{\Gamma_m}{\Omega_m}$, β and η. Thus equations (3.3) and (3.4) become

$$\dot{\alpha}_a = \left[i\left(\frac{\Delta_0}{\Omega_m} + x_a + \eta x_a^2 \right) - \frac{\kappa}{2\Omega_m} \right] \alpha_a + \frac{1}{2}, \tag{3.5}$$

$$\ddot{x}_a + \frac{\Gamma}{\Omega_m}\dot{x}_a + x_a - \beta x_a^3 = \Psi |\alpha_a|^2. \tag{3.6}$$

$\beta = \frac{\beta' x_{ZPF}^2}{g_M^2}$ and $\eta = \frac{\Omega_m x_{ZPF}}{2 g_M d_0}$ denote respectively the dimensionless geometrical nonlinear parameter and the dimensionless second order optical nonlinear parameter and, $\Psi = \frac{16 g_M^2 \kappa^2}{\hbar \omega_0 \Omega_m^4} P_{in}$.

By taking into account the nonlinear terms in the semiclassical limit, one gets an anharmonic Hamiltonian,

$$\begin{aligned} \hat{H} = &-\hbar \left(\Delta_0 + g_M x_m + \frac{g_M x_{ZPF}}{2 d_0} x_m^2 \right) \hat{\alpha}^\dagger \hat{\alpha} + \frac{\hbar \Omega_m}{2} \left(p_m^2 + x_m^2 - \frac{\beta' x_{ZPF}^2}{\Omega_m^2} x_m^4 \right) \\ &+ \hbar \sqrt{\kappa} E^{in} (\hat{\alpha}^\dagger + \hat{\alpha}) + \hat{H}_\kappa + \hat{H}_\Gamma, \end{aligned} \tag{3.7}$$

where $\frac{\beta' x_{ZPF}^2}{\Omega_m^2} x_m^4$ and $\frac{g_M x_{ZPF}}{2 d_0} x_m^2$ are the aforementioned geometrical nonlinearity and the second order optical nonlinearity. To obtain the equations in the semiclassical approach by starting from the Hamiltonian given by Eq.(3.7), we apply the Langevin equation described in subsection 2.3.1. The nonlinear quantum Langevin equations (NQLEs) then yield,

$$\dot{\alpha} = \left[i\left(\Delta_0 + \frac{g_M}{x_{ZPF}} x + \frac{g_M}{2 x_{ZPF} d_0} x^2 \right) - \frac{\kappa}{2} \right] \alpha + i\sqrt{\kappa} E^{in} + \sqrt{\kappa} \alpha^{in}, \tag{3.8}$$

$$\ddot{x} + \Gamma \dot{x} + \Omega_m^2 x - \frac{g_M \Omega_m x_{ZPF}}{d_0} |\alpha|^2 x - 2\beta' x^3 = \frac{\hbar g_M}{2 M x_{ZPF}} |\alpha|^2 + \sqrt{\frac{\hbar \Omega_m \Gamma_m}{M}} \xi. \tag{3.9}$$

By rescaling the parameters as in Eqs. (3.5) and (3.6), the dimensionless NQLEs are derived as,

$$\dot{\alpha}_a = \left[i\left(\frac{\Delta_0}{\Omega_m} + x_a + \eta x_a^2 \right) - \frac{\kappa}{2\Omega_m} \right] \alpha_a + \frac{1}{2} + \chi_0 \alpha^{in}, \tag{3.10}$$

$$\ddot{x}_a + \frac{\Gamma}{\Omega_m}\dot{x}_a + x_a - \frac{\Psi \Omega_m x_{ZPF}}{2 g_M d_0} |\alpha_a|^2 x_a - 2\beta x_a^3 = \frac{\Psi}{2} |\alpha_a|^2 + \chi_1 \xi, \tag{3.11}$$

where $\chi_0 = \sqrt{\frac{\hbar \omega_0}{8 \kappa P_{in}}}$ and $\chi_1 = \frac{g_M}{\Omega_m^3 x_{ZPF}} \sqrt{\frac{\hbar \Omega_m \Gamma_m}{M}}$ are the optical and mechanical noises intensity respectively with $\Gamma_m = \frac{M \Omega_m^3 x_{ZPF}^2}{\hbar} \left(1 - \frac{\beta g_M^2}{\Omega_m^2} \right)^2$.

The mechanical energy of the cantilever nanobeam is,

$$E_M = E_k + E_p = \frac{1}{2}M\dot{x}^2 + \frac{1}{2}M\Omega_m^2 x^2 - \frac{1}{4}M\beta' x^4, \tag{3.12}$$

where E_k and E_p respectively denote the kinetic and potential energy. In the dimensionless form, Eq.(3.12) becomes

$$\frac{E_M}{E_0} = A^2\left(\dot{x}_a^2 + x_a^2 - \frac{\beta}{2}x_a^4\right), \tag{3.13}$$

where $A = \frac{\Omega_m x_{ZPF}}{g_M x_{FWHM}}$ and $E_0 = \frac{1}{2}M\Omega_m^2 x_{FWHM}^2$ with x_{FWHM} the mechanical cantilever amplitude which moves the cavity just out of its resonance [83].

By using the experimental parameters of [26] given in Table 3.1, we have computed the following dimensionless parameters: $A = 7.36$; $\beta = 8\times10^{-3}$; $\eta = 2.18\times10^{-7}$; $\frac{\kappa}{\Omega_m} = 6.8\times10^{-2}$; $\frac{\Gamma}{\Omega_m} = 9.51\times10^{-6}$; $\frac{\Psi}{P_{in}} = 1,47\times10^{8}$; $\frac{\Gamma}{\Psi} = 50$; $\frac{\Psi\Omega_m x_{ZPF}}{2g_M d_0} = 9.6\times10^{-4}$ and $-2 \leq \frac{\Delta_0}{\Omega_m} \leq 2$. The driving strength Ψ should satisfy the condition $\frac{\Gamma_m}{\Psi} \gg 1$ that means that the dynamical multistability is precluded [91]. According to the small value of η, it will be neglected in this part of our simulations and so the value $\beta = 0$ corresponds to the linear case of the system.

$\Omega_m/2\pi$	$\Gamma_m/2\pi$	Q_m	$g_0/2\pi$	κ/π	P_0	T
3.6 GHz	35 kHz	1.05×10^5	910 kHz	529 MHz	0.7 mW	270 mK

Table 3.1: *Experimental parameters of Ref. [26].*

3.2.2 Dynamical behaviors

A comparative study between the classical and semiclassical limit in optomechanical systems is done in this section. These studies analyze the effects of both geometrical nonlinearity and the quantum noises on the dynamics of the system. Firstly, we present the results of optomechanical dynamics. After that, the effects of geometrical nonlinearity and both Brownian and shot noises on the mechanical energy of the cantilever mirror are analyzed.

Dynamical behavior of the system in classical limit

This dynamical behavior is presented by distinguishing the linear limit from the nonlinear one, in order to bring out the effect of the geometrical nonlinearity on the system. The equations use to this purpose are the Eqs.(3.5) and (3.6).

Linear limit The input laser beam used in our simulation is a continuous laser beam, which when it is sending in the cavity, various types of time dependent optical outputs are obtained [90]: sinusoidal (Fig.3.2a), pulsating (Fig.3.2b) and chaotic (Fig.3.2c and Fig.3.2d). As mentioned in paragraph 2.4.2, the Poincaré's map represented on Fig.3.2d does not consist of either a finite set of points or a closed curve. This Poincaré's section then reveals the chaotic state in the system.

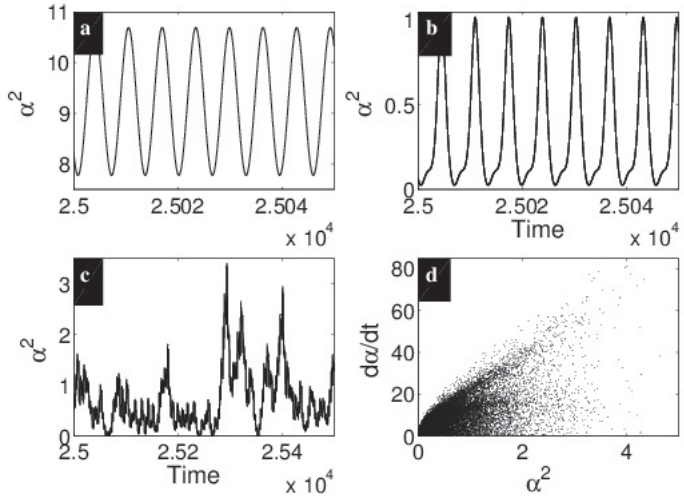

Figure 3.2: *Oscillation state of optical intracavity (a), pulsating state (b) and chaotic state (c). The Poincare's section (d) reveals more the chaotic behavior shown in (c). These curves are plotted for* $\frac{\Delta_0}{\Omega_m} = 0$ *(a and b) and for* $\frac{\Delta_0}{\Omega_m} = 1$ *(c and d). The values of input power used are:* $P_{in} = 5 \times 10^{-5} W$ *for (a),* $P_{in} = 8 \times 10^{-4} W$ *for (b) and* $P_{in} = 10^{-2} W$ *for (c).*

The optical energy stored in the cavity which is represented on Fig.3.3a, shows two peaks. In the resolved sideband limit ($\kappa \ll \Omega_m$) and weak driving, the cantilever nanobeam occupation peaks around the resonance between the cavity and the input laser $\left(\frac{\Delta_0}{\Omega_m} = 0\right)$. Therefore the number of photons in the cavity is large. Another peak appears around the first sideband ($\frac{\Delta_0}{\Omega_m} = 1$) corresponding to a resonance between a photon into the cavity and a phonon of the cantilever nanobeam. The first peak is higher than the second peak. But the mechanical amplitudes as well as the cantilever energy show the reversed effect. The highest maximum for these two quantities (Fig.3.3b and Fig.3.3c) appears around $\frac{\Delta_0}{\Omega_m} = 1$, rather than around $\frac{\Delta_0}{\Omega_m} = 0$. In the study of the optomechanical couplings, the zones of small amplitudes ($[-2; -0.41]$ and $[1.22; 2]$) are called stable zones while the zones of high amplitudes are known as unstable zones $]-0.41; 1.22[$. In the unstable zone, two jump phenomena (indicated by arrows) appear (Fig.3.3).

Figures 3.4 presents the amplitude of the mechanical oscillations and optical energy stored in the cavity versus the input power of the laser. The threshold power here is

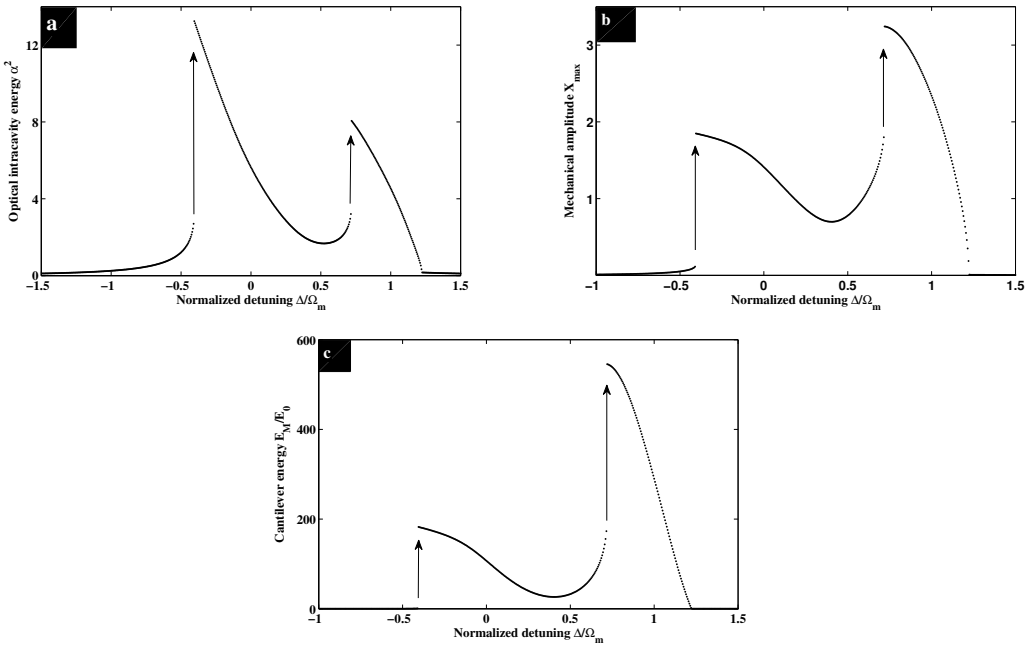

Figure 3.3: *Optical intracavity energy (a), Mechanical amplitude (b) and Cantilever energy (c) versus the detuning in the linear regime ($\beta = 0$). The input power used for these plots is $P_{in} = 3 \times 10^{-5}\,\mathrm{W}$.*

up to about $2 \times 10^{-6}\,\mathrm{W}$. The mechanical amplitude just increases until its saturation (Fig.3.4a). At the same time, the optical energy starts to increase from this threshold power, reaches its maximum at $P_{in} = 3.7 \times 10^{-6}\,\mathrm{W}$ and ends by a saturation toward the small values (Fig.3.4b).

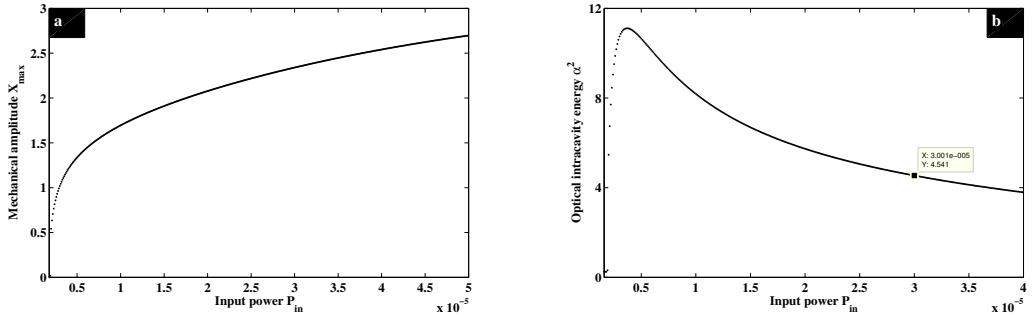

Figure 3.4: *Mechanical amplitude (a) and Optical intracavity energy (b) versus the input power in the absence of the nonlinearity and $\frac{\Delta_0}{\Omega_m} = 1$. These curves reach their saturation respectively towards the high amplitudes (a) and the small amplitudes (b).*

Nonlinear limit The introduction of nonlinear terms affect the dynamics of the system. Figure 3.5 shows that when the geometrical nonlinearity increases, the peaks heights are reduced consequently; but the stable zone remain unchanged. The reduction of peaks

expresses the diminution of cantilever energy. The gap between the linear and the nonlinear limits is more significant around the second peaks. For $\beta = 5 \times 10^{-2}$, the cantilever energy shifts from about 546 to 340. When β increases, the detuning value for which the jump phenomenon appears does not change in the first peak while in the second peak, that detuning is reduced: e.g. for $\beta = 0$, $\frac{\Delta_0}{\Omega_m} = 0.72$; for $\beta = 8 \times 10^{-3}$, $\frac{\Delta_0}{\Omega_m} = 0.7$ and for $\beta = 5 \times 10^{-2}$, $\frac{\Delta_0}{\Omega_m} = 0.64$. It appears that the geometrical nonlinear term affects the behavior of the intracavity energy the same way it affects the cantilever energy. But the difference is that what happens around the first peak of cantilever energy is what rather happens around the second peak of intracavity energy. We mentioned that antagonism between intracavity energy and the cantilever energy in the linear case. We then note that geometrical nonlinearity, in the classical limit, tends to stabilize or to control the behavior of the nano-mirror since it reduces its amplitudes of vibration.

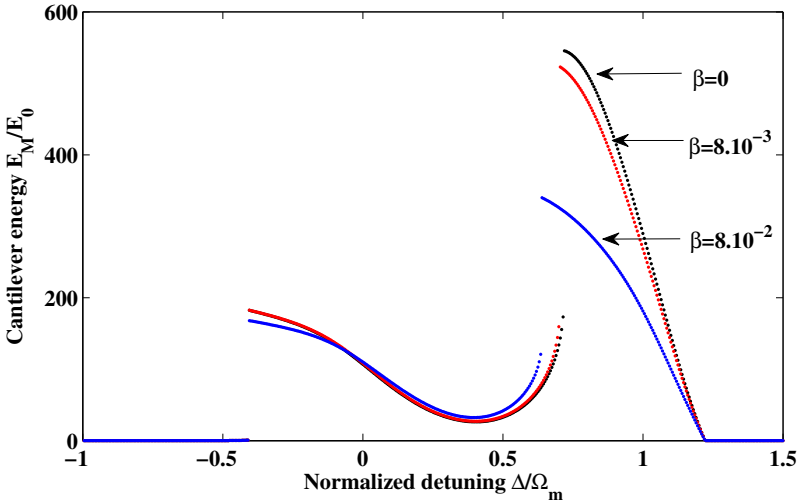

Figure 3.5: *Effect of the geometrical nonlinearity on the cantilever energy. When the nonlinearity increases, the amplitude of the cantilever energy decreases.*

Dynamical behavior of the system in semiclassical limit

In order to use the full nonlinear equation of motion for the operators given by the anharmonique Hamiltonian Eq.(3.7), we have to work in regime of very small mean photon number. In Ref. [83], it is shown that the amplitude of the optical field in the classical limit is greater than in the quantum case. In order to show that the classical Langevin equations try to mimick the quantum noise, it is sufficient to show numerically that the amplitude of the optical field in the semiclassical limit is small than in the classical case. Hence, numerical simulations are concerned by Eqs. (3.10) and (3.11).

Linear limit In the semiclassical approach, $|\alpha|^2$ denotes the photons number in the cavity. The input laser power used here is $P_{in} = 3 \times 10^{-5}\,\mathrm{W}$ and corresponds to the zone where optical intracavity energy reaches its saturation towards the small values of the mean photon number. The point indicated on Fig.3.4b corresponds to the value that we use in the following study. One shows that the amplitude of photons number in the cavity decreases in the semiclassical approach (Fig.3.6a), in comparison with the classical limit (Fig.3.3a). This result confirm that the semiclassical limit try to mimick the quantum behavior in the case of small mean photon number. The increase of the noise amplitude induces a slight increase of the photon number in the cavity (blue and dash-dot curve on Fig.3.6a). As suggested in [83], Fig.3.6b shows that the increase of the noise amplitude induces a slight decrease of the cantilever energy. When the noise amplitude becomes significant, another zone of instability appears around the second sideband $\frac{\Delta_0}{\Omega_m} = 2$. It is remarked that the point where the jump phenomenon appears (around $\frac{\Delta_0}{\Omega_m} = -0.5$) shifts toward the left to small values of detuning. Therefore, in the presence of noises, the cavity tends to become stable and new zones of oscillations appear.

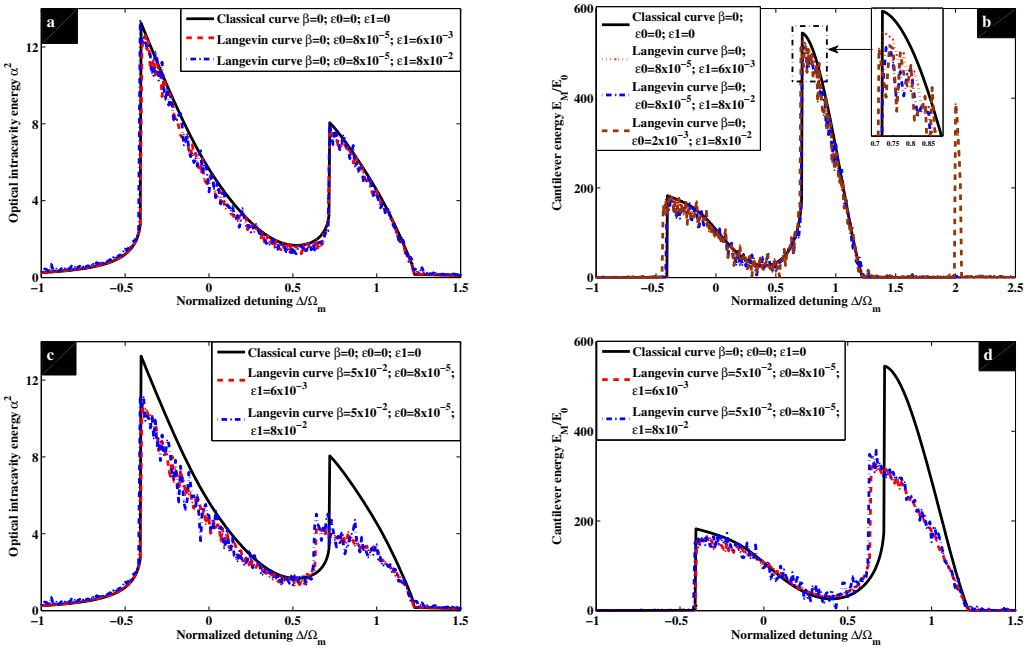

Figure 3.6: *Effect of noise on the optical and cantilever energy. (a) and (b) are in linear regime while (c) and (d) are in nonlinear regime where the nonlinear term is* $\beta = 5 \times 10^{-2}$.

Nonlinear limit In presence of the nonlinearity, it is observed a reduction of the values of both optical and cantilever energy mainly around the first sideband (Fig.3.6c and Fig.3.6d). Thus, in general in the semiclassical approach and in the presence of the

nonlinearity, not only the cantilever energy decreases, the first peak also move towards small values of the detuning. The significant decrease of the cantilever energy in Fig.3.6d is in good agreement with the quantum limit observations [83]. This means that, the quantum behavior is better approached when the effects of geometrical nonlinearity are taking into account in the semiclassical limit. The next subsection (3.2.3) studies the hysteresis loops for optical energy stored in the cavity in order to deduce the existence of the bistable zones. It also shows how the nonlinearity influences on the bistable zones both in the classical and semiclassical approach.

3.2.3 Optical bistability and effects of both geometrical nonlinearity and quantum noises

To approach the idea of bistability, the optical intracavity energy versus detuning characteristic is plotted both in forward and backward evolution of detuning.

In the classical approach and in the linear limit (Fig.3.7a), three hysteresis loops appear in the system. The first one is located within $\frac{\Delta_0}{\Omega_m} \in [-2;-0.41]$; the second within $\frac{\Delta_0}{\Omega_m} \in [0.67;0.71]$ and the third corresponds to the zone $\frac{\Delta_0}{\Omega_m} \in [1.7;2]$. The first and the third are unclosed loops while the second is a closed loop. One remarks that the unclosed hysteresis loops are located in the stable zones whereas the closed hysteresis loop is in the unstable zone. We deduce that the completely closed hysteresis loops characterize the instabilities in the cavity. One remarks that when we enlarge the horizontal axis, the opened hysteresis loop which appeared at the zone $[-2;-0.41]$ becomes a closed hysteresis loop while the other opened hysteresis loop which appeared at the zone $[1.7;2]$ disappears. In the nonlinear limit (Fig.3.7b), the first hysteresis loop ($\frac{\Delta_0}{\Omega_m} \in [-2;-0.41]$) reduces ($\frac{\Delta_0}{\Omega_m} \in [-1.05;-0.41]$) and becomes a closed hysteresis loop. It is also remarked that the second hysteresis loop widens ($\frac{\Delta_0}{\Omega_m} \in [0.42;0.64]$) while the third disappears.

In the semiclassical approach and in the linear limit, the hysteresis loops are at the same places as in the classical case. In the nonlinear case (Fig.3.7c), the hysteresis loop ($[-1.05;-0.41]$) reduces and becomes $[-0.75;-0.41]$. Therefore, by combining the noises and the nonlinearity in the system, the result is that, the width of the hysteresis loops are reduced (compare Fig.3.7b and Fig.3.7c). The width of the first and the second loops are now respectively $[-0.75;-0.41]$ and $[0.57;0.62]$. Similar result is also presented in [92], where stochastic force is used to reduce and/or suppress hysteresis zone in a Duffing oscillator. According to the fact that the quantum noise reduction is important near the bistability turning points [93], one deduces that this system behaves as an optical filter and improves so many quantum optomechanical applications.

Globally, we have noted that for large detuning range, the effects of nonlinear term as well as the effects of noise terms remain the same as in the zone $[-2;2]$. Nevertheless, it is noted that when the variable detuning zone is chosen large, some small details of optomechanical coupling are masked.

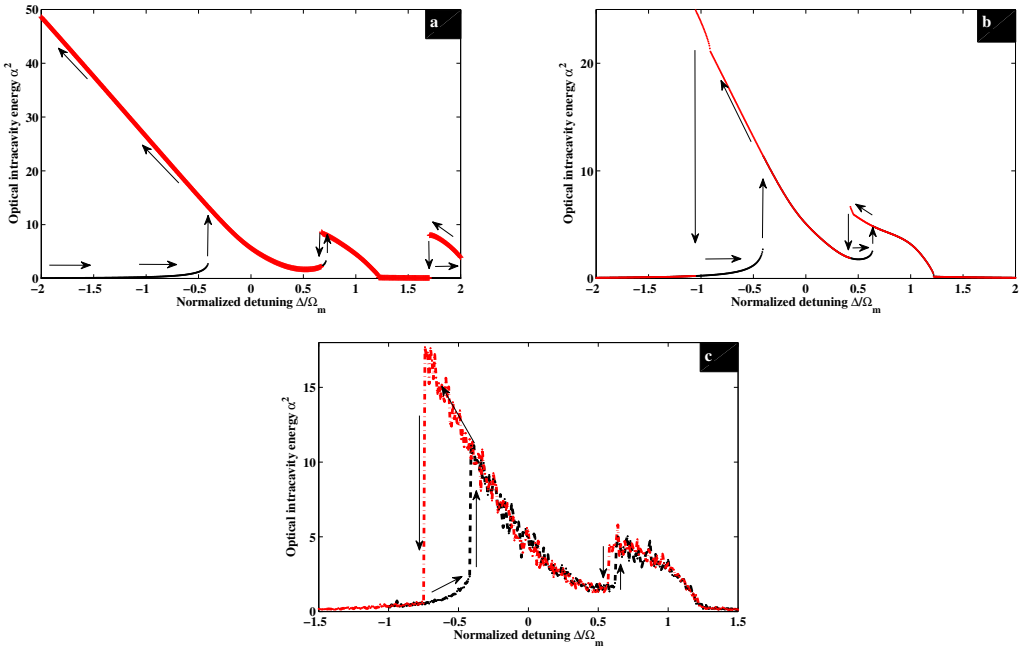

Figure 3.7: *Effects of noise and the nonlinearity on the bistability. In the classical limit, (a) and (b) represent the bistability in the linear and in the nonlinear regime respectively while (c) is the bistability in the nonlinear semiclassical limit.*

3.3 Quantum ground state cooling in nonlinear optomechanics

Enormous efforts have been done in quantum nanomechanical cooling during the last decade. Indeed, the phonon number less than unity is achieved in optomechanical laser cooling [26] and in electromechanical microwave cooling [27,28]. The enhancement of these results can be done through a nonlinear study at the single phonon level as suggested in [26]. This is why the effect of the geometrical nonlinearity is investigated on the cooling at the single phonon level here. As result, nonlinearity adds a small amount of phonon on the well known minimum theoretical phonon number (Eq.(1.4)). This means that geometrical nonlinearity behaves as thermal decoherence (or re-thermalization time $\tau_{th} = \frac{\hbar Q_m}{k_B T}$) and then constitutes a limiting factor for quantum cooling. Best cooling can

then be achieved by minimizing the value of geometrical nonlinear term, which also induces the suppression of the thermal decoherence. In the following, the dynamics fluctuations of the system is performed and the effects of geometrical nonlinearity on optical spring and phonon number are analyzed.

3.3.1 Quantum dynamics of the fluctuations

From the aforementioned steady state relations Eq.(2.2), one can obtains the following third-order polynomial equation for the mechanical steady state displacement,

$$x_s^3+\frac{2\Delta_0}{g_M}x_s^2+\frac{(4\Delta_0^2+\kappa^2)}{4g_M^2}x_s-\frac{4\kappa P_{in}}{\hbar\omega_0\Omega_m g_M}=0. \tag{3.14}$$

This polynomial equation is solved by the cardano's method (see paragraph 2.3.2) in order to get the steady state values. The quantum behavior of the optomechanical systems is then detected in the dynamics of the fluctuations around these steady states. Rewriting each Heisenberg operator of NQLEs as the classical steady state value plus an additional fluctuation operator with zero mean value, and neglecting high order terms in the equations (which is justified whenever $|\alpha_s|\gg 1$), one gets the following linearized NQLEs for the fluctuations,

$$\begin{aligned}\delta\dot{\alpha}=&\left[i\left(\Delta_0+\frac{g_M}{x_{ZPF}}x_s+\frac{g_M}{2x_{ZPF}d_0}x_s^2\right)-\frac{\kappa}{2}\right]\delta\alpha\\&+\frac{ig_M}{x_{ZPF}}\alpha_s\left(1+\frac{x_s}{d_0}\right)\delta x-i\delta E+\sqrt{\kappa}\delta\alpha^{in},\end{aligned} \tag{3.15}$$

$$\delta\ddot{x}+\Gamma_m\delta\dot{x}+\Omega_m^2\delta x-3\beta' x_s^2\delta x=\frac{\hbar g_M}{Mx_{ZPF}}\alpha_s(\delta\alpha+\delta\alpha^\dagger)+\frac{\delta F_{th}}{M}, \tag{3.16}$$

where the mechanical equations have been combined. Transforming these dynamics equations into the Fourier space and by using the hermeticity property for the displacement ($\delta x(t)=\delta x^\dagger(t)$), one obtains the following fluctuation equations

$$\begin{aligned}&\left[-i\left(\Delta_0+\frac{g_M}{x_{ZPF}}x_s+\frac{g_M}{2x_{ZPF}d_0}x_s^2+\Omega\right)+\frac{\kappa}{2}\right]\delta\alpha[\Omega]=\\&\frac{ig_M}{x_{ZPF}}\alpha_s\left(1+\frac{x_s}{d_0}\right)\delta x[\Omega]-i\delta E[\Omega]+\sqrt{\kappa}\delta\alpha^{in}[\Omega],\end{aligned} \tag{3.17}$$

$$\begin{aligned}&\left[i\left(\Delta_0+\frac{g_M}{x_{ZPF}}x_s+\frac{g_M}{2x_{ZPF}d_0}x_s^2-\Omega\right)+\frac{\kappa}{2}\right]\delta\alpha^\dagger[\Omega]=\\&-\frac{ig_M}{x_{ZPF}}\alpha_s\left(1+\frac{x_s}{d_0}\right)\delta x[\Omega]+i\delta E^\dagger[\Omega]+\sqrt{\kappa}\delta\alpha^{in}[\Omega],\end{aligned} \tag{3.18}$$

$$(\Omega_m^2-\Omega^2-i\Omega\Gamma-3\beta' x_s^2)\delta x[\Omega]=\frac{\hbar g_M}{Mx_{ZPF}}\alpha_s(\delta\alpha[\Omega]+\delta\alpha^\dagger[\Omega])+\frac{\delta F_{th}[\Omega]}{M}. \tag{3.19}$$

Equation (3.19) shows that the mechanical displacement δx is the sum of a displacement induced by the radiation pressure force fluctuations ($\delta F_{rp}=\frac{\hbar g_M}{Mx_{ZPF}}\alpha_s(\delta\alpha+\delta\alpha^\dagger)$) and a displacement induced by the thermal Langevin force fluctuations (δF_{th}). For room temperatures, thermal fluctuations mask the quantum effects of light. To observe this quantum effects, cryogenic treatment ($T\leq T_Q$) of the cavity is necessary. It should be Noted that $T_Q=\frac{\hbar\Omega_m}{k_B}$ is the the quantum temperature of the system, while T is the room temperature. As the quantity $i\delta E[\Omega]+\sqrt{\kappa}\delta\alpha^{in}[\Omega]$ and its conjugate are usually absorbed into the effective susceptibility, they will be neglected in the following.

To obtain the full dynamics of the mechanical part, the expressions of $\delta\alpha[\Omega]$ and $\delta\alpha^\dagger[\Omega]$, deduced from Eqs.(3.17) and (3.18), must be replaced in Eq.(3.19). At the room temperature, the expression of radiation pressure force is given by

$$\begin{aligned}\delta F_{rp}=&\frac{i\hbar g_M^2\alpha_s^2\left(1+\frac{x_s}{d_0}\right)}{2x_{ZPF}^2}\left\{\frac{\kappa}{(\Delta+\eta+\Omega)^2+\frac{\kappa^2}{4}}-\frac{\kappa}{(\Delta+\eta-\Omega)^2+\frac{\kappa^2}{4}}\right\}\delta x[\Omega]\\&-\frac{\hbar g_M^2\alpha_s^2\left(1+\frac{x_s}{d_0}\right)}{x_{ZPF}^2}\left\{\frac{\Delta+\eta+\Omega}{(\Delta+\eta+\Omega)^2+\frac{\kappa^2}{4}}+\frac{\Delta+\eta-\Omega}{(\Delta+\eta-\Omega)^2+\frac{\kappa^2}{4}}\right\}\delta x[\Omega],\end{aligned} \tag{3.20}$$

where we have set $\Delta=\Delta_0+\frac{g_M}{x_{ZPF}}x_s=\Delta_0+\eta_0$ as nonlinear or effective detuning and $\eta=\frac{g_M}{2x_{ZPF}d_0}x_s^2$ as the second order optical nonlinearity.

By setting

$$A_1=\frac{\hbar g_M^2\alpha_s^2\left(1+\frac{x_s}{d_0}\right)}{2x_{ZPF}^2}\left\{\frac{\kappa}{(\Delta+\eta+\Omega)^2+\frac{\kappa^2}{4}}-\frac{\kappa}{(\Delta+\eta-\Omega)^2+\frac{\kappa^2}{4}}\right\}, \tag{3.21}$$

and

$$A_2=\frac{\hbar g_M^2\alpha_s^2\left(1+\frac{x_s}{d_0}\right)}{x_{ZPF}^2}\left\{\frac{\Delta+\eta+\Omega}{(\Delta+\eta+\Omega)^2+\frac{\kappa^2}{4}}+\frac{\Delta+\eta-\Omega}{(\Delta+\eta-\Omega)^2+\frac{\kappa^2}{4}}\right\}, \tag{3.22}$$

Eq.(3.19) can be written under the theory of linear response as

$$\delta x[\Omega]=\chi_{eff}[\Omega]\delta F_{th}[\Omega]. \tag{3.23}$$

From Eq. (3.23), the effective mechanical susceptibility of the system χ_{eff} is defined as

$$\chi_{eff}[\Omega]=\frac{1}{M(\Omega_{eff}^2-\Omega^2-i\Gamma_{eff}\Omega)}, \tag{3.24}$$

where

$$\Omega_{eff}^2[\Omega] = \Omega_m^2 + \frac{A_2}{M} - 3\beta' x_s^2 \quad \text{and} \quad \Gamma_{eff}[\Omega] = \Gamma + \frac{A_1}{M\Omega}, \tag{3.25}$$

denote respectively the effective mechanical frequency and the effective damping of the nanomechanical oscillator. The quantity Ω_{eff}^2 which describes the optical spring effect and Γ_{eff} contain both important information about the quantum behavior of the system. Their detailed expressions are obtained by replacing in Eq.(3.25) the quantities A_1 and A_2 which are expressed in Eqs.(3.21) and (3.22). Thereafter, we define the Stokes coefficients A_- and A_+ as follows,

$$A_\pm = \frac{G^2}{\Omega_m} \frac{\frac{\kappa}{\Omega_m}}{4\left(\frac{\Delta}{\Omega_m} + \frac{\eta}{\Omega_m} \mp 1\right)^2 + \left(\frac{\kappa}{\Omega_m}\right)^2}, \tag{3.26}$$

where $G^2 = 4g_M^2\alpha_s^2\left(1 + \frac{x_s}{d_0}\right)$ denotes the optomechanical coupling parameter. To simplify the analytical calculations, we assume that the system is at a quasiresonance regime and then set $\Gamma_{eff}[\Omega] \approx \Gamma_{eff}[\Omega_m]$ and $\Omega_{eff}^2[\Omega] \approx \Omega_{eff}^2[\Omega_m]$. Therefore,

$$\Gamma_{eff}\left[\Omega_m\right] = \Gamma + A_- - A_+ = \Gamma + \Gamma_{opt} \tag{3.27}$$

and

$$\begin{aligned}\Omega_{eff}^2[\Omega_m] = \Omega_m^2 \Bigg[1 + \frac{2G^2}{\Omega_m^2} \Bigg\{ & \frac{\frac{\Delta}{\Omega_m} + \frac{\eta}{\Omega_m} + 1}{4\left(\frac{\Delta}{\Omega_m} + \frac{\eta}{\Omega_m} + 1\right)^2 + \left(\frac{\kappa}{\Omega_m}\right)^2} \\ & + \frac{\frac{\Delta}{\Omega_m} + \frac{\eta}{\Omega_m} - 1}{4\left(\frac{\Delta}{\Omega_m} + \frac{\eta}{\Omega_m} - 1\right)^2 + \left(\frac{\kappa}{\Omega_m}\right)^2} \Bigg\} - \frac{3\beta' x_s^2}{\Omega_m^2} \Bigg]\end{aligned} \tag{3.28}$$

where $\Gamma_{opt} = A_- - A_+$ and $\beta = \frac{3\beta' x_s^2}{\Omega_m^2}$ denote respectively the optical cooling rate and the mechanical nonlinearity. Using the experimental parameters of the Table 3.1 and the boundary conditions of the equations of beams in the ansatz approach, we obtain the dimensionless values of the geometrical nonlinearity in the Table 3.2, which are comparable to those obtained in [89]. Concerning the optical nonlinearities, one obtains $\frac{\eta_0}{\Omega_m} = 0.9813$ and $\frac{\eta}{\Omega_m} = 2.14 \times 10^{-7}$. The first term is the first order optical nonlinearity which is included into the nonlinear detuning while the second term is neglected.

Optomechanical cooling can be characterized by the optical cooling rate Γ_{opt} through the Stokes coefficients A_- and A_+. This is represented on Fig.3.8 where the Stokes processes are stronger at the sideband detuning points ± 1. The positive peak corresponds

Mean displacement of the nanobeam x_s	Length of the nanobeam (m)	Geometrical nonlinearity
10^{-7}	5×10^{-7}	2.34
	5×10^{-6}	2.34×10^{-2}
10^{-8}	10^{-7}	5×10^{-6}
	5×10^{-6}	2.34×10^{-4}

Table 3.2: *Values of the geometrical nonlinearity computed by using experimental parameters of Ref. [26].*

to the cooling ($\frac{\Delta}{\Omega_m}=-1$ where appears the anti-Stokes process or antiresonance) of the nanomechanical oscillator while the negative peak corresponds to its heating ($\frac{\Delta}{\Omega_m}=+1$ where appears the Stokes process or resonance). One remarks that the cooling appears in the stable zone where the mechanical displacements are weak, while the heating appears in the unstable zone where the mechanical displacements are important [83]. Therefore, the cooling takes place in the blue-detuning zone ($\Delta<0$) and the heating takes place in the red-detuning zone ($\Delta>0$). Figure 3.8 also shows that the cooling is efficient for weak values of optical linewidth $\frac{\kappa}{\Omega_m}$.

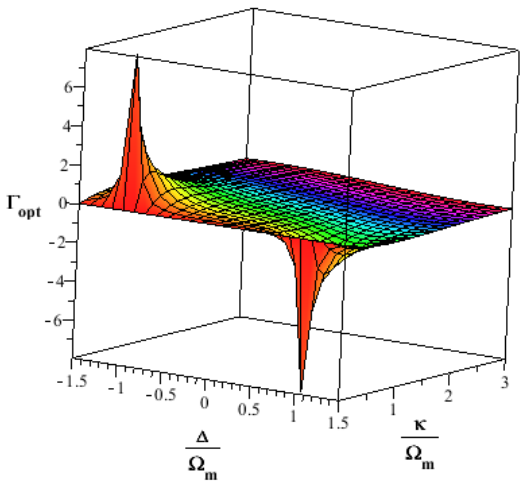

Figure 3.8: *Normalized cooling rate versus the detuning and optical linewidth. Stokes and anti-Stokes processes are efficient respectively, at $\frac{\Delta}{\Omega_m}=\pm1$ and for small values of the normalized optical linewidth.*

According to Eqs.(3.26) and (3.27), one remarks that the effective cooling is efficient in the strong optomechanical coupling regime (for large values of G), since the effective damping Γ_{eff} is proportional to G^2.

Another important parameter which characterizes the cooling or heating in nanomechanics is the final phonon number obtained. This is the focus point of next subsection.

3.3.2 Effective phonon number in nonlinear optomechanics

By assuming the cantilever nanobeam mirror as an harmonic oscillator, its energy can be defined as

$$\langle H\rangle = \frac{1}{2}\frac{\langle \delta p^2\rangle}{M} + \frac{1}{2}M\Omega_m^2\langle \delta x^2\rangle = \hbar\Omega_m\left(\langle n_{eff}\rangle + \frac{1}{2}\right), \tag{3.29}$$

where $n_{eff} = b^\dagger b$ is the phonon number operator, with b and $b^\dagger$ the phonon creation and annihilation operators. In the literature, the lowest attainable value of n_{eff} is given by the expression Eq.(1.4). By considering the anharmonic term β, this expression rigorously becomes

$$\langle n_{eff}\rangle = \left(\frac{\kappa}{4\Omega_{eff}}\right)^2 \propto \frac{1}{(1-\beta)}, \tag{3.30}$$

where Ω_{eff} is defined in Eq.(3.28). Eq.(3.30) shows that, in the nonlinear optomechanics which is quite described the real system, effective phonon number is inversely proportional to $(1-\beta)$. This explains how geometrical nonlinearity adds a small amount of phonon to the lowest phonon number and then, constitutes a limiting factor as the thermal decoherence. From the expressions of $\beta = \frac{3\beta' x_s^2}{\Omega_m^2}$ and the re-thermalization time $\tau_{th} = \frac{\hbar Q_m}{k_B T} = \frac{\hbar\Omega_m}{\Gamma k_B T}$, cooling can be enhanced in nonlinear optomechanics by increasing the mechanical frequency Ω_m of the oscillator. This action minimizes the value of β and increases the re-thermalization time τ_{th} allowing so the possibility to observe more quantum effects. Let us apply now this analysis to our system.

The spectrum of both Langevin force and radiation pressure force are respectively given by [94, 95],

$$S_{FF}^{th}(\Omega) = \hbar M\Gamma\Omega\coth\left(\frac{\hbar\Omega}{2k_BT}\right) \approx 2M\Gamma k_B T, \tag{3.31}$$

$$S_{FF}^{qn}(\Omega) = \frac{\hbar^2}{2x_{ZPF}}(A_- + A_+), \tag{3.32}$$

where the approximation done is valid for temperatures such that $k_BT \gg \hbar\Omega$. The total displacement spectrum is then given,

$$S_{xx}(\Omega) = |\chi_{eff}|^2[S_{FF}^{th}(\Omega) + S_{FF}^{qn}(\Omega)]. \tag{3.33}$$

Both position and momentum variances can then be respectively defined as,

$$\langle \delta x^2 \rangle = \int_{-\infty}^{+\infty} S_{xx}(\Omega) \frac{d\Omega}{2\pi}, \tag{3.34}$$

$$\langle \delta p^2 \rangle = M^2 \int_{-\infty}^{+\infty} \Omega^2 S_{xx}(\Omega) \frac{d\Omega}{2\pi}. \tag{3.35}$$

These variances are integrated by using the residue theorem described in paragraph 2.3.3. This yields to:

$$\langle \delta x^2 \rangle right\rangle = \frac{1}{M\Gamma_{eff}\Omega_{eff}^2} \left[k_B T\Gamma + \frac{A_- + A_+}{2} \hbar\Omega_m \right], \tag{3.36}$$

$$\langle \delta p^2 \rangle = \frac{M}{\Gamma_{eff}} \left[k_B T\Gamma + \frac{A_- + A_+}{2} \hbar\Omega_m \right]. \tag{3.37}$$

Replacing these variances in the phonon number extracted from Eq.(3.29), one obtains,

$$\langle n_{eff} \rangle = \left(1 + \frac{\Omega_m^2}{\Omega_{eff}^2} \right) \left(\frac{k_B T\Gamma}{2\hbar\Omega_m \Gamma_{eff}} + \frac{A_- + A_+}{4\Gamma_{eff}} \right) - \frac{1}{2}. \tag{3.38}$$

When $\Omega_{eff}^2 = \Omega_m^2$ in Eq.(3.38), one finds the usual expression of the phonon number. However, according to the values of the mechanical nonlinearity, one can have $\Omega_{eff}^2 < \Omega_m^2$, which adds supplemental phonon in the cavity.

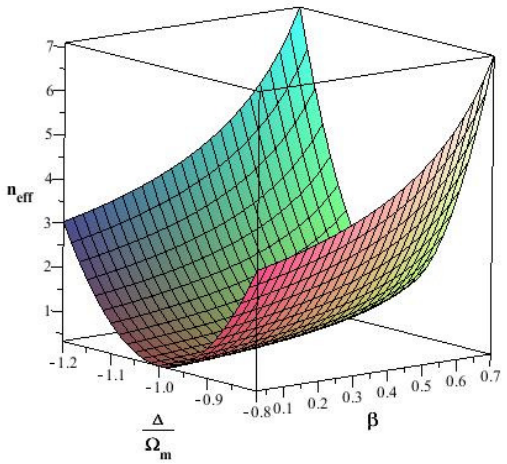

Figure 3.9: *Effective phonon number versus the detuning and mechanical nonlinearity. We see that the minimum phonon number depends on the mechanical nonlinearity.*

Two kinds of phonon are expressed in relation Eq.(3.38). The thermal phonon (n_{th}) which are generated by the Langevin thermal force, and the optical phonon (n_{opt}) gen-

erated by the radiation pressure force one. As previously mentioned in section 1.1,the challenge in optomechanical cooling is to reduce considerably the first one which implies implicitly a reduction of the thermal noise.

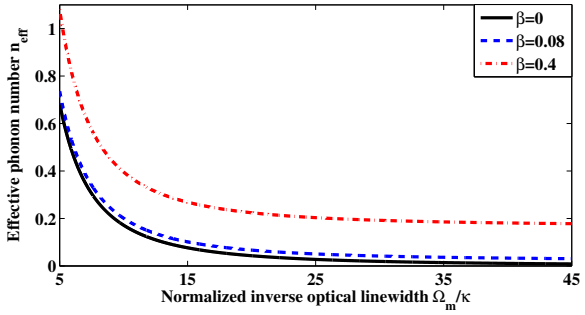

Figure 3.10: *Effect of the mechanical nonlinearity on the effective cooling in the regime of good cavity cooling ($\kappa < \Omega_m$). Cooling becomes less efficient when β increases.*

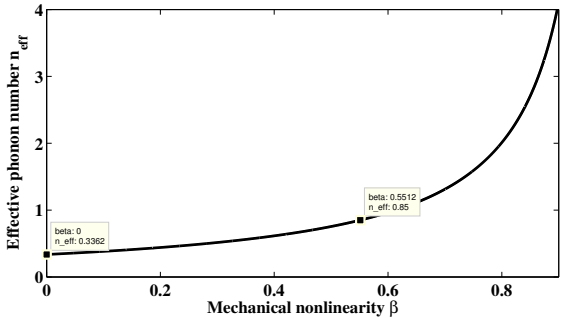

Figure 3.11: *Effect of β on the quantum cooling. The effective phonon number increases when β increase. For $\frac{\Delta}{\Omega_m} = -1$, the phonon number reaches is $n_{eff} = 0.33$ which corresponds to $\beta = 4 \times 10^{-3}$ while $n_{eff} = 0.85$ corresponds to $\beta = 0.55$.*

Figure 3.9 shows that when the mechanical nonlinearity is small (close to zero), the minimum effective phonon number is obtained at the detuning equal to -1. But when the mechanical nonlinearity becomes significant in the system, the minimum phonon number is reached at a detuning different to -1. Another effect of the mechanical nonlinearity is that it limits the cooling phenomenon. Indeed, the increase of the mechanical nonlinearity induces the increase of the effective phonon number (Figs.3.10 and 3.11). Figure 3.10 also reveals that optomechanical systems with high mechanical frequency are more affected by the mechanical nonlinearity effect, while those with low mechanical frequency are less sensitive to the effect of the mechanical nonlinearity since at low frequencies, the gap between the curves is smaller compared to the gap at high frequencies.

The influence of β on optical spring effect, plots versus the normalized detuning, is presented on Fig.3.12. This shows the decrease of the optical spring effect when geomet-

rical nonlinearity increases [94]. This result means that β limits the effects of radiation pressure in optomechanics, and confirms once again the fact that geometrical nonlinearity is a limiting factor for quantum effects in nanomechanics. This conclusion allows us, in the next sections, to look for the effects of geometrical nonlinearity on the generation of non-classical states which are used to enhance quantum applications such as quantum teleportation, quantum cryptography, dense coding, etc.

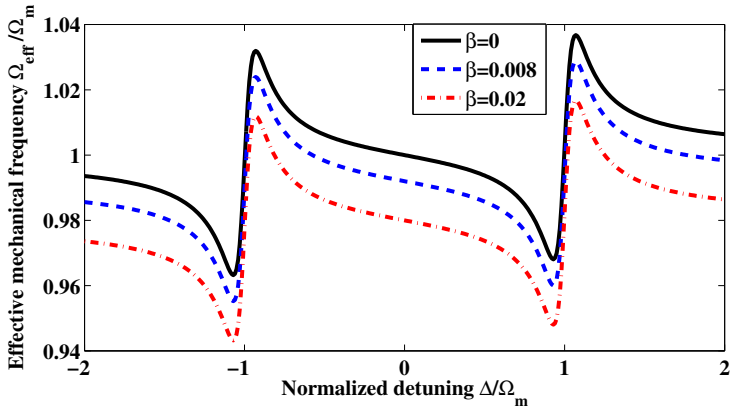

Figure 3.12: *Effect of β on the optical spring effect. The effective mechanical frequency decreases when β increases. This implies an increase of the effective phonon number (see Eq.3.38) and the decrease of optical spring effect, meaning that β limits both quantum cooling and optical effects in optomechanics.*

In order to validate quantitatively our results, we will make some comparisons with those obtained experimentally in Ref. [26]. Experimental minimum phonon number achieved in this work at $\frac{\Delta}{\Omega_m} = -1$ is $\langle n_{eff} \rangle = 0.85 \pm 0.08$. In the absence of nonlinearities ($\eta = \beta = 0$) and at $\frac{\Delta}{\Omega_m} = -1$, the minimum phonon number obtained analytically in our study is $\langle n_{eff} \rangle = 0.33$ (see Fig.3.11). The gap between the experimental result and our theoretical result is $\Delta(\langle n_{eff} \rangle) = 0,51 \pm 0.08$. Our investigation shows that the phonon number of $\langle n_{eff} \rangle = 0.85$ is reaches for $\beta = 0.55$ ($\eta = 0$) at the same detuning value. Since this experiment is carried out with the highest drive power which corresponds to a photon number equal to 2000, one suggests that the device studied in Ref. [26] exhibits a nonlinearity of about $\beta = 0.55$. Indeed, the high photon number used can induce the increase of the nanomechanical displacement and therefore, increases the geometrical nonlinearity.

3.4 Squeezed states generation in the nonlinear quantum optomechanics

This section analyzes the effects of both geometrical (β) and optical (η_0) nonlinearities on the squeezed states generation. The description of the squeezing is presented in paragraph 2.3.3.

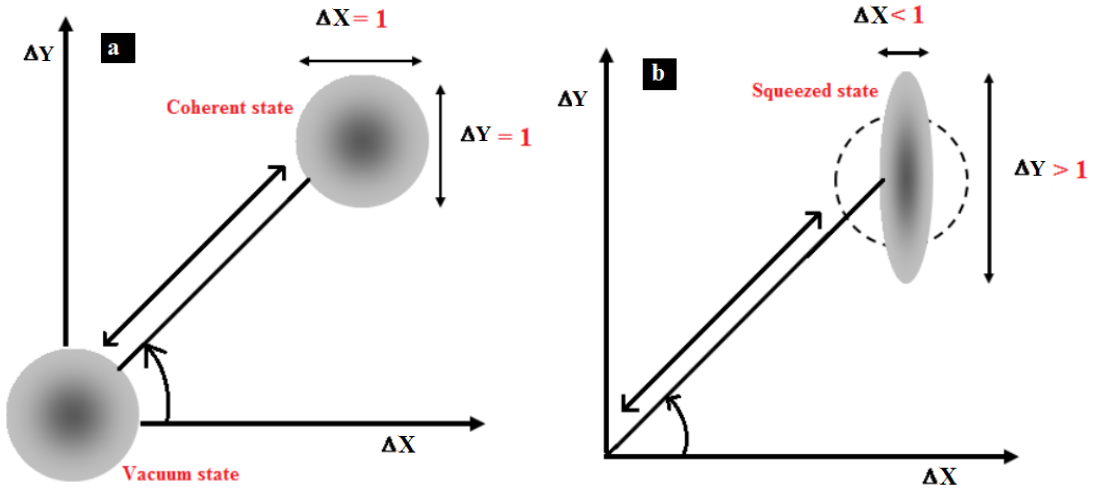

Figure 3.13: *These figures represent coherent (a) and squeezed states (b).*

According to the reduction of quantum fluctuations, squeezed states are useful to improve the quantum applications which are limited by the quantum fluctuations. Among these applications, one can mention quantum teleportation [96–99], quantum information processing [66], dense coding [100], quantum keys distribution [101, 102] and quantum measurement [103].

To generate squeezed states, the common technique consists to use an optical cavity filled with a nonlinear Kerr medium which is fed with an external pumping field. With the recent advances in cooling techniques for nano scale optomechanical systems, various setups have been designed to generate highly squeezed states.

Squeezing of the nanoresonator state produced by periodic measurement of position by a quantum point contact or a single-electron transistor is analyzed in Ref. [50]. The mechanism of this squeezing is the stroboscopic quantum nondemolition measurement generalized to the case of continuous measurement by a weakly coupled detector. The magnitude of squeezing is calculated for the harmonic and stroboscopic modulations of measurement, taking into account detector efficiency and nanoresonator quality factor. In Ref. [104], a parametrically driven nanomechanical resonator capacitively coupled to a microwave cavity is used to squeeze a quadrature of the nanoresonator motion.

Mechanical squeezing of nonlinear optomechanical systems in which an optical cavity mode is coupled quadratically rather than linearly to the position of mechanical oscillator have been studied in Ref. [17]. This mechanical oscillator is driving by two laser beams. The authors of [105] investigate nonlinear effects in an optomechanical system containing a quantum well and show that the transmitted field exhibits strong squeezing at certain hybrid resonance frequencies and system parameters. The quadrature squeezed states of a moving mirror in a Fabry-Perot cavity via a parametric scheme is proposed in Ref. [106]. This is achieved by exploiting the fact that when the cavity is driven by an external field with a large detuning, the moving mirror behaves as a parametric oscillator. It is shown that parametric resonance can be reached approximately by modulating the driving field amplitude at a frequency matching the frequency shift of the mirror. This parametric resonance leads to an efficient generation of squeezing, which is limited by the thermal noise of the environment. Similar scheme, explicitly based on modulation and without condition on the detuning, is used to generate strong squeezing in Ref. [16].

The squeezing of the oscillator amplitude is analyzed via an anharmonic term, originated from the static longitudinal compressive force F_0 close to a critical value at the Euler buckling instability in Ref. [89]. It is shown that this squeezing can be controlled by bringing F_0 close to or far from the critical value F_c.

Squeezed light is obtained from a silicon micromechanical resonator in Ref. [107]. Laser light sent into the cavity is used to measure the fluctuations in the position of the mechanical resonator at a measurement rate comparable to its resonance frequency and greater than its thermal decoherence rate. Despite the mechanical resonator's highly excited thermal state (10^4 phonons), it is observed, through homodyne detection, squeezing of the reflected light's fluctuation spectrum at a level 4.2 ± 0.2 per cent below that of vacuum noise over a bandwidth of a few megahertz around the mechanical resonance frequency of 28 megahertz. With further device improvements, on-chip squeezing at significant levels should be possible, making such integrated micro-scale devices well suited for precision metrology applications. The dissipative nature of the mechanical resonator is used to generate squeezed output light from an optomechanical cavity in Ref. [108]. The squeezing generated in this approach can be directly used to enhance the intrinsic measurement sensitivity of the optomechanical cavity.

In 2014, the Duffing nonlinearity, which behaves as a hardening geometrical nonlinearity, is used to generate robust squeezed state in optomechanics [109]. This work comes one year after ours one [110], which shows that softening geometrical and optical nonlinearities limit the robustness of mechanical and optical squeezed states respectively. Our

study is done at the specific points where these nonlinearities reach their maximum value in the system as we will see in the following sections.

3.4.1 Mechanical squeezing

After neglecting the second order optical nonlinearity as aforementioned in Section 3.2, the NQLEs of the system read,

$$\dot{x}_m = \Omega_m p_m, \tag{3.39a}$$
$$\dot{p}_m = -\Omega_m x_m - \Gamma_m p_m + g_M \alpha^\dagger \alpha + \beta'' + F_{th}, \tag{3.39b}$$
$$\dot{\alpha} = \left[i(\Delta_0 + g_M x_m) - \frac{\kappa}{2} \right] \alpha - iE + \sqrt{\kappa}\alpha^{in}, \tag{3.39c}$$
$$\dot{\alpha}^\dagger = \left[-i(\Delta_0 + g_M x_m) - \frac{\kappa}{2} \right] \alpha^\dagger + iE^* + \sqrt{\kappa}\alpha^{in\dagger}. \tag{3.39d}$$

where $\beta'' = \frac{\beta' x_{ZPF}^2 x_m^3}{\Omega_m}$ and $g_M x_m \alpha$ represent respectively the mechanical and optical anharmonic terms.

For $|\bar{\alpha}| \gg 1$ (satisfied with experimental data or Ref. [26]), one can linearize the above NQLEs by expanding the operators around their steady states: $x_m = \bar{x}_m + \delta x_m$ and $\alpha = \bar{\alpha} + \delta\alpha$. By introducing the vector of quadrature fluctuations $u(t) = (\delta x_m(t), \delta p_m(t), \delta I(t), \delta\varphi(t))^T$ and the vector of noises $n(t) = (0, F_{th}(t), \sqrt{\kappa}\delta I^{in}(t), \sqrt{\kappa}\delta\varphi^{in}(t))^T$, the linearized dynamics of the system can be written in a compact form

$$\dot{u}(t) = Au(t) + n(t), \tag{3.40a}$$

with

$$A = \begin{pmatrix} 0 & \Omega_m & 0 & 0 \\ \Omega_m(\beta - 1) & -\Gamma_m & G & 0 \\ 0 & 0 & -\frac{\kappa}{2} & -\Delta \\ G & 0 & \Delta & -\frac{\kappa}{2} \end{pmatrix}. \tag{3.40b}$$

It should be noted that $\delta I = (\delta\alpha^\dagger + \delta\alpha)$, $\delta\varphi = i(\delta\alpha^\dagger - \delta\alpha)$ are the intracavity quadratures of the intensity and the phase and δI^{in}, $\delta\varphi^{in}$ are their corresponding hermitian input noise operators respectively. The higher order of fluctuations are safely neglected ($|\bar{\alpha}| \gg 1$). The linearized NQLEs show that the mechanical mode is coupled to the cavity mode quadrature fluctuations by the effective optomechanical coupling $G = g_M|\bar{\alpha}|$, which can be made large by increasing the input laser power P_{in}. $\beta = \frac{3\beta' x_{ZPF}^2 x_s^2}{\Omega_m^2}$ and $\Delta = \Delta_0 + g_M x_s$

denote the new dimensionless geometrical nonlinearity and the effective detuning. The range values of the geometrical and optical nonlinearities are given in the Table 3.3. As expected in the Table 3.3, the optical and the mechanical effects are respectively highly pronounced at the optical ($\Delta_0 \approx 0$) and the mechanical ($\Delta_0 \approx \Omega_m$) resonances. This leads us to investigate the squeezing at this particular sidebands. The values of $\bar{x}$ obey the following steady state third order algebraic equation, solved for $P_{in} = 1\,\mathrm{mW}$ and the other parameters of Ref. [26],

$$\bar{x}^3 + \frac{2\Delta x_{ZPF}}{g_M}\bar{x}^2 + (4\Delta^2 + \kappa^2)\frac{x_{ZPF}^2}{4g_M^2}\bar{x} - \frac{4\kappa x_{ZPF}^3 P_{in}}{\hbar\Omega_m\omega_\ell g_M} = 0. \tag{3.41}$$

Detuning Δ_0	Mean displacement of the nanobeam $\bar{x}$(m)	Range of values of nonlinearities
0	2.77×10^{-11}	$\eta \in [2.54\times10^{-3}; 6.79\times10^{-2}]$
	7.42×10^{-10}	$\beta \in [7.87\times10^{-6}; 5.72\times10^{-4}]$
Ω_m	1.27×10^{-13}	$\eta \in [1.17\times10^{-5}; 1]$
	1.09×10^{-8}	$\beta \in [1.66\times10^{-10}; 1.22]$

Table 3.3: *The range of values of the optical nonlinearity η and the geometrical nonlinearity β at the detuning $\Delta = 0$ and $\Delta = \Omega_m$ respectively, using the parameters of Ref. [26].*

In the Fourier space, one obtains the following fluctuations dynamics of the system,

$$B(\Omega)u(\Omega) + n(\Omega) = 0, \tag{3.42a}$$

where

$$B(\Omega) = \begin{pmatrix} i\Omega & \Omega_m & 0 & 0 \\ \Omega_m(\beta-1) & (i\Omega - \Gamma_m) & G & 0 \\ 0 & 0 & (i\Omega - \frac{\kappa}{2}) & -\Delta \\ G & 0 & \Delta & (i\Omega - \frac{\kappa}{2}) \end{pmatrix}. \tag{3.42b}$$

Solving the matrix equation straightforwardly, we obtain the solution for the mechanical displacement operator to be

$$\begin{aligned} \chi_{eff}^{-1}(\Omega)\delta x_m(\Omega) = a_1 G\Omega_m\sqrt{\kappa}\left(\Delta^2 + \frac{\kappa^2}{4} - \omega^2 + i\kappa\Omega\right) \\ \times\left[-\Delta\delta\varphi^{in} + \left(-i\Omega + \frac{\kappa}{2}\right)\delta I^{in}\right] + \Omega_m F_{th}, \end{aligned} \tag{3.43}$$

where

$$a_1 = \left[\left(\Delta^2 + \frac{\kappa^2}{4} - \Omega^2\right)^2 + \kappa^2\Omega^2\right]^{-1}, \tag{3.44}$$

and

$$\chi_{eff}(\Omega) = (\Omega_{eff}^2 - \Omega^2 - i\Omega\Gamma_{eff})^{-1}, \tag{3.45}$$

is the effective susceptibility of the oscillator with the effective resonance frequency and damping rate given by

$$\Omega_{eff}^2(\Omega) = \Omega_m^2\left(1 + a_1 G^2 \frac{\Delta}{\Omega_m}\left(\Delta^2 + \frac{\kappa^2}{4} - \Omega^2\right) - \beta\right), \tag{3.46}$$

$$\Gamma_{eff}(\Omega) = \Gamma_m - a_1 G^2 \Omega_m \Delta\kappa. \tag{3.47}$$

By using the correlation functions of the noise sources for a coherent beam in the frequency domain, the oscillator position and the momentum variances are defined by,

$$\langle\delta x_m^2\rangle = \frac{1}{2\pi}\int_{-\infty}^{+\infty} d\Omega |\chi_{eff}|^2 S_x, \tag{3.48}$$

$$\langle\delta p_m^2\rangle = \frac{1}{2\pi}\int_{-\infty}^{+\infty} d\Omega \frac{\Omega^2}{\Omega_m^2} |\chi_{eff}|^2 S_x, \tag{3.49}$$

where the position noise spectrum is given by

$$\begin{aligned} S_x(\Omega) = {} & a_1 G^2 \Omega_m^2 \frac{\kappa}{2}\left(\Delta^2 - \Omega^2 + \frac{\kappa^2}{4} - i\kappa\Delta\right) \\ & + 2\Gamma_m\Omega_m\Omega\left(1 + \coth\left(\frac{\hbar\Omega}{2k_BT}\right)\right). \end{aligned} \tag{3.50}$$

At the quasi resonant frequency ($\Omega \approx \Omega_m$) and for $\coth\left(\frac{\hbar\Omega}{2k_BT}\right) \approx \frac{2k_BT}{\hbar\Omega}$ (satisfied with experimental parameters used), the exact solutions of integrals (3.48) and (3.49) are given by

$$\langle\delta x_m^2\rangle = \frac{\Omega_m^2}{4\Gamma_{eff}\Omega_{eff}^2} a_2, \tag{3.51}$$

$$\langle\delta p_m^2\rangle = \frac{1}{4\Gamma_{eff}} a_2, \tag{3.52}$$

where

$$a_2 = \frac{\frac{G^2}{\Omega_m^2}\kappa\left(\frac{\Delta^2}{\Omega_m^2} + \frac{\kappa^2}{4\Omega_m^2} - 1 - i\frac{\kappa\Delta}{\Omega_m^2}\right)}{\left(\frac{\Delta^2}{\Omega_m^2} + \frac{\kappa^2}{4\Omega_m^2} - 1\right)^2 + \frac{\kappa^2}{\Omega_m^2}} + 4\Gamma_m\left(1 + \frac{2k_BT}{\hbar\Omega_m}\right). \tag{3.53}$$

These position and momentum variances should satisfy the Heisenberg relation,

$$\langle \delta x_m^2 \rangle \langle \delta p_m^2 \rangle \geq |\frac{1}{2}[x_m, p_m]|^2, \tag{3.54}$$

that is,

$$\langle \delta x_m^2 \rangle \langle \delta p_m^2 \rangle \geq 1, \tag{3.55}$$

since $[x_m, p_m] = 2i$. At the SQL, the coherent states must satisfy $\langle \delta x_m^2 \rangle = \langle \delta p_m^2 \rangle = 1$. When one variance is below the SQL, i.e., $\langle \delta x_m^2 \rangle < 1$ or $\langle \delta p_m^2 \rangle < 1$, the corresponding quadrature is said to be squeezed. According to Eqs. (3.46) and (3.51), only $\langle \delta x_m^2 \rangle$ depends on the geometrical nonlinearity through the term $\frac{\Omega_m^2}{\Omega_{eff}^2}$. Contrariwise, the value of $\langle \delta p_m^2 \rangle$ is obtained by using experimental parameters of Ref. [26] in Eq. (3.52) and it appears to be squeezed up to about 37% (see Fig.3.14). Therefore, the position variance

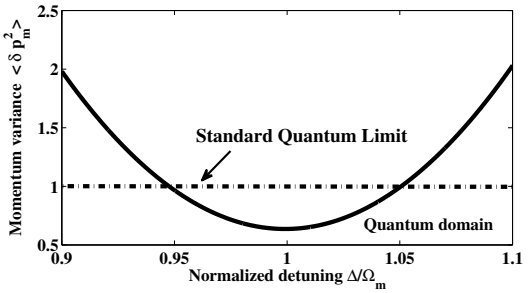

Figure 3.14: *Momentum variance $\langle \delta p_m^2 \rangle$ versus normalized detuning $\frac{\Delta_0}{\Omega_m}$ for $\eta = 0$, using experimental parameters of Table 3.1. The value of $\frac{\Delta_0}{\Omega_m} = 1$ corresponds to the momentum variance $\langle \delta p_m^2 \rangle = 0.6362$ which means that the momentum is squeezed up to about 37%.*

is deduced from the mean energy of the nanoresonator in the steady state,

$$E = \frac{\hbar \Omega_m}{4}(\langle \delta x_m^2 \rangle + \langle \delta p_m^2 \rangle) \equiv \hbar \Omega_m \left(n_{eff} + \frac{1}{2} \right), \tag{3.56}$$

by substituting the effective phonon number with the experimental value $n_{eff} = 0.85 \pm 0.08$ [26]. The value obtained is $\langle \delta x_m^2 \rangle \approx 4.44$ which is unsqueezed (see Fig.3.15). Indeed, the ratio $\frac{\Omega_m^2}{\Omega_{eff}^2}$ increases when β increases (for the high mechanical displacements) and rises up the position variance $\langle \delta x_m^2 \rangle$. So, as the re-thermalization time of the mechanical resonator or the decoherence time, the geometrical nonlinearity limits the squeezing and other quantum effects [111]. In fact, β depends on the bending moment of the resonator and takes into account its internal vibrations. For $\langle \delta x_m^2 \rangle \approx 4.44$, β is evaluated to be about 0.88 (see Fig.3.15) and is in the domain given in Table 3.3 and corresponds to the high mechanical displacements for the nanoresonators [26]. It also appears that for

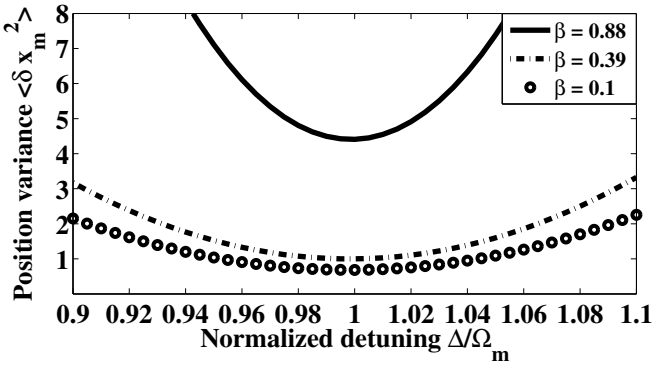

Figure 3.15: *Position variance $\langle \delta x_m^2 \rangle$ versus normalized detuning $\frac{\Delta_0}{\Omega_m}$ for different values of β when $\eta = 0$. The dot dashed line is plotted for $\beta = 0.39$ and corresponds to the SQL ($\frac{\Delta_0}{\Omega_m} = 1$; $\langle \delta x_m^2 \rangle = 1$). The full line is plotted with $\beta = 0.88$ and experimental parameters of Table 3.1. This shows that the position is unsqueezed ($\frac{\Delta_0}{\Omega_m} = 1$; $\langle \delta x_m^2 \rangle \approx 4.44$). The cercled line is plotted for $\beta = 0.1$ and shows that the position is squeezed ($\frac{\Delta_0}{\Omega_m} = 1$; $\langle \delta x_m^2 \rangle \approx 0.69$).*

$\beta = 0.1$, the position variance $\langle \delta x_m^2 \rangle$ is under the standard quantum limit (see Fig.3.15), allowing therefore the squeezing (up to about 31%). In order to investigate the effect of the optical nonlinearity η on the mechanical squeezing, we consider $\eta \neq 0$ in the expression $\frac{\Delta}{\Omega_m} = \frac{\Delta_0}{\Omega_m} + \eta$ which appears in Eqs. (3.51) and (3.52). Figure 3.16 shows the effect of η on the position variance $\langle \delta x_m^2 \rangle$ for $\beta = 0.1$. One remarks on Fig.3.16a that the position variance $\langle \delta x_m^2 \rangle$ becomes unsqueezed for high values of η ($\eta > 0.042$). This effect of η is similar to that of the β shown in Fig.3.15. It appears in Fig.3.16b that η shifts the optimal squeezing towards the left. Since η is always present in optomechanical systems, it is then important to quantify it in experiments in order to determine exactly at which detuning the optimal squeezing can be evaluated. On Fig.3.16c where the two mentioned effects of η are represented, $\langle \delta x_m^2 \rangle$ increases with η and the optimal position squeezing is not always at $\frac{\Delta_0}{\Omega_m} = 1$ but depends on the value of η in the range $\frac{\Delta_0}{\Omega_m} \in [0.9; 1]$. One also notes that the effects of η on the momentum variance are the same as these described on Fig.3.16.

After these analyzes of the geometrical and optical nonlinearities on the mechanical squeezing, the next section investigates their effects on the output optical beam from the cavity.

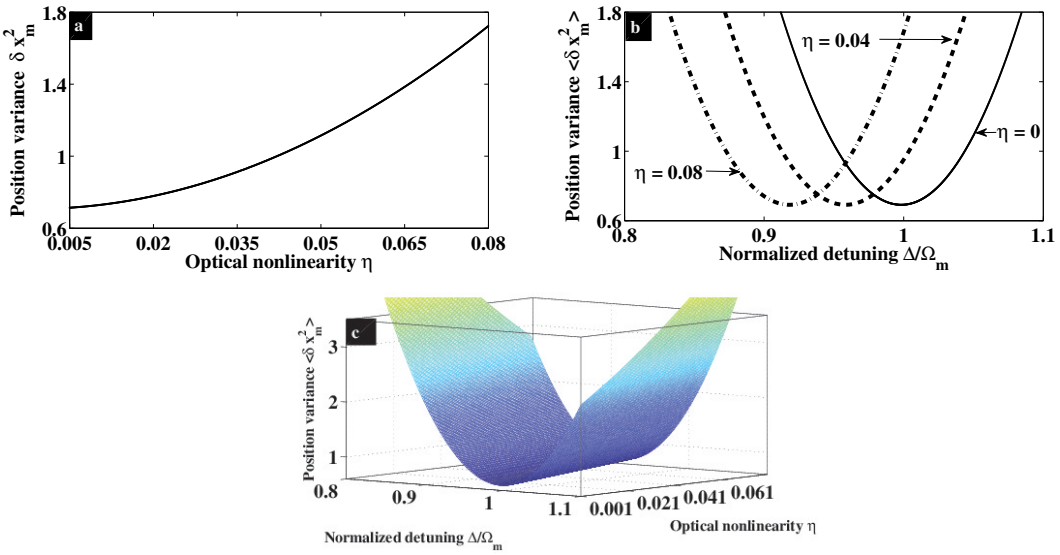

Figure 3.16: *Effect of optical nonlinearity η on the position variance for $\beta = 0.1$. (a) Position variance versus η shows that $\langle \delta x_m^2 \rangle$ becomes unsqueezed when η increases. (b) shows that optimum squeezing shifts towards the left when η increases. (c) shows the combined effects of η on $\langle \delta x_m^2 \rangle$.*

3.4.2 Optical output squeezing

From the matrix equation (3.42a) we also obtain the solutions for the intracavity phase and intensity quadratures operators to be

$$\delta I = -a_3 \left[\Delta G \delta x_m - \Delta \sqrt{\kappa} \delta \varphi^{in} + \sqrt{\kappa} \left(-i\Omega + \frac{\kappa}{2} \right) \delta I^{in} \right], \tag{3.57}$$

and

$$\delta \varphi = a_3 \left[(G \delta x_m + \sqrt{\kappa} \delta \varphi^{in}) \left(-i\Omega + \frac{\kappa}{2} \right) + \Delta \sqrt{\kappa} \delta I^{in} \right], \tag{3.58}$$

with

$$a_3 = \left[\left(-i\Omega + \frac{\kappa}{2} \right)^2 + \Delta^2 \right]^{-1}. \tag{3.59}$$

In order to analyze their squeezing, we use the well-known input-output relation [50]

$$\alpha^{out} = -\alpha^{in} + \sqrt{\kappa} \alpha, \tag{3.60}$$

and then deduce

$$\delta I^{out} = -a_3 \left[\Delta \sqrt{\kappa} G \delta x_m - \Delta \kappa \delta \varphi^{in} + \left(\Omega^2 + \frac{\kappa^2}{4} - \Delta^2 \right) \delta I^{in} \right], \tag{3.61}$$

and

$$\delta\varphi^{out} = a_3\left[\sqrt{\kappa}G\left(-i\Omega+\frac{\kappa}{2}\right)\delta x_m + \left(\Omega^2+\frac{\kappa^2}{4}-\Delta^2\right)\delta\varphi^{in} + \Delta\kappa\delta I^{in}\right]. \tag{3.62}$$

By using the spectral density

$$S_{A^{out}}(\Omega) = \frac{1}{2\pi}\int_{-\infty}^{+\infty} d\omega e^{-i(\Omega+\omega)t}\langle\delta A^{out}(\Omega)\delta A^{out}(\omega)\rangle, \tag{3.63}$$

we obtain the output spectrum of the intensity and phase as,

$$\begin{aligned} S_{I^{out}}(\Omega) &= a_1\Delta^2G^2\kappa|\chi_{eff}|^2S_x(\Omega) + \frac{a_1}{2}\left(\Omega^2+\frac{\kappa^2}{4}-\Delta^2\right)^2 \\ &\quad + a_1\Delta^2\kappa^2 + A(\Omega) - B(\Omega) - C(\Omega), \end{aligned} \tag{3.64}$$

$$\begin{aligned} S_{\varphi^{out}}(\Omega) &= a_1G^2\kappa\left(\frac{\kappa^2}{4}+\Omega^2\right)|\chi_{eff}|^2S_x(\Omega) + \frac{a_1}{2}\left(\Omega^2+\frac{\kappa^2}{4}-\Delta^2\right)^2 \\ &\quad + a_1\Delta^2\kappa^2 + G^2\kappa\Omega_m(D(\Omega)+E(\Omega)), \end{aligned} \tag{3.65}$$

where,

$$A(\Omega) = a\Delta G^2\Omega_m\kappa(\Omega_{eff}^2-\Omega^2)(\Delta-\Omega), \tag{3.66}$$

$$B(\Omega) = b\Delta G^2\Omega_m\kappa\Omega\Gamma_{eff}(\Delta-\Omega), \tag{3.67}$$

$$C(\Omega) = \Delta G^2\frac{\kappa^2}{4}\Omega_m[2b(\Omega_{eff}^2-\Omega^2) - 2a\Omega\Gamma_{eff}], \tag{3.68}$$

$$D(\Omega) = \left[(\Omega_{eff}^2-\Omega^2)\left(\Delta^2+\frac{\kappa^2}{4}-\Omega^2\right)+\kappa\Omega^2\Gamma_{eff}\right]\left(\frac{c}{2}-\Omega d\right)\kappa a_1, \tag{3.69}$$

$$E(\Omega) = \left[\kappa(\Omega_{eff}^2-\Omega^2) - \Gamma_{eff}\left(\Delta^2+\frac{\kappa^2}{4}-\Omega^2\right)\right]\left(\Omega c+\frac{\kappa^2}{2}d\right)\Omega a_1, \tag{3.70}$$

with

$$a = a_1^2\kappa\left[\Delta\left(\Delta^2+\frac{\kappa^2}{4}-\Omega^2\right) - \Omega\left(\Omega^2+\frac{\kappa^2}{4}-\Delta^2\right)\right], \tag{3.71}$$

$$b = a_1^2\left[\left(\Delta^2+\frac{\kappa^2}{4}-\Omega^2\right)\left(\Omega^2+\frac{\kappa^2}{4}-\Delta^2\right)+\Delta\kappa^2\Omega\right], \tag{3.72}$$

$$c = 2(\Omega-\Delta)\left(\Omega^2+\frac{\kappa^2}{4}-\Delta^2\right)+\kappa^2\Delta \tag{3.73}$$

$$d = 2\Delta(\Omega-\Delta) - \left(\Omega^2+\frac{\kappa^2}{4}-\Delta^2\right). \tag{3.74}$$

In Eqs. (3.64) and (3.65), the first terms are proportional to the position spectrum S_x (Eq. (3.50)) and to the effective mechanical susceptibility (Eq. (3.45)). These terms derive from the mechanical fluctuations of the oscillator. The other terms in Eqs. (3.64) and (3.65) originate to the fluctuations of the input beam. Assuming that the system is in the quasi resonant regime ($\Omega \approx \Omega_m$), all the contributions related to the input beam fluctuations take constant values. The expressions (3.64) and (3.65) can now be integrated. By using the residue theorem, one easily obtains

$$\langle \delta I^{out\,2} \rangle = \frac{\frac{\Delta^2}{\Omega_m^2}\frac{G^2}{\Omega_m^2}\kappa}{\left(\frac{\Delta^2}{\Omega_m^2}+\frac{\kappa^2}{4\Omega_m^2}-1\right)^2+\frac{\kappa^2}{\Omega_m^2}}\langle \delta x_m^2 \rangle, \tag{3.75}$$

and

$$\langle \delta \varphi^{out\,2} \rangle = \frac{\left(1+\frac{\kappa^2}{4\Omega_m^2}\right)\frac{G^2}{\Omega_m^2}\kappa}{\left(\frac{\Delta^2}{\Omega_m^2}+\frac{\kappa^2}{4\Omega a_m^2}-1\right)^2+\frac{\kappa^2}{\Omega_m^2}}\langle \delta x_m^2 \rangle, \tag{3.76}$$

where $\langle \delta x_m^2 \rangle$ is given by Eq. (3.51).

At the mechanical resonance ($\Delta \approx \Omega_m$) where it is established above that the position variance is unsqueezed ($\langle \delta x_m^2 \rangle = 4.44$), we deduce from Eqs. (3.75) and (3.76) that both optical variances are unsqueezed. However, the effective detuning $\Delta \approx \Delta_0 + g_M \bar{x}_m$ leads at the optical resonance ($\Delta_0 = 0$) to

$$\frac{\Delta}{\Omega_m} \approx \frac{g_M \bar{x}_m}{\Omega_m} = \eta. \tag{3.77}$$

Figure 3.17 shows that ΔI^{out} is squeezed when $|\eta| \leq 7.44 \times 10^{-5}$ which is obtained with

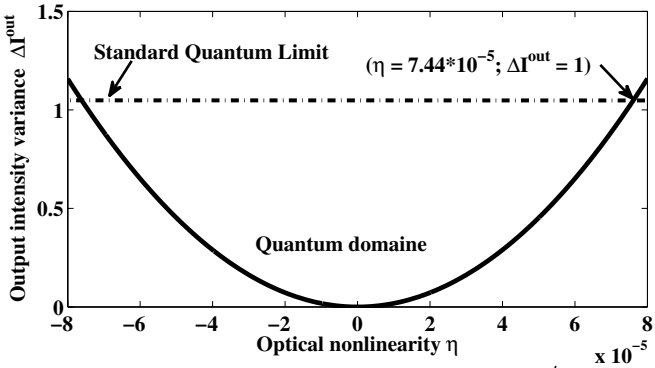

Figure 3.17: *Mean square fluctuation of the output light ΔI^{out} versus the optical nonlinearity η for $\beta = 5.72 \times 10^{-4}$. With the low input power used for the system $P_{in} \leq 30\,\mu$W [112], the output intensity is squeezed ($|\eta| \leq 7.44 \times 10^{-5}$).*

the input power $P_{in} \leq 30\,\mu$W [112]. This means that at the optical resonance and for the

low input power, the optomechanical cavity behaves as an optical filter or *noise eater* [93]. Thus, the quantum fluctuations (shot noise) in the input coherent laser beam ($\Delta I^{in} = 1$) are reduced after been reflected out of the optomechanical cavity ($\Delta I^{out} < 1$). To improve this squeezing at the optical resonance one can increase η (for the negative values of the detuning) or decrease η (for the positive values of the detuning) (see Fig.3.17). By using Eqs.(3.39c) and (3.60), one can expressed output field as

$$\alpha^{out} = \frac{a_4 + i a_5}{\left(\frac{\Delta_0}{\Omega_m} + \eta - 1\right)^2 + \frac{\kappa^2}{4\Omega_m^2}}, \tag{3.78}$$

with

$$a_4 = \frac{\kappa^2}{4\Omega_m^2}\alpha^{in} + \left(\frac{\Delta_0}{\Omega_m} + \eta - 1\right)\left(\left(\frac{\Delta_0}{\Omega_m} + \eta - 1\right)\alpha^{in} + \frac{\sqrt{\kappa}}{\Omega_m}E\right), \tag{3.79}$$

$$a_5 = \left(\left(\frac{\Delta_0}{\Omega_m} + \eta - 1\right)\frac{\kappa}{\Omega_m}\alpha^{in} - \frac{\kappa\sqrt{\kappa}}{2\Omega_m^2}E\right), \tag{3.80}$$

where $E^{in} = \sqrt{\frac{2\kappa P_{in}}{\hbar\Omega_m}}$. One remarks that α^{out} depends only on the optical nonlinearity which allows us to quantify his effect on the output field. Figure 3.18a shows that the output field decrease when η increases. This means that it is important to control the value of η in order to obtain the output field needed. This control of η also gives the value of the detuning at which the output field is optimal (see Fig.3.18b). Figure 3.18c shows the two mentioned effects of η on the output field α^{out}. It is also found that, as for the position, the decrease of temperature induces an improvement of intensity squeezing. Regarding the geometrical nonlinearity, it contributes to reduce the squeezing when it becomes large. But, it is generally weak around the optical resonance (see Table 3.3), so its effects are neglected at this sideband.

Another important quantum application which is enhanced at the quantum ground state is the entanglement. The following section analyzes effect of geometrical nonlinearity on the generation of continuous variable (CV) entangled states.

3.5 Entanglement in the nonlinear quantum optomechanics

As a Einstein-Podolsky-Rosen state (EPR), an entangled state characterizes (quantum) intrication between elements of m-partite system ($m > 1$). When the entanglement is ro-

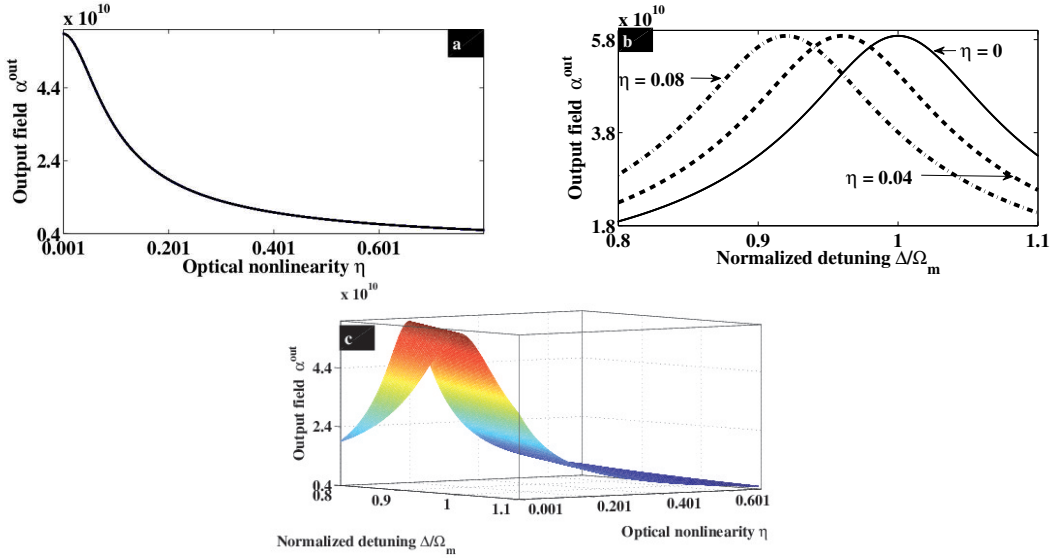

Figure 3.18: *Effect of optical nonlinearity η on the output field. (a) Output field versus η shows that α^{out} decreases when η increases. (b) The optimal output field shifts towards the left when η increases. (c) Combined effects of η on α^{out}.*

bust, the corresponding states can be used to improve the sharing information in quantum network applications [66, 96–103] and for quantum computational tasks [113].

Entanglement is considered as a distinguishing feature that separates quantum from classical physics and then, it can be used to inform us about the quantum theory's limit [114]. This is for example why scientists are interested nowadays to know difference between quantum entanglement and classical synchronization [115–117]. This study does not given a satisfactory conclusion and this research field remains an actual preoccupation.

There are two types of entanglement depending on the fact that the variables used are discrete [85, 118] or continuous. Our study is focused on the continuous variables entanglement according to their easy manipulation in an experimental context.

According to the great interest attached to the nanomechanics during this last decade, optomechanical systems, superconducting microwave cavities and hybrid systems have been very recently used as a novel tool for generating strong CV entangled quantum states. This consists to couple optical and/or microwave mode to the mechanical mode of the resonator which vibrates under the electromagnetic field. There are many configurations which have been proposed to this end. In [119], stationary entanglement between optical field and mechanical mode of vibrating end mirror is generated from optical Fabry-Perot cavity. Strong quantum correlation between the mirror and the optical Stokes sideband is explained in [120] as being generated by a scattering process. The configuration used in [121] consists of a whispering-gallery mode (WGM) cavity with a

movable boundary. Entanglement between mechanical and radiation mode is achieved in [74] by using a suitable modulation of the driving field. Pulsed field is used to create EPR-type entanglement between mechanical mode and light pulses and microwave pulses respectively in optomechanical cavity [97] and microwave cavity [122]. In [100], a membrane-in-the-middle geometry is used to generate output entangled light from a fixed end Fabry-Perot cavity. The optical-microwave quantum interface is used in [123, 124] to produce robust entangled signal which can be used for high-fidelity transfer of quantum states between optical and microwave fields. All these schemes aim to generate robust entangled states against decoherence which limits their lifetime [99] and their performance in quantum applications. This decoherence is often manifested by various factors such as the stability conditions that place constraints on the magnitude of the effective optomechanical couplings and the thermal noise of the mechanical mode.

3.5.1 Dynamical equations

We proposed here a scheme based on the geometrical nonlinearity which generates robust entangled states against thermal decoherence [125]. The study is done at the blue detuning and the parameters are those of Table 3.1. We assume that range of the nonlinearity β is given in the Tables (3.2) and (3.3).

To analyze the stability of our system, we have used the Routh-Hurwitz criterion which yields the two following nontrivial conditions on the system parameters,

$$\begin{aligned} s_1 = \Gamma_m\kappa\Bigg\{&\left[\frac{\kappa^2}{4}+(\Omega_m-\Delta)^2\right]\left[\frac{\kappa^2}{4}(\Omega_m+\Delta)^2\right] \\ &+\Gamma_m\left[(\Gamma_m+\kappa)\left(\frac{\kappa^2}{4}+\Delta^2\right)+\kappa\Omega_m^2\right]\Bigg\}-\Delta\Omega_m G^2(\Gamma_m+\kappa)^2>0, \end{aligned} \tag{3.81}$$

$$s_2 = \Omega_m\left(\Delta^2+\frac{\kappa^2}{4}\right)+G^2\Delta>0. \tag{3.82}$$

With respect to physical parameters in Table 3.1, these stability conditions lead at the blue sideband of the cavity ($\Delta=-\Omega_m$) to $G<2.26\times10^{10}\,\mathrm{s}^{-1}$ or $\alpha_s<2.07\times10^3$ while at the red sideband ($\Delta=\Omega_m$), one has $G<2.89\times10^7\,\mathrm{s}^{-1}$ or $\alpha_s<0.26$. Optomechanical entanglement is then possible within the blue sideband detuning range where the coupling is strong. We describe the mirror Brownian noise $F_{th}(t)$ as,

$$\frac{1}{2}\langle F_{th}(t)F_{th}(t')+F_{th}(t')F_{th}(t)\rangle\approx\Gamma_m(2n_{th}+1)\delta(t-t'), \tag{3.83}$$

which is delta-correlated [66], with the mean thermal excitation number sets as $n_{th}=$

$(e^{\hbar\Omega_m/k_BT}-1)^{-1}$. This means that $F_{th}(t)$ is a Markovian process. As the parameters used here lead to a large mechanical factor, $Q=\frac{\Omega_m}{\Gamma_m}\approx 1.05\times 10^5 \gg 1$, the quantum effects can be achieved.

Since the quantum noises F_{th} and α^{in} are zero-mean quantum Gaussian noises and the dynamics is linearized, the quantum steady state for the fluctuations is a zero-mean bipartite Gaussian state, fully characterized and described as in subsection 2.3.4. This description allows us to quantity the Gaussian CV entanglement in our system. Thus, we use the definition of the logarithmic negativity $E_{\mathcal{N}}$ (Eq.2.66) for this purpose and the system is said to be entangled if only $E_{\mathcal{N}}>0$.

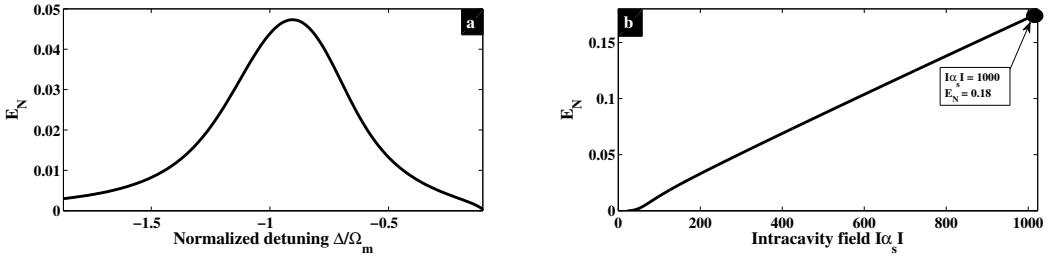

Figure 3.19: *Linear regime obtained with the physical parameters in Tab.3.1. (a) Logarithmic negativity $E_{\mathcal{N}}$ versus normalized detuning $\frac{\Delta}{\Omega_m}$. The entanglement is maximal around the blue-detuning $\frac{\Delta}{\Omega_m}=-1$. (b) Logarithmic negativity $E_{\mathcal{N}}$ versus intracavity field with high input power $P_0=10\,\mathrm{mW}$. The entanglement is enhanced for high input power.*

3.5.2 Effect of geometrical nonlinearity on stationary entanglement

The parameters of Table 3.1 not only satisfy our aforementioned stability conditions, but also lead to a generation of a lightly mechanical and optical mode entanglement in linear regime. This entanglement, which is present only in a finite interval of detuning values around the blue-sideband $\frac{\Delta}{\Omega_m}=-1$ (Fig.3.19a), can be increased by significant optomechanical coupling as shown in [90,119,121], which consists for example to increase the input power P_{in}. This is shown on Figure 3.19b where the high power is $P_0=10\,\mathrm{mW}$, which corresponds to the intracavity field of $|\alpha_s|=10^3$, and is in accordance both with current state-of-art optics and our stability condition. The above value of intracavity field have been recently used to generate entangled states [121] and squeezed states [124] in optomechanical systems. Such a high input power induces large mechanical displacement of the nanoresonator which exhibits a geometrical nonlinearity in the system [65,97,112]. A more interesting situation is depicted in Fig.3.20a which represents the logarithmic negativity versus the normalized detuning for different values of nonlinear parameter

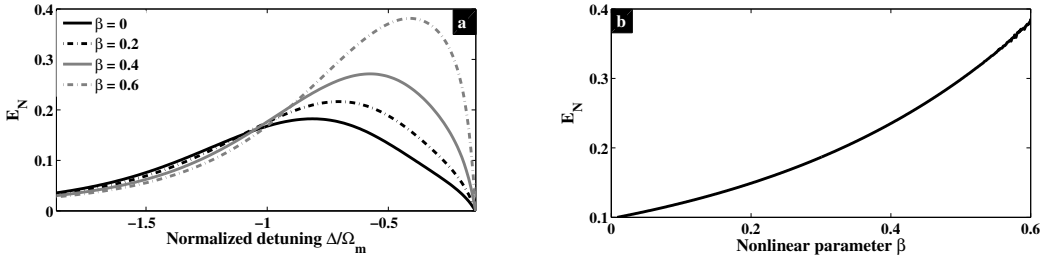

Figure 3.20: *These figures are plotted for an input power of $P_0 = 10\,\mathrm{mW}$ and the others parameters are those in Tab.3.1. (a) The logarithmic negativity versus the normalized detuning for different values of geometrical nonlinearity. The increase of nonlinear parameter enhances the entanglement and shifts its maximum value towards high detuning values (compare gray dash-dots line and full black line). (b) The logarithmic negativity versus the geometrical nonlinearity for $\frac{\Delta}{\Omega_m} = -0.5$. This shows the robustness of the entanglement in the presence of geometrical nonlinearity.*

β. One remarks that the entanglement increment is related to the increasing of the nonlinear parameter for $\frac{\Delta}{\Omega_m} \in [-1.1; -0.16]$, with a significant enhancement around the normalized detuning $\frac{\Delta}{\Omega_m} = -0.5$. In other terms, the entanglement becomes robust with the nonlinearity within the above interval of $\frac{\Delta}{\Omega_m}$. In the case where $\beta = 0$ (linear case), the optimal entanglement remains near $\Delta = -\Omega_m$ (full black line on Fig.3.20a), and for $\beta \neq 0$ it is shifted towards high detuning values (other curves on Fig.3.20a). Reverse effects are induced on entanglement in [126] and [119] by the resonator mass and the Kerr nonlinearity respectively. This means that softening nonlinear effect study here is a promising way to improve quantum information processing such as quantum teleportation and quantum key distribution. For the small normalized detuning values, $\frac{\Delta}{\Omega_m} \in [-2; -1.1]$, the increase of the nonlinearity induces a decrease of the entanglement. However, this opposite effect of the parameter β on the entanglement is not important in the system. In

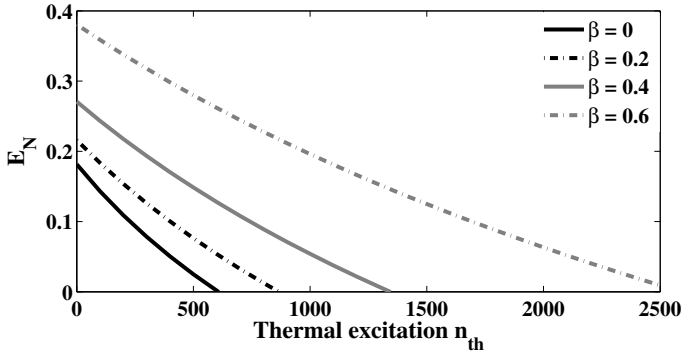

Figure 3.21: *Plot of the logarithmic negativity versus the mean bath occupation for different values of nonlinear parameter with an input power of $P_0 = 10\,\mathrm{mW}$. This shows the robustness of entanglement against thermal decoherence depending on the nonlinear term. For $\beta = 0.6$ this robustness persists far to $n_{th} = 2500$ (gray dash-dots line).*

Fig.3.20b we have fixed the normalized detuning at $\frac{\Delta}{\Omega_m} = -0.5$ and varied the nonlinear parameter β. This curve shows the robustness of entanglement when the nonlinearity increases in the system. Thus, in the system which exhibits geometrical nonlinearity, the optimal entanglement depends on the value of the detuning and should be checked around the detuning $\frac{\Delta}{\Omega_m} = -0.5$ but not around $\frac{\Delta}{\Omega_m} = -1$ as in linear system [119].

Finally, Fig.3.21 shows the robustness of the entanglement against the environmental temperature in the presence of such nonlinearity. As expected, in the linear regime ($\beta = 0$), there is a decrease of the entanglement with respect to the bath temperature. However, the entanglement persists until $n_{th} = 600$ or $T = 98\,\mathrm{K}$, which is several order magnitude larger than the temperature needed to cool a mechanical resonator to its quantum ground state. This enlightens the performance of the system studied here to resist to thermal decoherence. Figure 3.21 mostly reveals that by increasing the geometrical nonlinearity, one definitely improve the robustness of the entanglement against thermal decoherence in an optomechanical system. Indeed, gray dash-dots shows that entanglement persists until $n_{th} = 2500$, which corresponds to the room temperature. It should be noted that similar results have recently been found in [120] and [124] with the inverse bandwidth and quantum optomechanical interface respectively. Particularly in [124], where the hybrid system is studied, the entanglement remains strong even for $n_{th} = 10^4$ which is greater than that found here ($n_{th} = 2500$). This may be understood by the fact that hybrid systems combine two optomechanical couplings, optical and microwave couplings, to drive a nanoresonator.

Since the physical parameters used here have been recently experimented and the fact that they satisfy the system's stability condition for the feasible input power of $P_0 = 10\,\mathrm{mW}$, our results can then be implemented. This technique of entanglement which used the geometrical nonlinearity is further promising to observe the quantum effects even for high environmental temperatures. This could lead to the improvement of the robustness of quantum teleportation protocols and other quantum applications.

3.6 Conclusion

In this chapter we have studied the nonlinear effects in optomechanics.

In the classical limit, we have shown that the geometrical nonlinearity reduces the mechanical amplitudes of the nanomirror. In the semiclassical limit, the combined effects of quantum noises and geometrical nonlinearity allow to obtain similar results than those of the quantum limit. It is also shown that these combined effects reduce optical bistability

in the system studied.

The effect of geometrical nonlinearity on the quantum ground state achievement is shown to be the same as the one of the thermal decoherence. Thus, by reducing the effect of the geometrical nonlinearity, we have shown how it is possible to reduce the thermal decoherence in quantum mechanics. This opens a way to a long time quantum effects observation in optomechanics.

For the generation of the nonclassical states, we have found that both geometrical and optical nonlinearities limit the robustness of the squeezing at certain points. Indeed, at the mechanical and optical resonance where geometrical and optical nonlinearities reach their maximum respectively, the squeezing is limited by nonlinear effect. However, the robustness of entanglement against thermal decoherence is proved at the blue detuning.

In the next chapter, we will used a quadratic coupling, exhibited from superconducting microwave circuit, to control the dynamical behavior of a nanoresonator. The effect of this coupling will be also investigated on ground state cooling and on the entanglement.

General Conclusion

The main purpose of this thesis was to analyze the effects of nonlinearities on quantum ground state achievement and on the quantum states generation in order to improve quantum applications. To do this, we have organized our thesis in three chapters.

The first chapter overviews the progresses done in the field of quantum ground state cooling. This chapter allows us to bring out the challenge of this field and then to state the problem that we try to solve.

In the second chapter, we have described the rate equations of optomechanical systems. The mathematical formalism as well as the numerical methods used for our analysis are presented and explained. Analytical formalism used to generate squeezed and entangled states are also briefly explained.

The main results obtained are presented in the third chapter and are summarized in the following points: The first point studied the effect of geometrical nonlinear term as well as the quantum noises on both the dynamical system behavior and optical bistability. Indeed, we have shown that geometrical nonlinearity reduces the mechanical amplitudes of vibration in classical limit. This means that it can be used to control instabilities in an optomechanical system. In semiclassical limit, the combined effect of geometrical nonlinearity and the operator's noises has produced the results which are similar to those in the quantum limit. As the dynamics in nano-scale is better described in quantum mechanical terms, this result means that, nonlinearity and noise should be taking into account to give a good dynamical behavior of a nano-structure. This result is confirmed when we have studied the optical bistability in the system. Indeed, we have shown that the combined effect of geometrical nonlinearity and noises reduces the optical bistability, which is the signature of instabilities in the system (jump phenomenon here).

In the second point, we have shown that geometrical nonlinearity behaves as a thermal decoherence and then, limits the ground state cooling in nanomechanics. To improve cooling in this situation, we have shown that an increase of the mechanical frequency reduces intensity of geometrical nonlinear, inducing an increase of the thermal decoherence time. This is a good thing for quantum applications which can then be observed in a longer

time. This result shows how it is necessary to build very high finesse optomechanical cavities having the GHz frequency range.

In the third point, we have shown that the CV mechanical squeezing is limited by the geometrical nonlinearity at the mechanical resonance where it reaches its maximum value. Optical CV squeezing is shown to be limited by the optical resonance at the optical resonance where it also reaches its maximum value.

The fourth point is devoted to the generation of CV entanglement based on the geometrical nonlinearity. Precisely, we have generated the CV entanglement at the blue sideband detuning and we have shown how geometrical nonlinearity enhances the robustness of this entanglement even against thermal decoherence.

Outlook

Here, we highlight some points which can further improve the present work. Firstly, deeply dynamical study of this system regarding to the geometrical nonlinear term is necessary. In fact, as the nonlinear effect can be used for the classical control of the system, we think that it has a profound influence on the different phase transition points. Secondly, we intend to deeply investigate on the fact that a reduction of nonlinear term induce the decoherence suppression, in order to further explain this result. This will be more important for the improvement of the quantum applications. Thirdly, the sideband detuning at which the squeezing can be enhanced by the nonlinear term must be checked. This will enhance the quantum information processing.

As the geometrical nonlinearity is used to generate robust CV entanglement, it can be used to perform applications such as quantum teleportation, quantum cryptography and dense coding protocol.

In order to further cool close to the quantum ground state, we think that both the effects of geometrical and quadratic nonlinearities should be investigated in the superconducting microwave circuits capacitively coupled. Since the gap between the two gates of the coupling capacitance in such systems is small ($\lesssim 100\,\mathrm{nm}$), then the effects of both Casimir and Wan der waals forces on the quantum ground state cooling should also be checked.

In the nearest future, we intend to show the effect of quantum synchronization in quantum sharing information. This preoccupation comes from the fact that we need to quantify the performance of quantum sharing information based one hand on entanglement and the other hand on quantum synchronization.

Bibliography

[1] Von R. Frisch, Expementeller Nachweis des Einsteinschen Strahlungsrüsckstobes, Zeitschrift für Physik B **86**, 42 (1933).

[2] R. A. Beth, Mechanical Detection and Measurement of the Angular Momentum of Light, Phys.Rev. **50**, 115 (1936).

[3] S. Stenholm, The semiclassical theory of laser cooling, Rev. Mod. Phys. **58**, 699 (1986)

[4] T. W. Hansch and A. L. Schawlow, Cooling of gases by laser radiation, Optics Communications **13**, 68 (1975).

[5] D. J. Wineland, R. E. Drullinger and F. L. Walls, Radiation-pressure cooling of bound resonant absorbers, Phys. Rev. Lett. **40**,1639 (1978).

[6] S. Chu, L. Hollberg, J. E. Bjorkholm, A. Cable and A. Ashkin, 3-dimensional viscous confinement and cooling of atoms by resonance radiation pressure, Phys. Rev. Lett. **55**, 48 (1985).

[7] A. Ashkin, Applications of laser radiation pressure, Science **210**,1081 (1980).

[8] A. Ashkin, J. M. Dziedzic, J. E. Bjorkholm and S. Chu, Observation of a single-beam gradient force optical trap for dielectric particles, Optics Letters **11**, 288 (1986).

[9] H. J. Metcalf and P. van der Straten, Laser Cooling and Trapping, Springer-Verlag New York, p. 317 (1999).

[10] I. Bloch, J. Dalibard, W. Zwerger, Many-body physics with ultracold gases, Rev. Mod. Phys. **80**, 885 (2008).

[11] F. Diedrich, J. C. Bergquist, Wayne M. Itano and D. J. Wineland, Laser cooling to the zero-point energy of motion, Phys. Rev. Lett.**62**(4), 406 (1989).

[12] D. Leibfried, R. Blatt, C. Monroe and D. Wineland, Quantum dynamics of single trapped ions, Rev. Mod. Phys. **75**(1), 324 (2003).

[13] W. M. Itano, J. C. Bergquist, J. J. Bollinger and D. J. Wineland, Laser cooling of trapped ions, Laser Manipulation of Atoms and Ions, North-Holland, Amsterdam, p.p. 519-537 (1992).

[14] S. Gigan, H. R. Bohm, M. Paternostro, F. Blaser, G. Langer, J. B. Hertzberg, K. C. Schwab, D. Bauerle, M. Aspelmeyer and A. Zeilinger, Self-cooling of a micromirror by radiation pressure, Nature (London) **444**, 67 (2006).

[15] O. Arcizet, P.-F. Cohadon, T. Briant, M. Pinard and A. Heidmann, Radiation-pressure cooling and optomechanical instability of a micromirror, Nature (London) **444**, 71 (2006).

[16] A. Schliesser, P. DelHaye, N. Nooshi, K. J. Vahala and T. J. Kippenberg, Radiation Pressure Cooling of a Micromechanical Oscillator Using Dynamical Backaction, Phys. Rev. Lett. **97**, 243905 (2006).

[17] I. Wilson-Rae, N. Nooshi, W. Zwerger and T. J. Kippenberg, Theory of Ground State Cooling of a Mechanical Oscillator Using Dynamical Backaction, Phys. Rev. Lett. **99**, 093901 (2007).

[18] I. Favero and K. Karrai, Cavity cooling of a nanomechanical resonator by light scattering, New J. Phys. **10**, 095006 (2008).

[19] A. Schliesser, O. Arcizet, R. Rivière, G. Anetsberger and T. J. Kippenberg, Resolved-sideband cooling and position measurement of a micromechanical oscillator close to the Heisenberg uncertainty limit, Nature Physics **5**, 509 (2009).

[20] A. Naik, O. Buu, M. D. LaHaye, A. D. Armour, A. A. Clerk, M. P. Blencowe and K. C. Schwab, Cooling a nanomechanical resonator with quantum back-action, Nature **443**, 193 (2006).

[21] S. Gröblacher, J. B. Hertzberg, M. Vanner, G. Cole, S. Gigan, K. C. Schwab and M. Aspelmeyer, Demonstration of an ultracold microoptomechanical oscillator in a cryogenic cavity, Nature Physics **5**, 485 (2009).

[22] A. Nunnenkamp, K. Børkje, J. G. E. Harris and S. M. Girvin, Cooling and squeezing via quadratic optomechanical coupling, Phys. Rev. A **82**, 021806(R) (2010).

[23] A. Mari and J. Eisert, Gently Modulating Optomechanical Systems, Phys. Rev. Lett.**103**, 213603 (2009); A. Mari and J. Eisert, Opto- and electro-mechanical entanglement improved by modulation, New J. Phys. **14**, 075014 (2012); A. Farace and V. Giovannetti, Enhancing quantum effects via periodic modulations in optomechanical systems, Phys. Rev. A **86**, 013820 (2012).

[24] C. Yang, Progress Toward Observing Quantum Effects in an Optomechanical System in Cryogenics, PhD Thesis, Yale University, 2011.

[25] Y. Hadjar, Etude du couplage optomécanique dans une cavité de grande finesse. Observation du mouvement Brownien d'un miroir, Ph.D. thesis, Université Paris VI (2004).

[26] P. Rabl, C. Genes, K. Hammerer and M. Aspelmeyer, Phase-noise induced limitations on cooling and coherent evolution in optomechanical systems, Phys. Rev. A **80**, 063819 (2009).

[27] G. A. Phelps and P. Meystre, Laser phase noise effects on the dynamics of optomechanical resonators, Phys. Rev. A **83**, 063838 (2011).

[28] M. Abdi, Sh. Barzanjeh, P. Tombesi and D. Vitali, Effect of phase noise on the generation of stationary entanglement in cavity optomechanics, Phys. Rev. A **84**, 032325 (2011).

[29] T. J. Kippenberg, A. Schliesser and M. L. Gorodetsky, Phase noise measurement of external cavity diode lasers and implications for optomechanical sideband cooling of GHz mechanical modes, New J. Phys. **15**, 015019 (2013).

[30] A. H Safavi-Naeini, J. Chan, J. T. Hill, S. Gröblacher, H. Miao, Y. Chen, M. Aspelmeyer and O. Painter, Laser noise in cavity-optomechanical cooling and thermometry, New J. Phys. **15**, 035007 (2013).

[31] M. Aspelmeyer, T. J. Kippenberg, F. Marquardt, Cavity Optomechanics, arXiv:1303.0733v1.

[32] J. Chan, T. P. Mayer Alegre, A. H. Safavi-Naeini, J. T. Hill, A. Krause, S.Gröblacher, M. Aspelmeyer and O.Painter, Laser cooling of a nanomechanical oscillator into its quantum ground state Nature (London) **478**, 89 (2011); S. Meenehan, J. D. Cohen,

S. Gröblacher, J. T. Hill, A. H. Safavi-Naeini, M. Aspelmeyer and O. Painter, Thermalization properties at mk temperatures of a nanoscale optomechanical resonator with acoustic-bandgap shield, arXiv:1403.3703v1.

[33] J. D. Teufel, T. Donner, Dale Li, J. W. Harlow, M. S. Allman, K. Cicak, A. J. Sirois, J. D. Whittaker, K. W. Lehnert and R. W. Simmonds, Sideband cooling of micromechanical motion to the quantum ground state, Nature **475**, 359 (2011).

[34] A. D.O'Connell, M. Hofheinz, M. Ansmann, R. C. Bialczak, M. Lenander, Erik Lucero, M. Neeley, D. Sank, H. Wang, M. Weides, J. Wenner, J. M. Martinis and A. N. Cleland, Quantum ground state and single-phonon control of a mechanical resonator, Nature **464**, 697 (2010).

[35] M. Aspelmeyer, P. Meystre and K. Schwab, Quantum optomechanics, Phys. Today **65**(7), 29 (2012).

[36] V. B. Braginsky, Y. I. Vorontsov and K. Thorne, Quantum Nondemolition Measurements, Science **209**, 557 (1980).

[37] V. B. Braginsky and F. Ya. Khalili, Quantum nondemolition measurements: the route from toys to tools, Rev. Mod. Phys. **68**, 11(1996).

[38] V. B. Braginsky, M. L. Gorodetsky, F. Ya. Khalili, A. B. Matsko, K. S. Thorne and S. P. Vyatchanin, Noise in gravitational-wave detectors and other classical-force measurements is not influenced by test-mass quantization, Phys. Rev. D **67**, 082001 (2003).

[39] M. I. Dykman, Heating and cooling of local and quasilocal vibrations by a nonresonance field, Soviet Physics - Solid State, **20**, 1311 (1978).

[40] A. Dorsel, J. D. McCullen, P. Meystre, E. Vignes and H. Walther, Induced by Radiation Pressure Optical Bistability and Mirror Confinement, Phys. Rev. Lett. **51**, 1550 (1983).

[41] V. B. Braginskii and A. B. Manukin, Ponderomotive effects of electromagnetic radiation, Soviet Physics JETP Letters **25**(4), 655 (1967).

[42] V. B. Braginskii, A. B. Manukin and M. Yu. Tikhonov, Investigation of dissipative ponderomotive effects of electromagnetic radiation, Soviet Physics JETP **31** 830 (1970).

[43] V. B. Braginsky and A. B. Manukin, Measurement of Weak Forces in Physics Experiments, University of Chicago Press (1977).

[44] V. B. Braginsky, S. E. Strigin and V. P. Vyatchanin, Parametric oscillatory instability in Fabry-Perot interferometer, Phys. Lett. A **287**(5-6), 338 (2001).

[45] V. B. Braginsky and S. P. Vyatchanin, Low quantum noise tranquilizer for Fabry-Perot interferometer, Phys. Lett. A **293**, 234 (2002).

[46] C. M. Caves, Quantum-mechanical radiation-pressure fluctuations in an interferometer, Phys. Rev. Lett.**45**(2), 79 (1980); C. M. Caves, Quantum-mechanical noise in an interferometer, Phys. Rev. D **23**, 1693(1981).

[47] A. Heidmann, Y. Hadjar and M. Pinard, Quantum non-demolition measurement by optomechanical coupling, Applied Physics B **64**, 180 (1997).

[48] S. Mancini and P. Tombesi, Quantum noise reduction by radiation pressure, Phys. Rev. A **49**, 4055 (1994).

[49] C. Fabre, M. Pinard, S. Bourzeix, A. Heidmann, E. Giacobino and S. Reynaud, Quantum-noise reduction using a cavity with a movable mirror, Phys. Rev. A **49**,1337 (1994).

[50] R. Ruskov, K.Schwab and A. N. Korotkov, Squeezing of a nanomechanical resonator by quantum nondemolition measurement and feedback, Phys. Rev. B **71**, 235407 (2005); R. Ruskov, K. Schwab and A. N. Korotkov, Quantum Nondemolition Squeezing of a Nanomechanical Resonator, IEEE transactions on nano-technology **4**, 132 (2005).

[51] A. Mari and J. Eisert, Gently modulating optomechanical systems, Phys. Rev.Lett. **103**, 213603 (2009).

[52] S. Mancini, V. Giovannetti, D. Vitali and P. Tombesi, Entangling Macroscopic Oscillators Exploiting Radiation Pressure, Phys. Rev. Lett. **88**, 120401 (2002).

[53] L. Yong-Chun, Hu Yu-Wen, Wong Chee Wei and Xiao Yun-Feng, Review of cavity optomechanical cooling, Chin.Phys. B **22**(11), 114213 (2013).

[54] W. W. Johnson and M. Bocko, Approaching the Quantum Limit for Force Detection, Phys. Rev. Lett. **47**, 1184 (1981).

[55] M. F. Bocko and R. Onofrio, On the measurement of a weak classical force coupled to a harmonic oscillator: experimental progress, Rev. Mod. Phys. **68**, 755 (1996).

[56] O. Arcizet, T. Briant, A. Heidmann and M. Pinard, Beating quantum limits in an optomechanical sensor by cavity detuning, Phys. Rev. A **73**, 033819 (2006).

[57] G. Anetsberger, O. Arcizet, Q. P. Unterreithmeier, R. Riviere, A. Schliesser, E. M. Weig, J. P. Kotthaus, T. J. Kippenberg, Near-field cavity optomechanics with nanomechanical oscillators, Nature Physics **5**,909 (2009).

[58] J. D. Teufel, T. Donner, M. A. Castellanos-Beltran, J. W. Harlow and K.W.Lehnert, Nanomechanical motion measured with precision beyond the standard quantum limit, Nat. Nanotech. **4**, 820 (2009).

[59] A. G. Krause, Martin Winger, T. D. Blasius, Q. Lin and O. Painter, A high-resolution microchip optomechanical accelerometer, Nature Photonics **6** (11), 768 (2012).

[60] T. J. Kippenberg and K. Vahala, Cavity Opto-Mechanics, Optics Express **15**, 17205 (2007).

[61] T. J. Kippenberg and K. J. Vahala, Cavity Optomechanics: Back-Action at the Mesoscale, Science **321**, 176 (2008).

[62] A.N. Cleland, Foundations of Nanomechanics (SpringerVerlag, Berlin, 2003).

[63] R.Lifshitz and M.C. Cross, Nonlinear Dynamics of Nanosystems (WILEY-VCH Verlag GmbH & Co. KGaA, Weinheim, 2010).

[64] L. G. Villanueva, R. B. Karabalin, M. H. Matheny, D. Chi, J. E. Sader and M. L. Roukes, Nonlinearity in nanomechanical cantilevers, Phys. Rev. B **87**, 024304 (2013).

[65] X. Zhou, F. Hocke, A. Schliesser, A. Marx, H. Huebl, R. Gross and T. J. Kippenberg, Slowing, advancing and switching of microwave signals using circuit nanoelectromechanics, Nat. Phys. **9**, 179 (2012).

[66] S. Rips, M. Kiffner, I. Wilson-Rae and M. J. Hartmann, Steady-state negative Wigner functions of nonlinear nanomechanical oscillators, New Journal of Physics **14**, 023042(2012); S. Rips and M. J. Hartmann, Quantum Information Processing with Nanomechanical Qubits, Phys. Rev. Lett.**110**, 120503 (2013); S. Rips, I. Wilson-Rae and M. J. Hartmann, Nonlinear nanomechanical resonators for quantum optoelectromechanics, Phys. Rev. A **89**, 013854 (2014).

[67] S.Gröblacher, S. Gigan, H. R. Bohm, A. Zeilinger and M. Aspelmeyer, Radiation-pressure self-cooling of a micromirror in a cryogenic environment, Eur. Phys. Lett. **81**, 54003 (2008).

[68] A. A. Clerk, M. H. Devoret, S. M. Girvin, F. Marquardt and R. J. Schoelkopf, Introduction to quantum noise, measurement and amplification, Rev. Mod. Phys. **82**,1155 (2010).

[69] C. Genes, D. Vitali, P. Tombesi, S. Gigan and M. Aspelmeyer, Ground-state cooling of a micromechanical oscillator: Comparing cold damping and cavity-assisted cooling schemes, Phys. Rev. A **77**, 033804 (2008).

[70] S. Huang and G. S. Agarwal,Enhancement of cavity cooling of a micromechanical mirror using parametric interactions, Phys. Rev. A **79**, 013821 (2009).

[71] C. Genes, Atom-membrane cooling and entanglement using cavity electromagnetically induced transparency, Phys. Rev. A **84**, 051801(R) (2011).

[72] C. Genes, H. Ritsch and D. Vitali, Micromechanical oscillator ground-state cooling via resonant intracavity optical gain or absorption, Phys. Rev. A **80**, 061803 R (2009).

[73] S. Machnes, J. Cerrillo, M. Aspelmeyer, W. Wieczorek, M. B. Plenio and A. Retzker, Pulsed Laser Cooling for Cavity Optomechanical Resonators, Phys. Rev. Lett. **108**, 153601 (2012).

[74] Li Ge, S. Faez, F. Marquardt and H. E. Türeci, Gain-tunable optomechanical cooling in a laser cavity, Phys. Rev. A **87**, 053839 (2013).

[75] T. Weiss and A. Nunnenkamp, Quantum limit of laser cooling in dispersively and dissipatively coupled optomechanical systems, Phys. Rev. A **88**, 023850 (2013).

[76] A. Hopkins, K. Jacobs, S. Habib and K. Schwab, Feedback cooling of a nanomechanical resonator, Phys. Rev. B **68**, 235328 (2003).

[77] M. D. LaHaye, O. Buu, B. Camarota and K. C. Schwab, Approaching the Quantum Limit of a Nanomechanical Resonator, Science **304**, 74 (2004).

[78] J. D. Thompson, B. M. Zwickl, A. M. Jayich, F. Marquardt, S. M. Girvin and J. G. E. Harris, Strong dispersive coupling of a high-finesse cavity to a micromechanical membrane, Nature **452**, 72 (2008).

[79] A. M. Jayich, J. C. Sankey, B. M. Zwickl, C. Yang, J. D. Thompson, S. M. Girvin, A. A. Clerk, F. Marquardt and J. G. E. Harris, Dispersive optomechanics: a membrane inside a cavity, New J. Phys. **10**, 095008 (2008).

[80] P. Meystre, A short walk through quantum optomechanics, Ann. Phys. (Berlin) **525** (3), 215 (2013).

[81] C. K. Law, Interaction between a moving mirror and radiation pressure: A Hamiltonian formulation, Phys. Rev. A 51, 2537 (1995).

[82] M. Eichenfield, J. Chan, R.M. Camacho, K.J. Vahala, O. Painter, Optomechanical Crystals, Nature 462, 78 (2009).

[83] Max Ludwig , Björn Kubala and Florian Marquardt, The optomechanical instability in the quantum regime, New J. Phys. **10**, 095013 (2008).

[84] P. Langevin, Sur la théorie du mouvement brownien, C. R. Acad. Sci. **146**, 530 (1908).

[85] G. Vidal and R. F. Werner, Computable measure of entanglement, Phys. Rev. A **65**, 032314 (2002).

[86] G. Adesso, A. Serafini and F. Illuminati, Extremal entanglement and mixedness in continuous variable systems, Phys. Rev. A **70**, 022318 (2004).

[87] J. Laurat, G. Keller, J. A. Oliveira-Huguenin, C. Fabre, T. Coudreau, A. Serafini, G. Adesso and F. Illuminati, J. Opt. B: Quantum Semiclass. Opt. **7**, 577 (2005).

[88] S. Huang and G. S. Agarwal, Entangling nanomechanical oscillators in a ring cavity by feeding squeezed light, New J. Phys. **11** 103044 (2009).

[89] A. Kolkiran and G. S. Agarwal, amplitude noise reduction in nano-mechanical oscillator, Mathematical and Computational Applications **16**, 290 (2011).

[90] P. Djorwé, J.H. Talla Mbé, S.G. Nana Engo and P. Woafo, Classical and semiclassical studies of nonlinear nano-optomechanical oscillators, Eur. Phys. J. D **67** (45), 1 (2013).

[91] F. Marquardt, J. G. E. Harris and S. M. Girvin, Dynamical Multistability Induced by Radiation Pressure in High-Finesse Micromechanical Optical Cavities, Phys. Rev. Lett. **96**, 103901 (2006).

[92] S. Datta and J. K. Bhattacharjee, Effect of stochastic forcing on the Duffing oscillator, Phys. Lett. A **283**, 323 (2001).

[93] S. Reynaud, C. Fabre, E. Giacobino, A. Heidmann, Photon noise reduction by passive optical bistable systems, Phys.Rev. A 40 (3), 1440 (1989).

[94] P. Djorwé, J.H. Talla Mbé, S.G. Nana Engo, P. Woafo, Nonlinearity-induced limitations on cooling in optomechanical systems, Phys. Rev. A **86**, 043816 (2012).

[95] Albert Schliesser, Cavity Optomechanics and Optical Frequency Comb Generation with Silica Whispering-Gallery-Mode Microresonators, PhD thesis, Ludwig-Maximilians-University, Munchen (2009).

[96] A. Mari and D. Vitali, Optimal fidelity of teleportation of coherent states and entanglement, Phys. Rev. A **78**, 062340 (2008).

[97] S. G. Hofer, W. Wieczorek, M. Aspelmeyer and K. Hammerer, Quantum entanglement and teleportation in pulsed cavity optomechanics, Phys. Rev. A **84**, 052327 (2011).

[98] C. A. Muschik, K. Hammerer, E.S. Polzik and I. J. Cirac, Quantum Teleportation of Dynamics and Effective Interactions between Remote Systems, Phys. Rev. Lett. **111**, 020501 (2013).

[99] M. Abdi, S. Pirandola, P. Tombesi and D. Vitali, Continuous-variable-entanglement swapping and its local certification: Entangling distant mechanical modes, Phys. Rev. A **89**, 022331 (2014).

[100] S. Barzanjeh, S. Pirandola and C. Weedbrook, Continuous-variable dense coding by optomechanical cavities, Phys. Rev. A **88**, 042331 (2013).

[101] P. Horak, The role of squeezing in quantum key distribution based on homodyne detection and post-selection, J. Mod. Opt **51** (8), 1249 (2004).

[102] V. C. Usenko and R. Filip, Squeezed-state quantum key distribution upon imperfect reconciliation, New J. of Phys. **13**, 113007 (2011).

[103] H. Vahlbruch, M. Mehmet, S. Chelkowski, B. Hage, A. Franzen, N. Lastzka, S. Gobler, K. Danzmann and R. Schnabel, Observation of Squeezed Light with $10-dB$ Quantum-Noise Reduction, Phys. Rev. Lett. **100**, 033602 (2008).

[104] M. J. Woolley, A. C. Doherty, G. J. Milburn and K. C. Schwab, Nanomechanical squeezing with detection via a microwave cavity, Phys. Rev.A **78**, 062303 (2008).

[105] E. A. Sete and H. Eleuch, Controllable nonlinear effects in an optomechanical resonator containing a quantum well, Phys. Rev. A **85**, 043824 (2012).

[106] Jie-Qiao Liao and C. K. Law, Parametric generation of quadrature squeezing of mirrors in cavity optomechanics, Phys. Rev. A **83**, 033820 (2011).

[107] A. H. Safavi-Naeini, S. Gröblacher, J. T. Hill, J. Chan, M. Aspelmeyer and O. Painter, Squeezed light from a silicon micromechanical resonator, Nature **500**, 185 (2013).

[108] A. Kronwald, F. Marquardt and A. A. Clerk, Dissipative optomechanical squeezing of light, New J. Phys. **16**, 063058 (2014).

[109] X-Y. Lu, J-Q Liao, L. Tian and F. Nori, Steady-state Mechanical Squeezing in an Optomechanical System via Duffing Nonlinearity, arXiv:1403.0049v1 [quant-ph] 1 Mar 2014.

[110] P. Djorwé, S. G. Nana Engo, J. H. Talla Mbé and P. Woafo, Limiting effects of geometrical and optical nonlinearities on the squeezing in optomechanics, Physica B **422**, 72 (2013).

[111] C. Genes, A. Mari, D. Vital, P. Tombesi, Quantum effects in optomechanical systems, Adv. Atom. Mol. Opt. Phy. **57**, 33 (2009).

[112] A. H. Safavi-Naeini, T. P. M. Alegre, J. Chan, M. Eichenfield, M. Winger, Q. Lin, J. T. Hill, D. E. Chang and O. Painter, Electromagnetically induced transparency and slow light with optomechanics, Nature **472**, 69 (2011).

[113] J. Stolze and D. Suter, Quantum Computing: A short course from Theory to Experiment (WILEY-VCH GmbH & Co. KGaA, Dortmund, 2004).

[114] K. Hammerer, Quantum Mechanics Tackles Mechanics, Science **342**, 702 (2013).

[115] V. M. Vinokur, T. I. Baturina, M. V. Fistul, A. Yu. Mironov, M. R. Baklanov and C. Strunk, Superinsulator and quantum synchronization, Nature **452**, 613 (2008).

[116] M. Bagheri, M. Poot, L. Fan, F. Marquardt and H. X. Tang, Photonic Cavity Synchronization of Nanomechanical Oscillators, Phys. Rev. Lett. **111**, 213902 (2013).

[117] A. Mari, A. Farace, N. Didier, V. Giovannetti and R. Fazio, Measures of Quantum Synchronization in Continuous Variable Systems, Phys. Rev. Lett. **111**, 103605 (2013).

[118] M. B. Plenio and S. F. Huelga, Entangled Light from White Noise, Phys. Rev. Lett. **88**, 197901-1(2002).

[119] D. Vitali, S. Gigan, A. Ferreira, H. R. Bohm, P. Tombesi, A. Guerreiro, V. Vedral, A. Zeilinger and M. Aspelmeyer, Optomechanical Entanglement between a Movable Mirror and a Cavity Field, Phys. Rev. Lett. **98**, 030405 (2007).

[120] C. Genes, A. Mari, P. Tombesi and D. Vitali, Robust entanglement of a micromechanical resonator with output optical fields, Phys. Rev. A **78**, 032316 (2008).

[121] Z. Ying and Y-J. Han, Generating EPR beams in a cavity optomechanical system, Phys. Rev. A **79**, 024301 (2009).

[122] T. A. Palomaki, J. D. Teufel, R. W. Simmonds and K. W. Lehnert, Entangling Mechanical Motion with Microwave Fields, Science **342**, 710 (2013).

[123] Sh. Barzanjeh, M. Abdi, G. J. Milburn, P. Tombesi and D. Vitali, Reversible Optical-to-Microwave Quantum Interface, Phys. Rev. Lett.**109**, 130503 (2012).

[124] L. Tian, Robust Photon Entanglement via Quantum Interference in Optomechanical Interfaces, Phys. Rev. Lett.**110**, 233602 (2013).

[125] P. Djorwé, S. G. Nana Engo and P. Woafo, Robustness of continuous-variable entanglement via geometrical nonlinearity, arXiv:1405.4483v1.

[126] S. Shahidani, M. H. Naderi, M. Soltanolkotabi and S. Barzanjeh, Steady-state entanglement, cooling, and tristability in a nonlinear optomechanical cavity, J. Opt. Soc. Am. B **31**, 1095 (2014).

Publications from this thesis

1. **P. Djorwé**, S. G. Nana Engo and P. Woafo, *Robustness of continuous-variable entanglement via geometrical nonlinearity*, accepted in Phys. Rev. A (2014).

2. **P. Djorwé**, S. G. Nana Engo, J. H. Talla Mbé and P. Woafo, *Limiting effects of geometrical and optical nonlinearities on the squeezing in optomechanics*, Physica B **422**, 72 (2013).

3. **P. Djorwé**, J. H. Talla Mbé, S. G. Nana Engo and P. Woafo, *Classical and semi-classical studies of nonlinear nano-optomechanical oscillators*, Eur. Phys. J. D **67**, 45 (2013).

4. **P. Djorwé**, J. H. Talla Mbé, S. G. Nana Engo and P. Woafo, *Nonlinearity-induced limitations on cooling in optomechanical systems*, Phys. Rev. A **86**, 043816 (2012).

Conferences presentation

1. **P. Djorwé**, S.G Nana Engo and P. Woafo, *Entanglement enhanced by geometrical nonlinearity in optomechanical systems*, School on Non-linear Dynamics, Dynamical Transitions and Instabilities in Classical and Quantum Systems, 14 July - 1 August 2014, Miramare-Trieste (Italia). *Poster*.

2. **P. Djorwé**, Student Chapter Leadership Workshop, Official Officer Travel Grant Award for SPIE Photonics Europe 2014, $13-17$ April, Brussels, Belgium. *Poster*.

3. **P. Djorwé**, S.G Nana Engo and P. Woafo, *Semiclassical study of Casimir effect on pull-in phenomenon and on quantum ground state cooling*, 3^{rd} International conference of the Cameroon Physical Society, Yaoundé, $25-29$ November 2013. *Oral presentation*.

4. **P. Djorwé**, S.G Nana Engo, J.H.Talla Mbé and P. Woafo, *Limiting effects of geometrical and optical nonlinearities on squeezing in optomechanics*, 3^{rd} International conference of the Cameroon Physical Society, Yaoundé, $25-29$ November 2013. *Oral presentation*.

5. **P. Djorwé**, S.G Nana Engo, J.H.Talla Mbé and P. Woafo, *Nonlinear phononics study at the single-phonon level in optomechanics*, Frontiers of Nanomechanics conference, Miramare-Trieste (Italia), $9-13$ September 2013. *Poster*.

6. **P. Djorwé**, J.H.Talla Mbé, S.G Nana Engo and P. Woafo, *Dynamical behaviour of optomechanical systems: classical, semi-classical and quantum limits*, 2^{nd} International Conference of the Cameroon Physical Society, Yaoundé, $6-8$ December 2011. *Poster*.